DETERMINING MICRO- AND MACRO- GEOMETRY OF FABRIC AND FABRIC REINFORCED COMPOSITES

by

LEJIAN HUANG

B.S., LANZHOU UNIVERSITY OF TECHNOLOGY, CHINA, 2004
M.S., SHANDONG UNIVERSITY, CHINA, 2007

AN ABSTRACT OF A DISSERTATION

submitted in partial fulfillment of the requirements for the degree

DOCTOR OF PHILOSOPHY

Department of Mechanical and Nuclear Engineering
College of Engineering

KANSAS STATE UNIVERSITY
Manhattan, Kansas

2013

Abstract

Textile composites are made from textile fabric and resin. Depending on the weaving pattern, composite reinforcements can be characterized into two groups: uniform fabric and near-net shape fabric. Uniform fabric can be treated as an assembly of its smallest repeating pattern also called a unit cell; the latter is a single component with complex structure. Due to advantages of cost savings and inherent toughness, near-net shape fabric has gained great success in composite industries, for application such as turbine blades.

Mechanical properties of textile composites are mainly determined by the geometry of the composite reinforcements. The study of a composite needs a computational tool to link fabric micro- and macro-geometry with the textile weaving process and composite manufacturing process.

A textile fabric consists of a number of yarns or tows, and each yarn is a bundle of fibers. In this research, a fiber-level approach known as the digital element approach (DEA) is adopted to model the micro- and macro-geometry of fabric and fabric reinforced composites. This approach determines fabric geometry based on textile weaving mechanics. A solver with a dynamic explicit algorithm is employed in the DEA.

In modeling a uniform fabric, the topology of the fabric unit cell is first established based on the weaving pattern, followed by yarn discretization. An explicit algorithm with a periodic boundary condition is then employed during the simulation. After its detailed geometry is obtained, the unit cell is then assembled to yield a fabric micro-geometry. Fabric micro-geometry can be expressed at both fiber- and yarn-levels.

In modeling a near-net shape fabric component, all theories used in simulating the uniform fabric are kept except the periodic boundary condition. Since simulating the entire component at the fiber-level requires a large amount of time and memory, parallel program is used during the simulation.

In modeling a net-shape composite, a dynamic molding process is simulated. The near-net shape fabric is modeled using the DEA. Mold surfaces are modeled by standard meshes. Long vertical elements that only take compressive forces are proposed. Finally, micro- and macro-geometry of a fabric reinforced net-shape composite component is obtained.

DETERMINING MICRO- AND MACRO- GEOMETRY OF FABRIC AND FABRIC REINFORCED COMPOSITES

by

LEJIAN HUANG

B.S., LANZHOU UNIVERSITY OF TECHNOLOGY, CHINA, 2004
M.S., SHANDONG UNIVERSITY, CHINA, 2007

A DISSERTATION

submitted in partial fulfillment of the requirements for the degree

DOCTOR OF PHILOSOPHY

Department of Mechanical and Nuclear Engineering
College of Engineering

KANSAS STATE UNIVERSITY
Manhattan, Kansas

2013

Approved by:

Major Professor
Dr. Youqi Wang

Copyright

Abstract

Textile composites are made from textile fabric and resin. Depending on the weaving pattern, composite reinforcements can be characterized into two groups: uniform fabric and near-net shape fabric. Uniform fabric can be treated as an assembly of its smallest repeating pattern also called a unit cell; the latter is a single component with complex structure. Due to advantages of cost savings and inherent toughness, near-net shape fabric has gained great success in composite industries, for application such as turbine blades.

Mechanical properties of textile composites are mainly determined by the geometry of the composite reinforcements. The study of a composite needs a computational tool to link fabric micro- and macro-geometry with the textile weaving process and composite manufacturing process.

A textile fabric consists of a number of yarns or tows, and each yarn is a bundle of fibers. In this research, a fiber-level approach known as the digital element approach (DEA) is adopted to model the micro- and macro-geometry of fabric and fabric reinforced composites. This approach determines fabric geometry based on textile weaving mechanics. A solver with a dynamic explicit algorithm is employed in the DEA.

In modeling a uniform fabric, the topology of the fabric unit cell is first established based on the weaving pattern, followed by yarn discretization. An explicit algorithm with a periodic boundary condition is then employed during the simulation. After its detailed geometry is obtained, the unit cell is then assembled to yield a fabric micro-geometry. Fabric micro-geometry can be expressed at both fiber- and yarn-levels.

In modeling a near-net shape fabric component, all theories used in simulating the uniform fabric are kept except the periodic boundary condition. Since simulating the entire component at the fiber-level requires a large amount of time and memory, parallel program is used during the simulation.

In modeling a net-shape composite, a dynamic molding process is simulated. The near-net shape fabric is modeled using the DEA. Mold surfaces are modeled by standard meshes. Long vertical elements that only take compressive forces are proposed. Finally, micro- and macro-geometry of a fabric reinforced net-shape composite component is obtained.

Table of Contents

List of Figures

List of Tables

Acknowledgements

I would like to express my sincere appreciation to my major advisor, Dr. Youqi Wang, for her intellectual guidance and insight in completion of this research work. I would like to thank my co-advisor, Dr. Daniel Swenson, for his guidance and help throughout my Ph.D. study.

I would also like to thank Dr. Kevin Lease, Dr. Daniel Andresen, Dr. Sherry Haar, and Dr. Bharat Ratra for their willingness to serve on my supervisory committee.

This research work is financially supported by the U.S. Army Research Laboratory (ARL) and Albany Engineered Composites, Inc. (AEC). Special thanks are due to Dr. Chian-fong Yen from ARL and Mr. Jon Goering from AEC for their most appreciated help in finishing the project.

I would also like to thank my group members, Dr. Yuyang Miao, Xiaoyan Yang, Ying Ma, Habib Ahmadi, and Mario Dippolito, for their inspiration to my research and career.

Finally, I thank my wife, Yijie Liu, for her sacrifice and encouragement in completion of this degree.

Dedication

To my father and mother, my wife and my son.

Chapter 1 - Introduction

Textile fabrics and composites have demonstrated outstanding success in both military and civilian fields. In Boeing 787 Dreamliner, nearly half of its materials are made by advanced composites. The light-weight construction of using composite also saves 20 percent in fuel compared to other equivalents. In the past, 2-D laminated composites were commonly used in aerospace industry, such as manufacturing of airplane fuselages and wings. However, production of 2-D laminated composite requires laborious laminating work and has poor impact resistance and delamination strength. In order to overcome these deficiencies, 3-D fabric manufacturing technologies, especially near-net shape fabric manufacturing, have been developed. Various complex 3-D composite products have accordingly arisen, including airplane engine blades, airplane door frames, rib structures, biomedical devices and ballistic panels. In addition, 3-D fabrics have gained attention for creating next-generation body armor.

Characterization of the mechanical behavior of textile fabrics and composites is a growing need because of their expanding applications. Composite mechanical properties rely on the structure of the fabric which is also called composite reinforcement, which, in turn, is determined by the textile weaving process. Composite design and analysis requires a computer tool not only to link composite properties to fabric micro- and macro-geometry, but also to link fabric micro-geometry to the weaving pattern. Consequently, in this dissertation, micro- and macro-geometries of fabrics created by the textile weaving process and fabric reinforced composites formed by the composite manufacturing process are studied.

At the outset of composite design and analysis, the hierarchy of a composite part is addressed, as shown in Figure 1-1. A composite part is made by commingling textile fabric and matrix (e.g.

resin) through a specific manufacturing process, such as resin transfer molding (RTM). A fabric is typically created on a weaving machine. To weave a fabric, repeated patterns are usually adopted and hence the smallest structural repeat of fabric, also called unit cell, can be found. A unit cell consists of a number of yarns or tows. A yarn or a tow is an assembly of thousands of fibers.

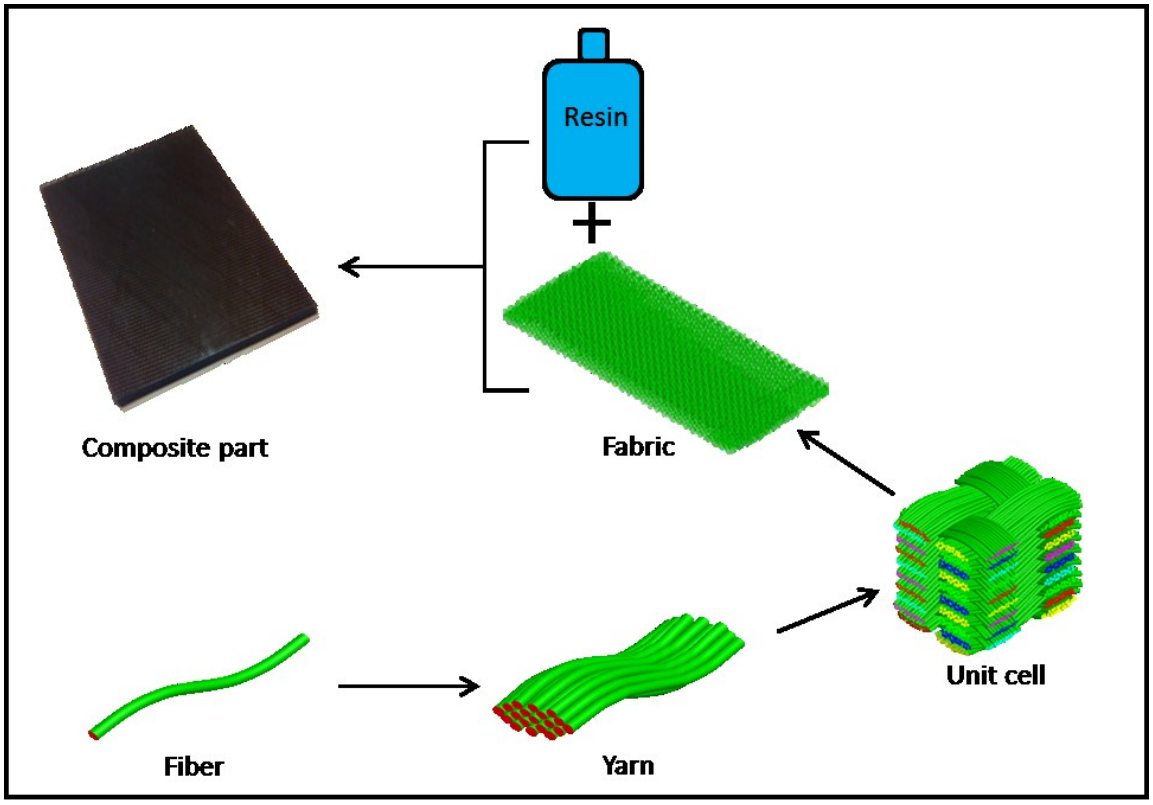

Figure 1-1 Hierarchy of Composite Part

Micro-geometry of fabric or its unit cell can be analyzed at the yarn level or the fiber level. For yarn-level analysis, the yarn micro-geometry is defined by its axial path and cross-section shape. For fiber-level analysis, the yarn path is defined by the axial path of each fiber; the yarn

cross-section shape is determined by the arrangement of circular cross-sectional fibers on the yarn cross-section.

Yarn-level analyses have predominately been performed to estimate fabric micro-geometry with the assumption of a regular yarn cross-section shape, such as semi-circular ended rectangle, ellipse, or lenticil. The assumptions are relatively effective for modeling simple structures, such as 2-D woven structures, but not for structures with complex yarn shapes. Also, the numerical assumption of yarn shape based on experimental observation is time consuming. As well, it is necessary to develop a robust method able to represent complex yarn geometries and stand alone from experimental investigations.

Since a fabric or its unit cell consists of many yarns and each yarn is a bundle of fibers, fabric micro-geometry can be better reflected by a fiber-level analysis. As such, a fiber-level based approach, known as the digital element approach (DEA), has arisen.

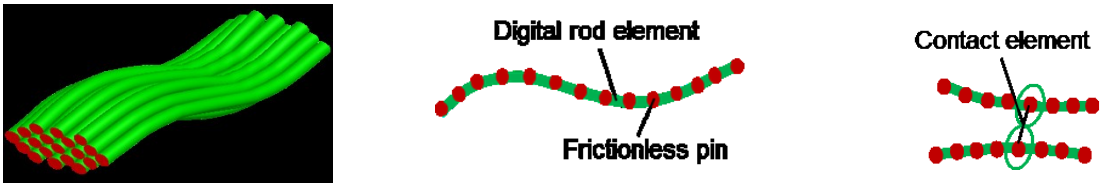

(a) Digital yarn (b) Digital fiber (c) Contact element

Figure 1-2 Key Concepts of Digital Element Approach [1]

The DEA was developed by Wang and her colleagues at Kansas State University to simulate textile weaving and braiding processes and to determine fabric micro-geometry [2]-[4]. It is based on three key concepts: digital yarn, digital fiber, and contact element, as demonstrated in Figure 1-2. A digital yarn consists of a number of digital fibers. Each digital fiber is an assembly of circular cross-sectional rod elements connected by frictionless pins. A fiber is fully

represented when the rod element length approaches zero. A contact element is inserted when interference occurs between two fibers. The fabric deforms when external forces are applied. Because the DEA follows textile processing mechanics, it has become a very promising method for determining fabric micro-and macro -geometries.

The solver used in the DEA has undergone several phases, including quasi-static, static, and current dynamic algorithms [1]-[10]. The quasi-static algorithm generates fabric micro-geometry by simulating the textile weaving or braiding process step by step, which consumes a large amount of computer resources. The static algorithm, solving the global matrix of a fabric using an implicit algorithm, is more efficient than the quasi-static algorithm. The dynamic algorithm, using an explicit algorithm instead of solving the global matrix, is more efficient than the static algorithm. In this research, dynamic relaxation with periodic boundary conditions will be used to determine the fabric unit cell micro-geometry. Unit cells are then assembled to form a fabric.

As stated, advanced technologies have been developed in order to manufacture complex composite parts. Near-net shape technology has shown potential in manufacturing composite reinforcements by saving costs in surface processing and also guaranteeing mechanical properties of the net-shape composite. A near-net shape fabric often has a complex shape and has caused researchers many difficulties in modeling the weaving pattern and detailed yarn shapes. The DEA is a method based on weaving mechanics and is able to handle complex fabrics. It models fabric micro-geometry at the fiber level and needs a large amount of computer resources to model large-scale fabrics. Hence, in this research, parallel computation will be conducted to accomplish the full-field fabric simulation.

A near-net shape fabric is then typically formed into a net-shape composite component through a composite manufacturing process, such as resin transfer molding. Although

manufacturing details vary, common modeling issues are consistent among the processes: fabric representation, mold surface representation, and mold-to-fabric contact. Because of fabric model simplifications, few research works were able to predict a precise fabric deformation process. In this research, the DEA will demonstrate its power to simulate the molding process and model the relative fabric reinforced composite.

Research work in this dissertation includes

- 3-D Woven Fabric Unit Cell Micro-geometry

A dynamic DEA with periodic boundary conditions is developed to model the fabric unit cell micro-geometry. Numerical simulations are validated with experimental results.

- 3-D Woven Near-Net Shape Fabric Component

A 3-D woven near-net shape fabric is modeled using dynamic DEA. Parallel processing is employed for full-field fabric simulation. Numerical simulations are compared with experimental results.

- 3-D Woven Net-shape Composite and Molding Process

In addition to fabric representation using the DEA, mold surface and mold-to-fabric contact are also modeled. A fabric reinforced composite is modeled and the dynamic molding procedure is also explained.

Chapter 2 - Literature Review

Textile composite properties are determined by textile fabric micro-geometry and textile fabric micro-geometry is determined by the textile weaving process. A weaving process with repeated pattern yields a uniform fabric with unit cell features. An increasing number of advanced technologies, including the near-net shape fabric manufacturing, have been developed to manufacture composite reinforcement. After its creation, a fabric is generally processed into a composite part. Fabric deforms accordingly. Numerical simulations of geometries of fabric and fabric reinforced composite play an essential part in composite design and analysis. In this chapter, a review of relevant research is discussed in three sections: 1) Fabric geometry analysis, 2) Near-net shape fabric manufacturing, and 3) Fabric reinforced composites and fabric deformation process.

2.1 Fabric Geometry Analysis

Fabric geometry can be modeled at the macro-scale or the micro-scale. At the macro-scale, fabric is normally treated as a continuum, modeled by finite shell or membrane elements. This type of fabric representation is commonly used in fabric thermal conductivity, rapid prototyping, and impact analysis. At the macro-scale, the fabric unit cell can be identified if it is present. In this case, it is necessary to only model the micro-geometry of the fabric unit cell and construct spatially translated copies of it. The fabric unit cell micro-geometry can be expressed at either yarn-level or fiber-level. In this section, fabric geometry is studied at the micro-scale and both yarn-level and fiber-level models are addressed.

This section contains three parts: 1) Fabric structures, 2) Fabric structure modeling methods, and 3) Fabric micro-geometry modeling software.

2.1.1 Fabric Structures

Understanding composite/fabric structure is essential for composite design and analysis. Various textile manufacturing processes create different fabric structures, such as woven, braided, stitched, and knitted. Among the structures, the woven structure is most common and is highlighted in this research. Woven fabric can be classified into 2-D woven and 3-D woven structures.

2.1.1.1 2-D Woven Structure

In a 2-D woven fabric, weft and warp interlace in one layer, typically at an angle of 90^0, as seen in Figure 2-1. Three types of 2-D woven fabric structures are shown in Figure 2-2: plain weave, twill weave, and satin weave. In the plain weave structure, each weft passes over and under each warp alternatively, as demonstrated in Figure 2-2a. In the twill weave structure, one or more wefts pass over and under one or more warps alternatively. Figure 2-2b illustrates the case when every two wefts pass over and under every two warps alternatively. This structure is called a 2×2 plain weave. In the satin weave, four or more wefts pass over a single warp, or vice versa. The number of wefts passing over a single warp is called the Harness number. Figure 2-2c shows a 4-Harness satin weave structure. Black dashed lines in the pictures mark the unit cell domain. These three structures contain 16, 4, and 4 unit cells, respectively.

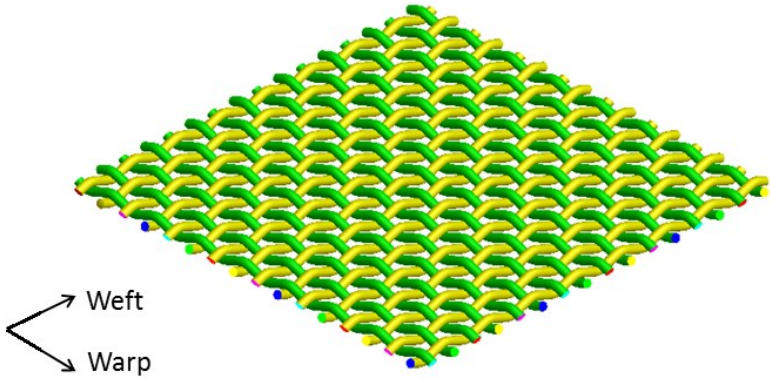

Figure 2-1 2-D Woven Fabric

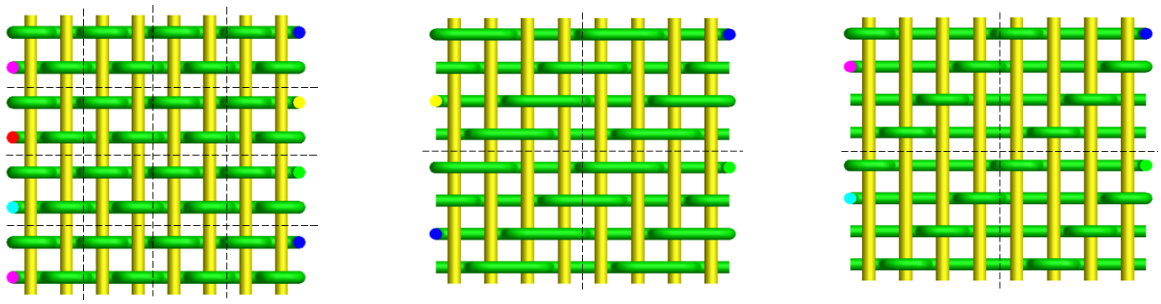

(a) Plain weave (b) Twill weave (2×2) (c) Satin weave (4-Harness)

Figure 2-2 Typical 2-D Woven Structures (Top View)

2.1.1.2 3-D Woven Structure

A 3-D woven fabric generally consists of multiple layers of weft yarns and a number of warp yarns intertwining weft yarns. Three types of 3-D woven fabrics are shown in Figure 2-3, layer-to-layer, orthogonal, and angle interlock. The top pictures are top views and the bottom pictures are front views. The layer-to-layer fabric consists of multiple layers of fabrics. Each layer has individual sets of wefts and warps and is connected with neighboring layers by interlacing yarns. The orthogonal fabric consists of three types of yarns, weft, warp stuffer, and warp weaver.

Warp stuffer is typically straight yarn and warp weaver is curvy yarn in order to bind the wefts. In angle interlock weaves, warps travel through the fabric and bind wefts together. The warp traveling plane is angled, instead of perpendicular, to weft plane.

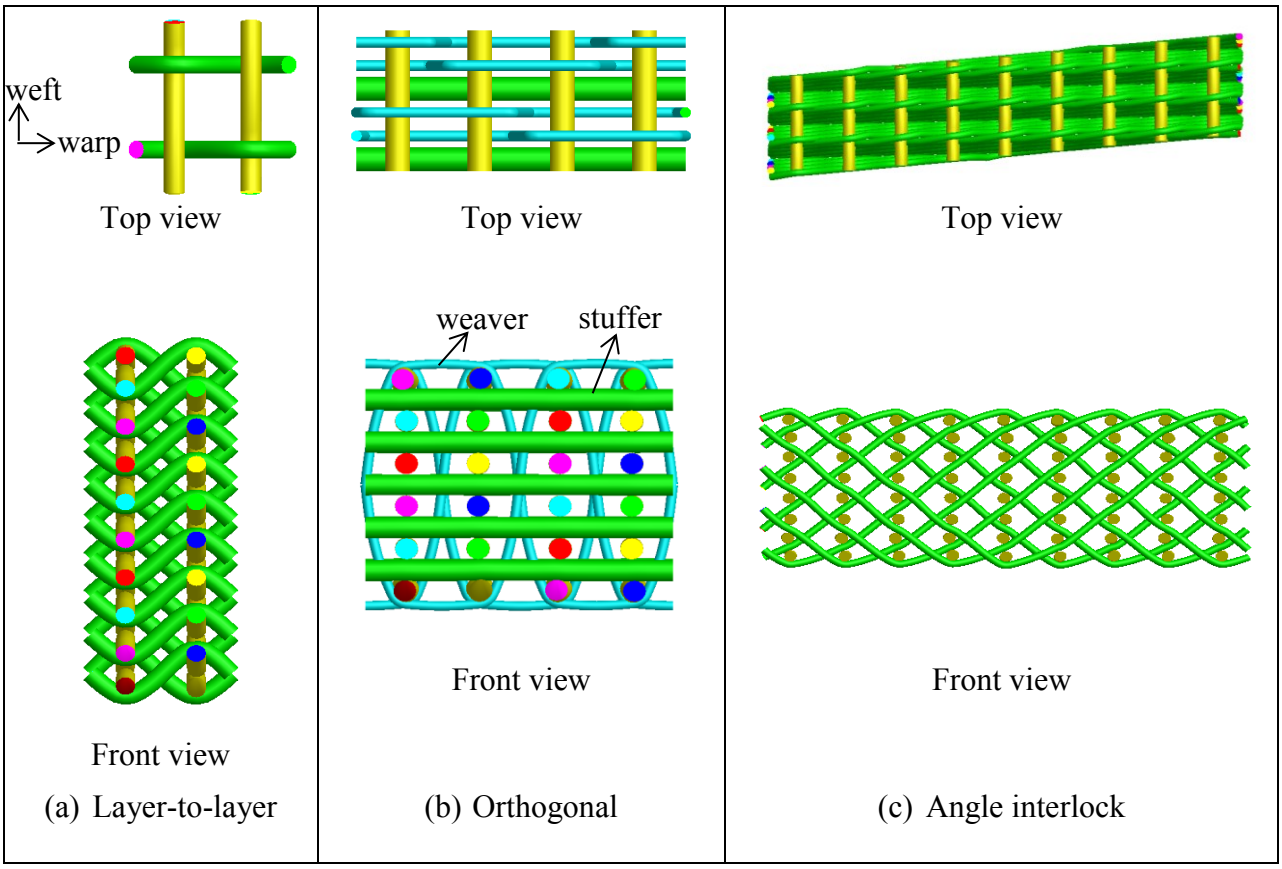

Figure 2-3 Typical 3-D Woven Structures

2.1.2 Fabric Structure Modeling Methods

Modeling methods conducted on fabric micro-structure can be categorized into the tow- or yarn-level analysis and fiber-level analysis. For the tow- or yarn- level analysis, yarn geometry is defined by yarn axial path and yarn cross-section shape. For the fiber-level analysis, yarn geometry is defined by fiber path and fiber arrangement on the yarn cross-section.

2.1.2.1 Yarn-Level Analysis

Yarn axial path is determined by the weaving pattern. Yarn cross-section shape varies according to the weaving kinetics. Based on the yarn cross-section shape, yarn-level analyses can be elaborated into two groups: constant yarn cross-section and variable yarn cross-section.

2.1.2.1.1 Constant yarn cross-section model

Constant yarn cross-section shapes are commonly assumed as circle, semi-circular ended rectangle, ellipse, and lenticil, as seen in Figure 2-4. Applications of the assumptions are heavily dependent on weaving realities.

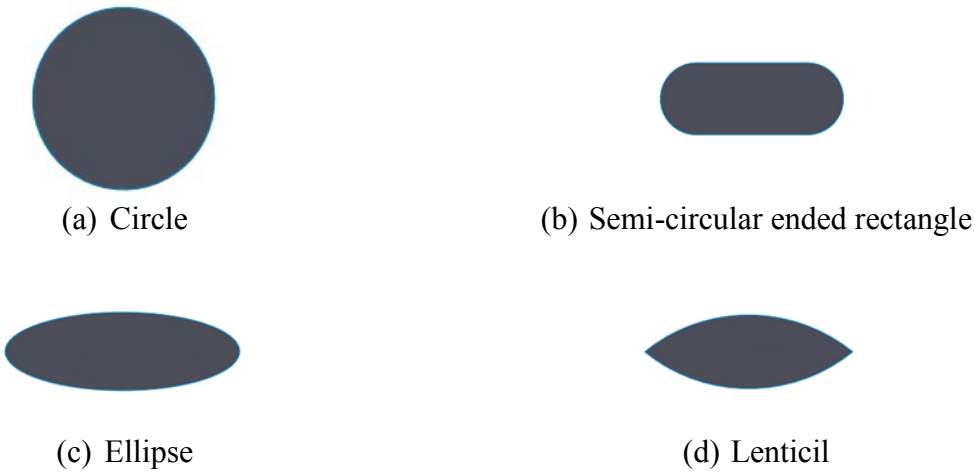

(a) Circle (b) Semi-circular ended rectangle

(c) Ellipse (d) Lenticil

Figure 2-4 Common Assumptions of Yarn Cross-section Shapes

Characterization of textile fabric geometry originated in 1930s when Peirce [11] developed a geometric model to describe a plain weave fabric. In his model, yarns were treated as perfectly flexible and inextensible cylinders. Yarn path was expressed by a combination of linear and circular segments. Refer to Figure 2-5. Mathematical relations of geometric parameters were

studied. This model was applicable in only a limited number of structures, such as the fabric with loose density.

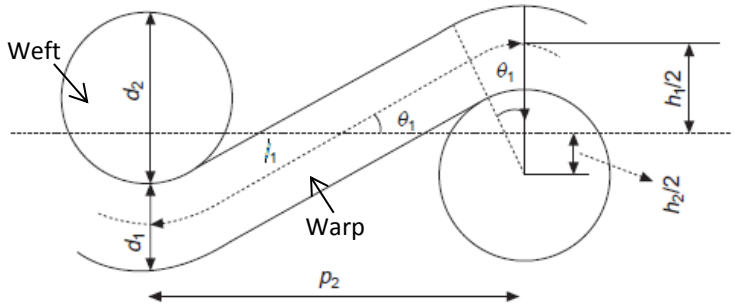

Figure 2-5 Unit Cell with Circular Cross-sectional Yarn [11][12]

In regard to yarn flattening, in the 1950s Kemp [13] proposed a race track model based on Peirce's model. As demonstrated in Figure 2-6, yarn cross-section was assumed as a rectangle enclosed by two semi-circular ends. Length and width of weft cross-section was denoted by a_2 and b_2, respectively. Other modifications were then correspondingly applied. Yarn flattening was implemented by changing the pick spacing p_2, crimp height h_1, and yarn diameter b_2.

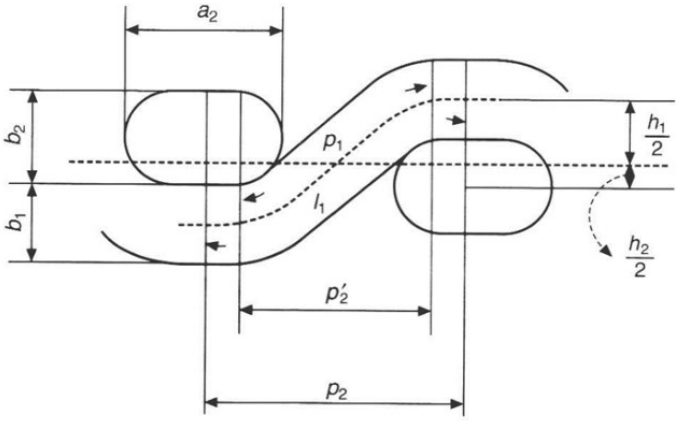

Figure 2-6 Racetrack Model [12][13]

In the 1970s, Hearle and Shanahan [14] concluded that Kemp's model was satisfactory in purely geometric models but not mechanical models. They stated that Kemp's model increased bending energy because of high curvatures at the semi-circular ends. They proposed a model with lenticular cross-section, as seen in Figure 2-7, and believed the continuous length of lower curvature would not create a rapid increase of bending energy in the contact region. The cross-section shape was formed by two arcs with equal radius on either side. Other assumptions followed what Peirce had used.

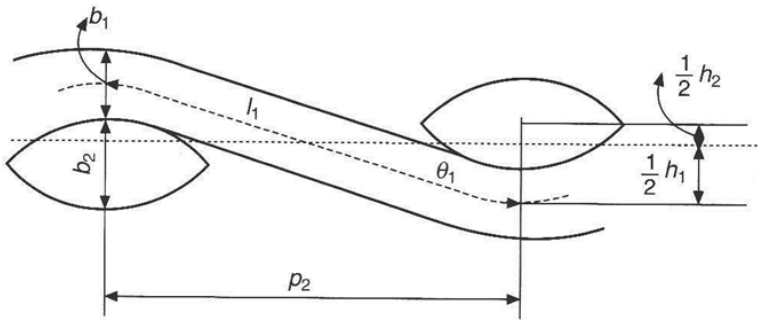

Figure 2-7 Unit Cell with Lenticular Cross-sectional Yarn [12][14]

In the 1990s, Ito and Chou [15] used single sinusoidal function to define yarn geometry in the plain weave structure, as seen in Figure 2-8. Axial path of the longitudinal yarn (z_0) is defined using a sine function curve and yarn thickness (h_y) is assumed constant. Thus, the upper and lower bonds (z_1 and z_2) of the longitudinal yarn and the cross-sections of transverse yarns are sine function curves. Similar assumptions were also adopted by Naik et al. [16] and McBride and Chen [17].

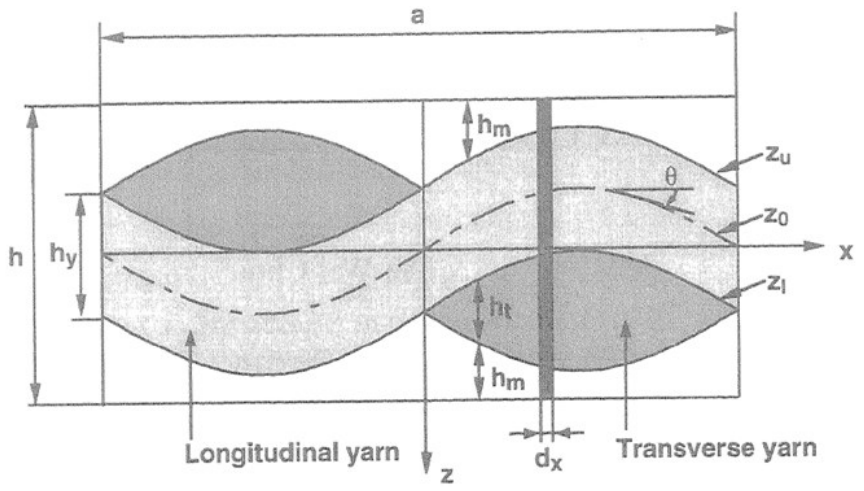

Figure 2-8 Yarn Shape Defined by Sinusoidal Function [15]

As long as a regular or constant yarn cross-section shape is assumed, interference could exist between yarns, especially in complex fabric structures. The interference will cause difficulties in further finite element analysis.

2.1.2.1.2 Variable yarn cross-section model

In most cases, yarn cross-section shape is not constant because of yarn-to-yarn interactions. Microscopic images have also demonstrated that yarn cross-section varies from section to section [18].

In the 1990s, Kuhn and Charalambides [19] described the fabric unit cell as three regions and assigned relatively different cross-section shapes within those regions. As shown in Figure 2-9a, these three regions are the interlace region, gap region, and bridge region, denoted by *cghd*, *hmnj*, *dhje*, respectively. As illustrated in Figure 2-9b, yarn cross-section is formed by a combination of top and bottom sinusoidal curves with different amplitudes. In the interlace region, the portion contacting the adjacent yarns has a lower amplitude than the opposing portion. The cross-section

shapes in the interlace region remain constant and those in the bridge region are interpolated from adjacent interlace regions.

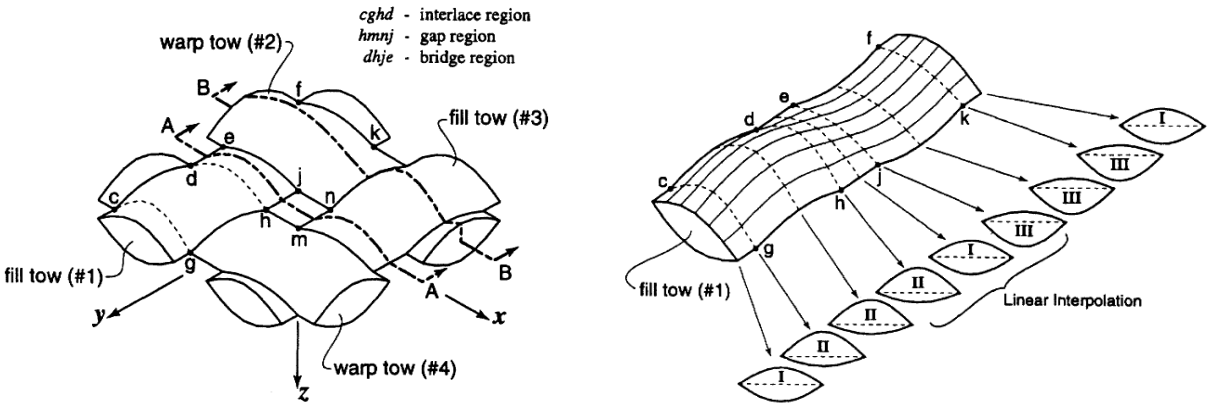

(a) Unit cell divided into three regions (b) Cross-section variations along a yarn

Figure 2-9 Yarn with Variable Cross-sections [19]

Similarly, in the 2000s, Hivet and Boisse [18][20][21] characterized yarn using three different zones and defined yarn geometry accordingly. As demonstrated in Figure 2-10a, curves s_1s_2, s_3s_4, and s_2s_3 as well as s_4s_1 denote yarn cross-section shapes in contact free zone, contact zone, and lateral zone, respectively. Yarn axial path is formed by a combination of a straight segment in the contact free zone and a conic curve in the contact zone, as seen in Figure 2-10b. A parametric description of yarn geometry of a twill weave structure is shown in Figure 2-10c.

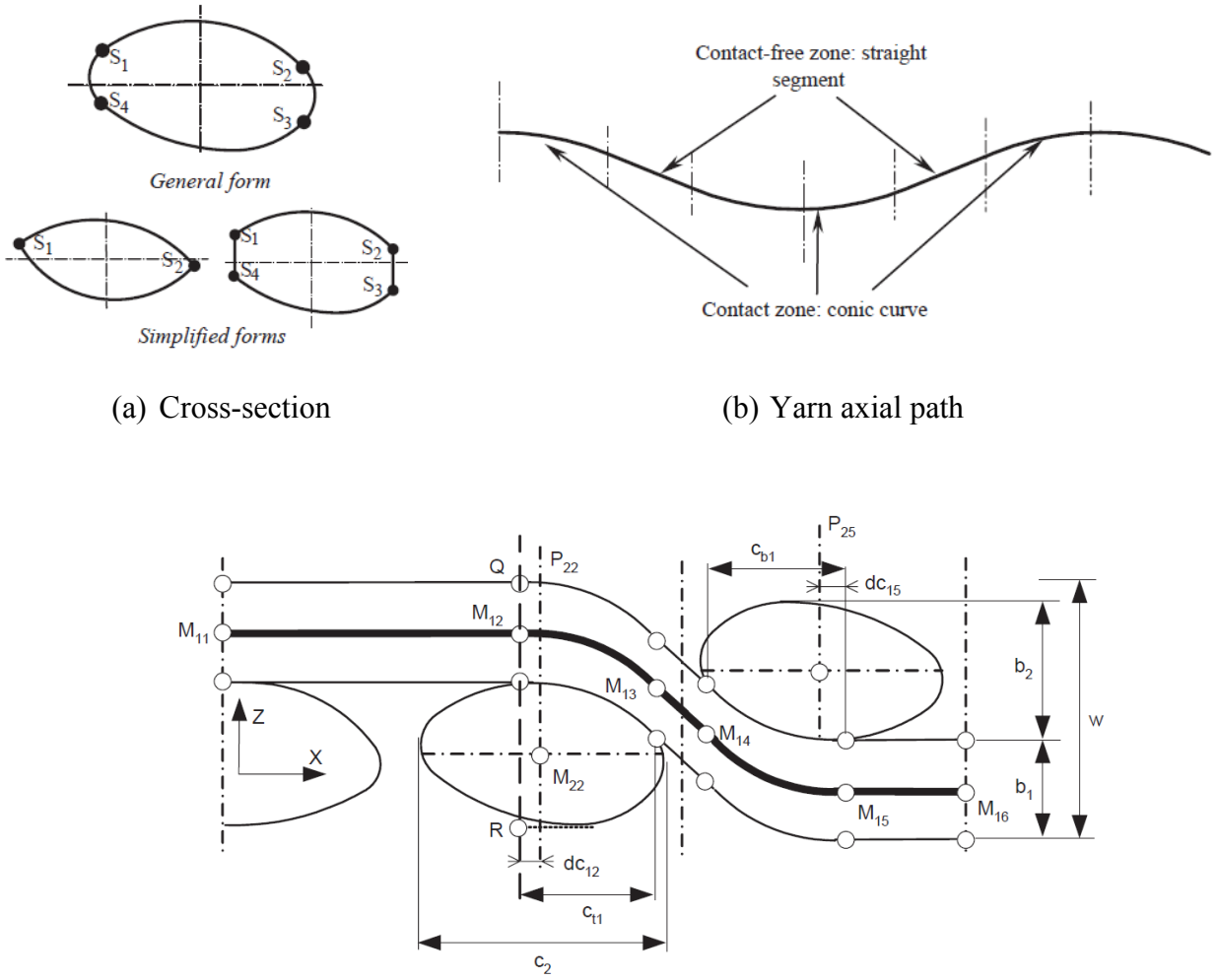

(a) Cross-section (b) Yarn axial path

(c) Parameterization of the unit cell transverse cut

Figure 2-10 Yarn Shape Defined by Parameterized Function [18]

Assumption of variable yarn cross-section has the potential to generate more accurate yarn shape, but it is highly dependent on experimental or empirical results and is hardly applicable to complex fabric structures.

2.1.2.2 Fiber-Level Analysis

Textile composites, especially those with complex weaving patterns, contain various yarn cross-section shapes. Microscopic pictures of two 3-D woven composite structures are provided

in Figure 2-11. In the first sample, weavers show variable cross-section shapes along yarn paths. In the second sample, all yarns present irregular cross-section shapes. Consequently, assumption of constant or simple variable yarn cross-section is no longer applicable.

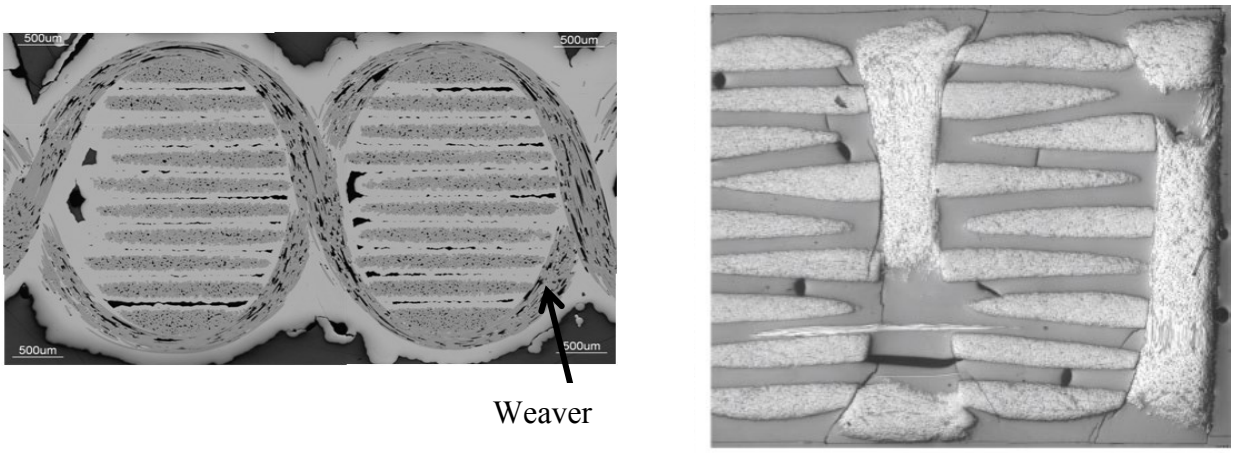

(a) Sample 1 [22] (b) Sample 2 [23]

Figure 2-11 Experimental Observations

Fabric is commonly comprised of yarns, and yarn is an assembly of fibers. Yarn shape is affected by the relative motion of fibers inside the yarn. Consequently, fabric micro-geometry can be accurately reflected at the fiber level. For the fiber-level analysis, fiber cross-section shape is assumed to be circular and the local yarn cross-section shape is determined by fiber arrangement in that yarn. One method of fiber-level analysis is called “digital element approach”.

2.1.2.2.1 Digital element approach

The digital element approach (DEA) is a micro-mechanics based sub-yarn level approach developed by Wang and her colleage [1]-[10]. Initially, the method was used to determine the unit cell topology of 3-D braided fabrics [2][3]. In her model, each yarn was modeled as a digital rod element chain with frictionless pin connections, as seen in Figure 2-12a. Yarn-to-yarn

contact was modeled by a contact element inserted between two contact nodes, as seen in Figure 2-12b. A quasi-static numerical procedure was employed to simulate the 3-D braiding process step-by-step.

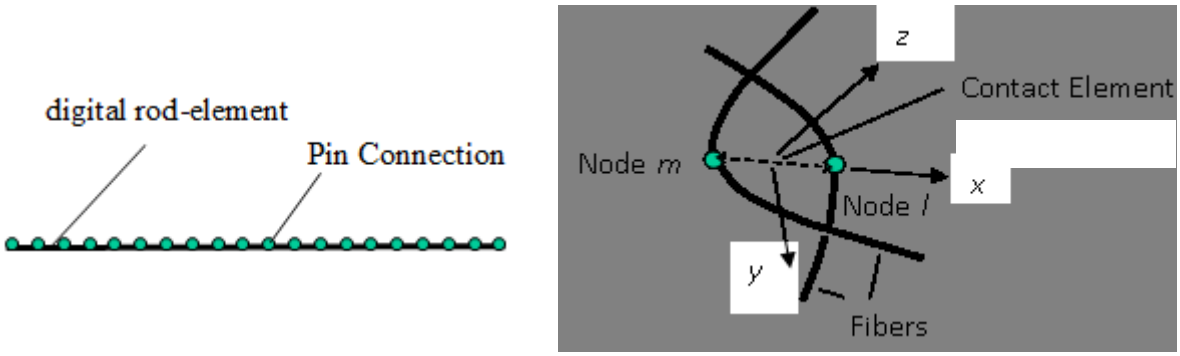

(a) Yarn discretization (b) 3-D contact element

Figure 2-12 Single Digital Chain Model [3]

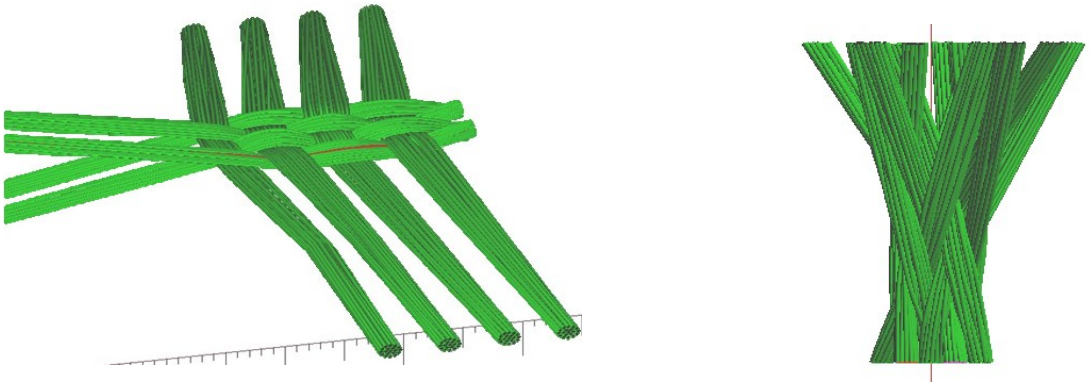

(a) 2-D weaving (b) 3-D braiding

Figure 2-13 Multi-Digital Chain Model [4]

The DEA was later refined at the sub-yarn level to simulate the 2-D weaving process and the 3-D braiding process [4]. A yarn was modeled as a bundle of digital fibers, as seen in Figure

2-13. Yarn cross-section deformed due to the relative motion of fibers inside the yarn during the textile processing. Therefore, both yarn paths and yarn cross-section shapes can be derived.

The major obstacle of the quasi-static method is the great computer resource required by the step-by-step simulation. In order to resolve this issue, a static relaxation procedure was developed [5]. In this procedure, fabric topology was established based upon the textile process kinematics, as seen in Figure 2-14a. Then, a tension was applied to each yarn. Non-equilibrium nodal forces were calculated. Next, a global stiffness matrix was assembled and nodal displacements were calculated. Final geometry is shown in Figure 2-14b. The static relaxation procedure required less than 5% of computer resources used by the step-by-step simulation.

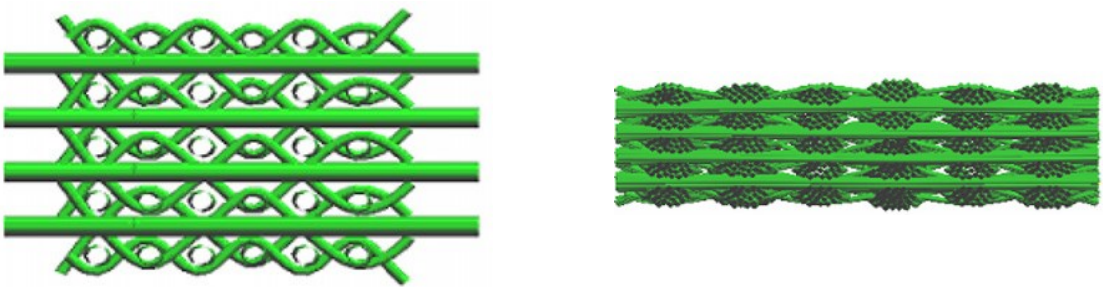

(a) Fabric topology (b) Fabric detailed geometry

Figure 2-14 3-D Woven Model with Multi-Fibers Per Yarn [5]

The unit cell in DEA is a non-continuum domain. During simulation, boundary changes and interior area nodes may move to the boundary. A static algorithm for a non-continuum domain with a periodic boundary condition would be complex. Hence, an explicit dynamic relaxation algorithm with a periodic boundary condition is proposed. The explicit dynamic approach is elaborated in Chapter 3.

2.1.2.2.2 Other approaches

Based on the DEA, Madhadik and Hallett [24][25] modeled fabric micro-geometry using commercial software LS-DYNA, as shown in Figure 2-15. Each yarn was treated as an assembly of 19 fibers and each fiber was modeled using finite beam elements. A linear thermal loading decrease was adopted in order to model tensile forces applied on yarns, thus causing a decrease in fabric thickness.

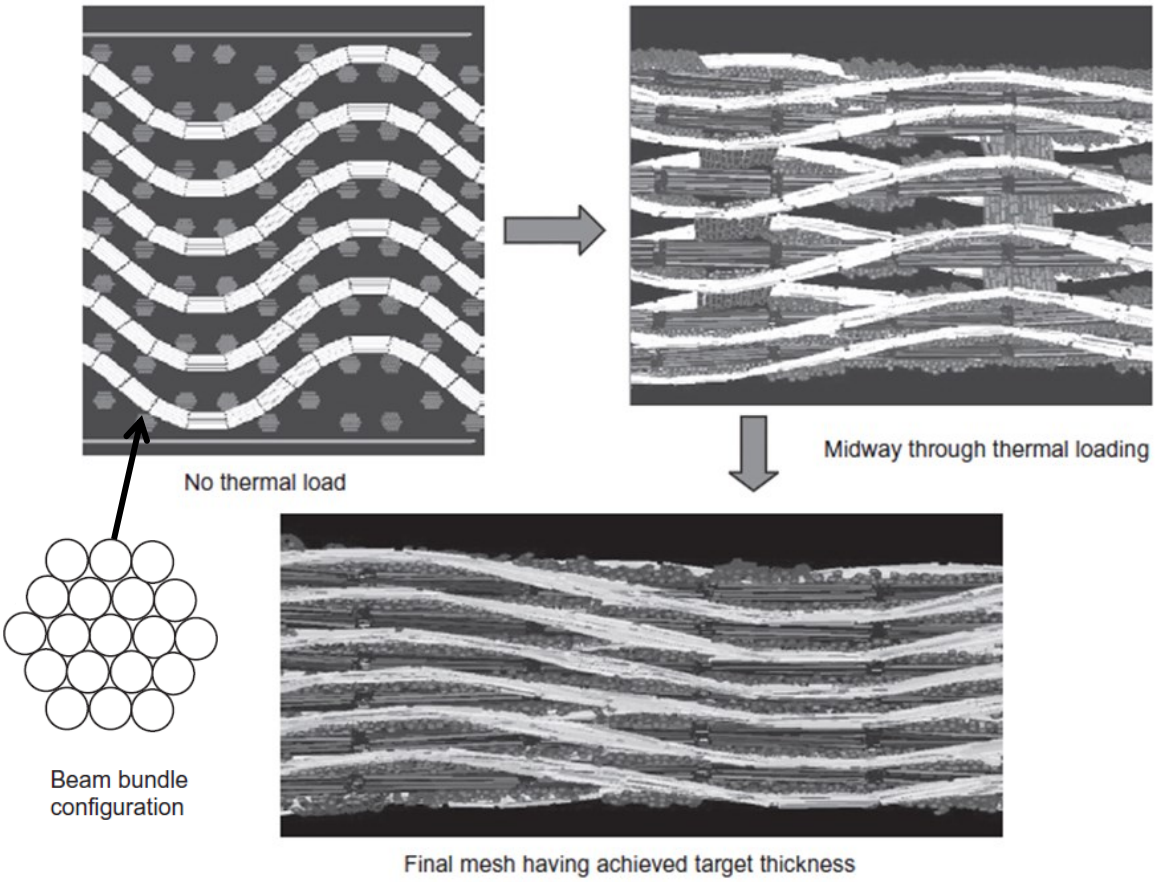

Figure 2-15 3-D Woven Structure with Multi-Fibers Per Yarn [25]

Durville [26]-[28] modeled the micro-geometry of 2-D woven fabrics. A yarn was defined as a bundle of fibers and each fiber was modeled using 3-D finite strain beam elements. All yarns

were initially laid on the same plane with a superimposing order, as seen in Figure 2-16a. Yarns and relevant fibers were gradually separated and moved toward target positions set by normal contact directions according to the weaving pattern. An implicit solver was employed during the simulation. Running time of the entire process was two to three days.

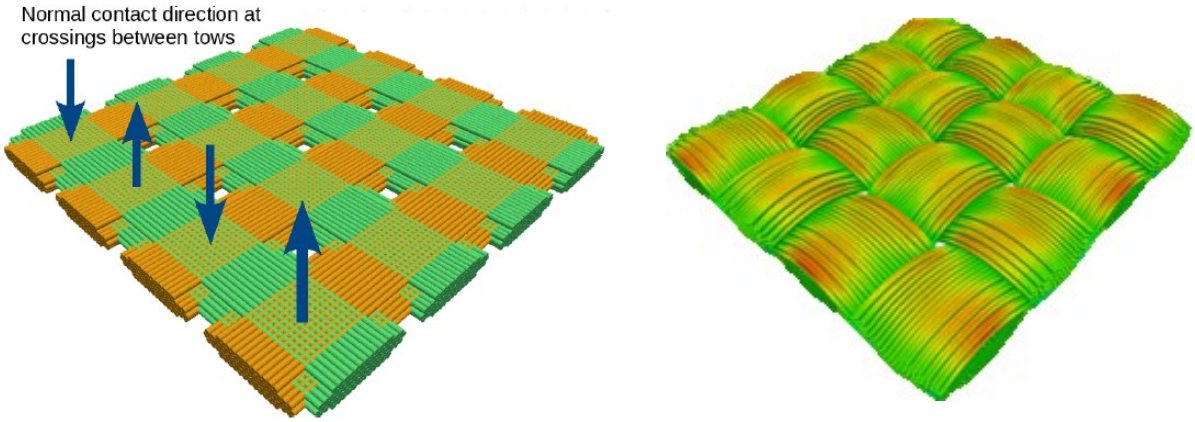

(a) Initial geometry (b) Final geometry

Figure 2-16 2-D Woven Structure with Multi-Fibers Per Yarn [28]

2.1.3 Fabric Micro-geometry Modeling Software

Since the 1990s, an increasing number of advanced textile composites have arisen in modern industry. Computer tools are desired in order to model those structures. In this section, three composite/fabric structure modeling software packages are introduced: WiseTex, TexGen, and DFMA.

2.1.3.1 WiseTex

WiseTex, developed at the Katholieke Universiteit Leuven, Belgium [29]-[33], is a commercial software package used to model textile fabric and textile composite. This package is able to model fabric micro-geometry (WiseTex, LamTex, WeftKnit, FETex), composite micro-

geometry (TexComp), permeability of textile composites (FlowTex), and textile virtual reality (VRTex).

In order to model fabric micro-geometry, WiseTex defines fabric architecture with assigned fiber and yarn properties. Unit cell topology is defined through matrix coding according to the textile weaving pattern. Input yarn properties include linear density, yarn dimension, yarn compression, yarn bending rigidity, and yarn transverse compressive stiffness. Yarn path is expressed as a parameterized polynomial function, and yarn cross-section is assumed to be elliptical or lenticular. Polynomial coefficients and major and minor axes lengths of the yarn cross-section are derived by minimizing the bending energy. Fabric micro-geometry is consequently generated. A 3-D woven fabric structure created by WiseTex is shown in Figure 2-17.

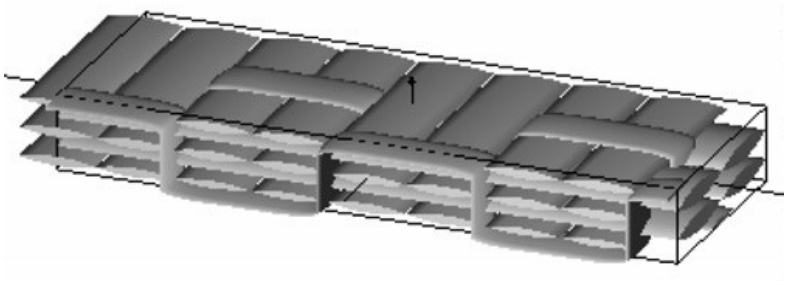

Figure 2-17 3-D Woven Fabric Created by WiseTex [31]

2.1.3.2 TexGen

TexGen was developed at the University of Nottingham, UK [34]-[40] as an open source code. This software has experienced increased usage in recent years.

In TexGen, yarn axial path is described by using a set of control points. Spline interpolations are implemented between those control points in order to obtain a smooth yarn path. The yarn cross-section shape is assigned based on experimental or empirical results, and common yarn

cross-section shapes used are ellipse, lenticil, or polygon. Detailed yarn shape is then created by sweeping the assumed cross-sections along the yarn path. A 3-D woven fabric unit cell created by TexGen is shown in Figure 2-18.

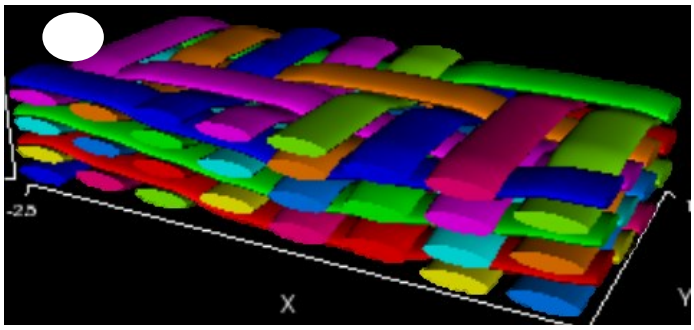

Figure 2-18 3-D Woven Unit Cell Created by TexGen [37]

The primary difference between WiseTex and TexGen in regard to creating fabric micro-geometry is that WiseTex is a mechanical based computer tool, and TexGen is a geometrical based computer tool. Both software programs highly depend on empirical or experimental results to define yarn cross-section. Constant cross-section shapes assigned to yarns are inaccurate and may also create yarn-to-yarn interference which causes difficulties for finite element analysis.

2.1.3.3 DFMA

Digital Fabric Mechanics Analyzer, DFMA, is developed at Kansas State University. Mechanical theory in this software uses DEA developed by Wang et al. [1]-[10]. The DEA is able to model the textile weaving process, textile fabric micro-geometry, and fabric deformation process.

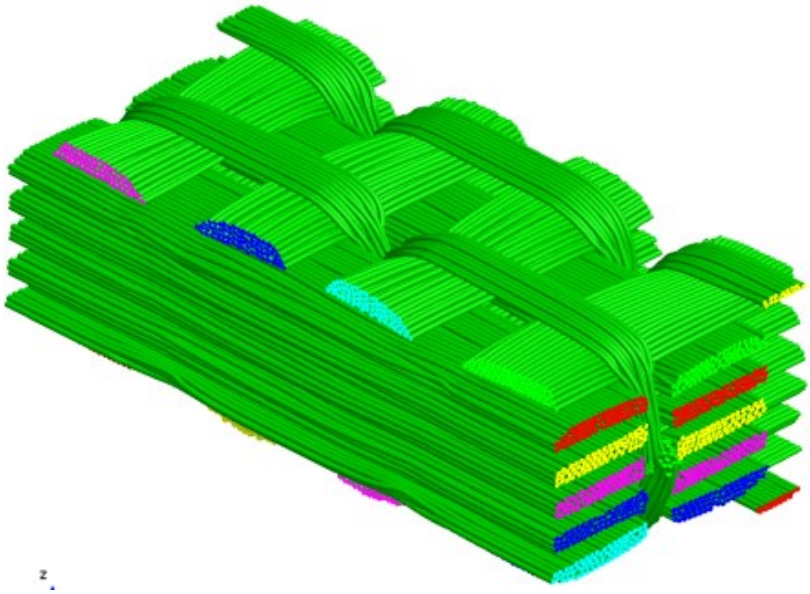

(a) Fiber level

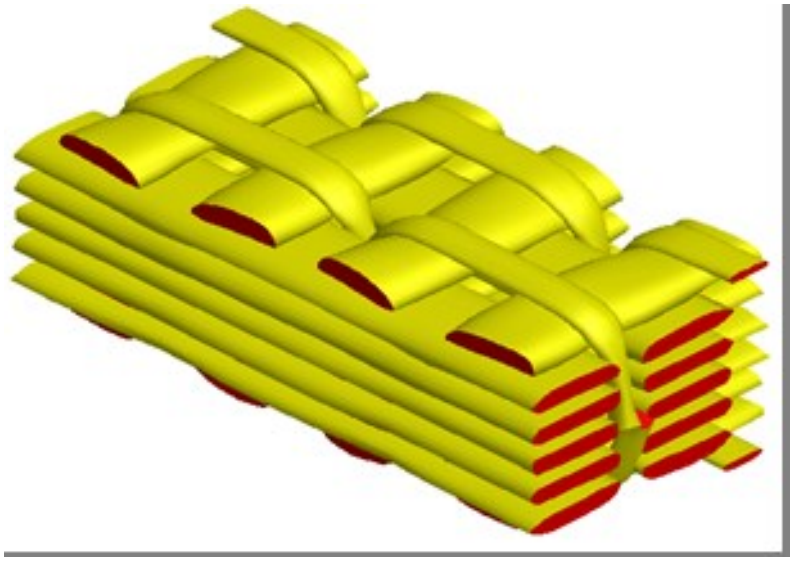

(b) Yarn level

Figure 2-19 3-D Woven Unit Cell Created by DFMA [1]

DFMA generates fabric micro-geometry by following textile weaving mechanics. Fabric topology is defined based on the textile weaving pattern. Input data of yarn properties include:

yarn cross-section area, fiber longitudinal and transverse moduli, and fiber density. Yarn is represented by a bundle of digital fibers and each digital fiber is a digital element chain. An explicit dynamic relaxation approach is employed. Fabric micro-geometry can be expressed at both fiber and yarn levels. A 3-D woven fabric unit cell created by DFMA for both yarn-level and fiber-level is shown in Figure 2-19. The simulation procedure and corresponding theories are detailed in Chapter 3.

2.2 Near-net Shape Fabric Manufacturing

Near-net shape technology produces a product that resembles the shape of the net/final product as closely as possible. Therefore, the final product can then be made with minimum cutting or surface finishing based on the near-net shape product.

In the composite industry, many textile fabrics can be manufactured through near-net shape technology. Various textile processes, such as weaving, braiding, and knitting, have adopted this technology. Those processes can yield a near-net shape fabric that guarantees toughness within the product without additional reinforcement treatment. In this section, processes of weaving, braiding, and knitting, and the relative near-net shape products, are introduced.

2.2.1 Weaving

In a typical weaving process, three primary actions occur: weft insertion, beating up, and warp weaving [8], as demonstrated in Figure 2-20. In a weft insertion action, the shuttle takes a weft yarn and moves across the weaving loom. In a beating up action, the reed beats the inserted weft against the newly formed fabric. In the ensuing weaving action, warps move either upward or downward to create fabric with a specific pattern. A fabric is thus created.

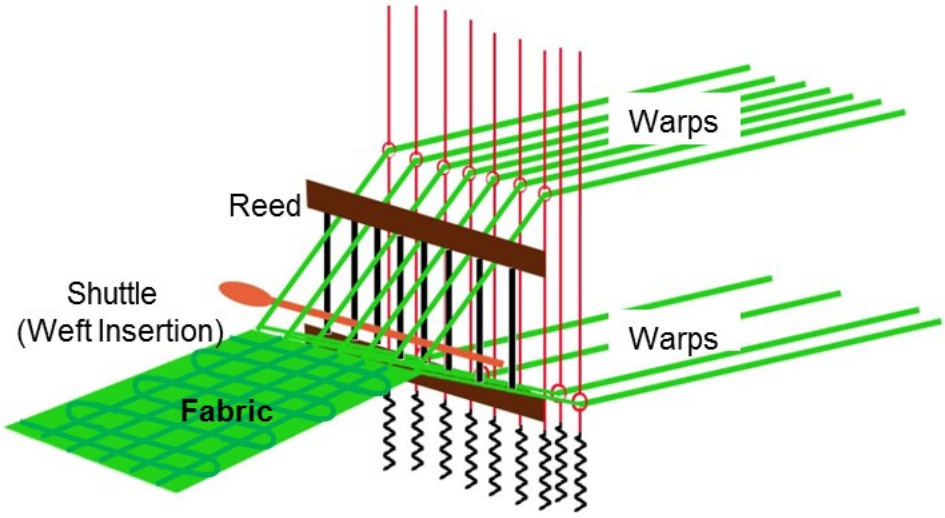

Figure 2-20 Schematics of Dynamic Weaving [8]

Figure 2-21 shows a 3-D woven near-net shape fabric and net shape composite, produced by Albany Engineered Composites, a leading organization in composite design and manufacturing [41]-[44]. The near-net shape fabric is a single component woven by the Jacquard weaving, and then processed into the final product by resin transfer molding. The figure indicates two shapes are so similar that surface tailoring or polishing is rarely needed.

Figure 2-21 Near-net Shape Fabric (Left) and Net Shape Composite (Right) [42]

2.2.2 Braiding

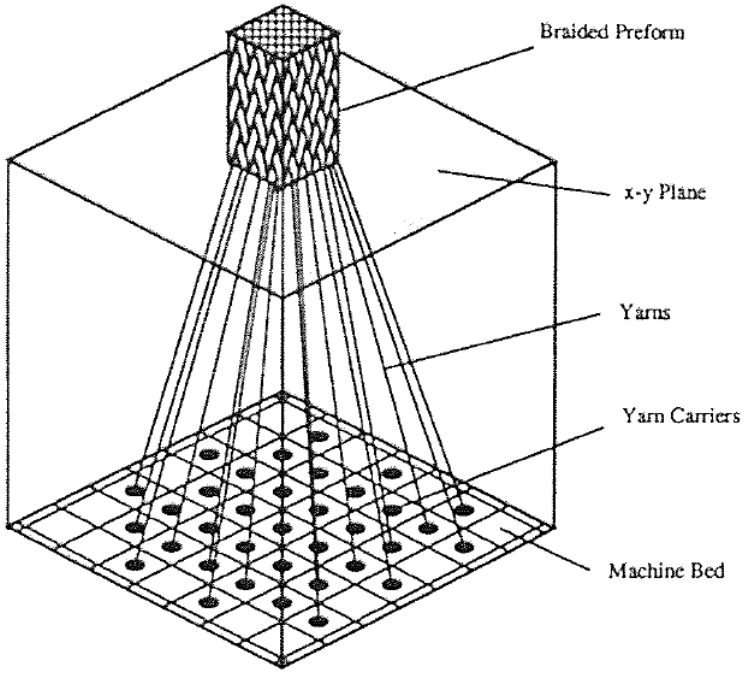

Figure 2-22 Schematics of 3-D Rectangular Braiding [45]

Braiding is defined as the intertwining of three or more yarns diagonally so that each yarn passes over and under other yarns alternatively. Figure 2-22 shows an illustration of 3-D rectangular braiding [45]. Yarn carriers take the yarns and travel in x and y directions alternately on the machine bed by following a specific pattern. After several cycles of a certain step (e.g., 4-step) movement, yarns interwine with each other and the specimen is created, as demonstrated in the top portion of the figure.

Figure 2-23 shows two 3-D fabrics braided at Kansas State University Composites Lab. The left picture and the right picture are L shape and ⊔ shape, respectively.

Top view

Section view

(a) L shape

Top view

Section veiw

(b) ⊔ shape

Figure 2-23 3-D Braided Fabrics

Recently, Ko et al. [46]-[48] has developed the 3D-hexagonal braiding technology capable of manufacturing complex three-dimensional braided structures. The relative computer tool has also been developed. A selection of hexagonal braiding patterns is shown in Figure 2-24. These patterns range from straight line to triangle, diamond, and star shapes. Voids inside the patterns are hexagonal shapes. This novel technology is applicable in the biomedical industry.

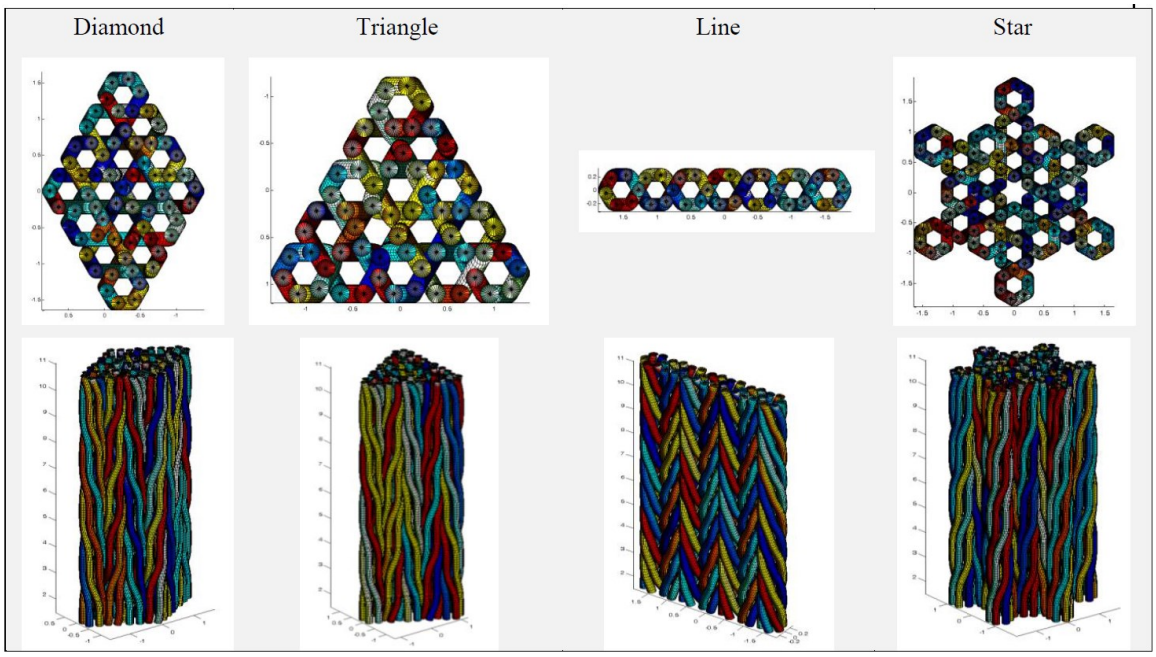

Figure 2-24 Hexagonal Braiding Patterns [46]

2.2.3 Knitting

Knitting is defined as the inter-looping of one yarn system into horizontal rows and vertical columns of loops. The corresponding loops are called courses and wales, respectively. Two primary types of knitting include weft knitting and warp knitting. In weft knitting, yarns (weft threads) meander along the course direction by adding stitches to each wale in sequence, as shown in Figure 2-25a. The entire fabric can be manufactured using one or multiple yarns. In warp knitting, yarns (warp threads) meander along the wale direction, by simultaneously adding stitches to each wale through the warp guides, as shown in Figure 2-25b. In this case, the entire fabric should be manufactured using a number of yarns.

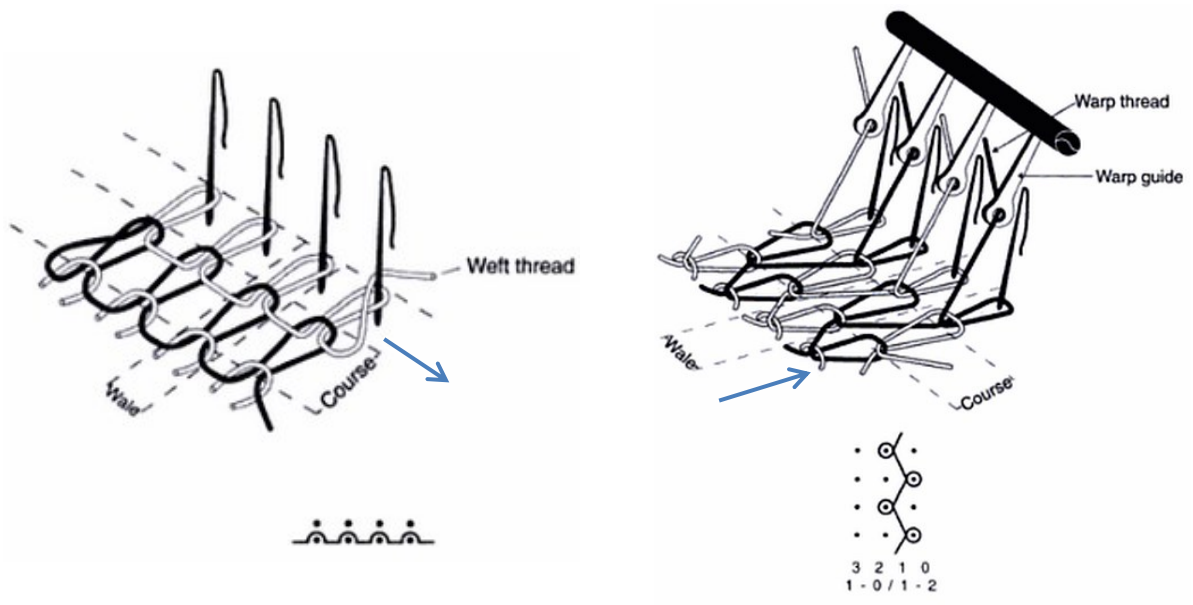

(a) Weft knitting (b) Warp knitting

Figure 2-25 Schematics of Knitting [49]

Figure 2-26 shows two fabrics produced by biaxial weft knitting [50]. The left picture is a nearly spherical shape, and the right picture is a spirally circular disk.

Near-net shape fabric manufacturing technology has potential for the composite industry. However, numerical simulations of near-net shape fabric are rarely seen, possibly because fabric patterns are too complex to numerically formulate by simply identifying and assembling unit cells. For near-net shape fabric without unit cell feature, a full field modeling is necessary. Details of modeling near-net shape fabric are discussed in Chapter 4.

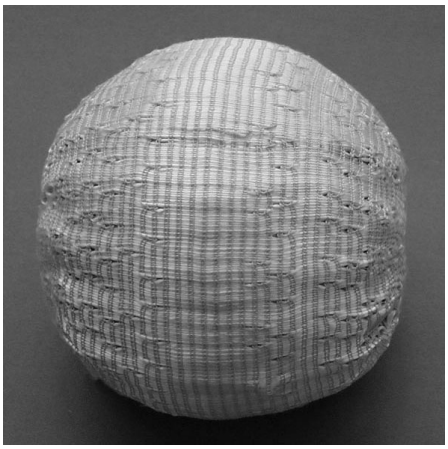

(a) Spherical shape

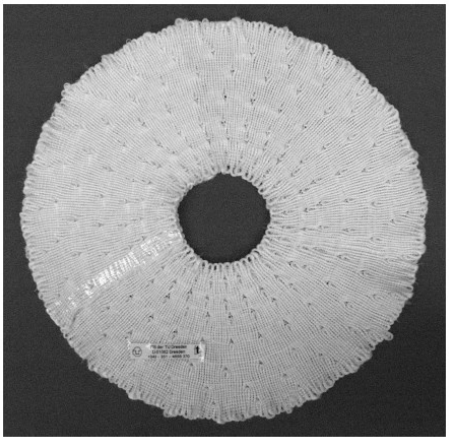

(b) Spirally circular disk

Figure 2-26 Biaxial Weft Knitted Fabrics [50]

2.3 Fabric Reinforced Composites and Fabric Deformation Process

After a fabric is created, it is processed into a targeted product, such as fabric reinforced composite. Fabric deforms accordingly. Figure 2-27 shows three typical fabric deformation processes: draping, stamping (or deep drawing), and molding. In the draping process, a typically soft fabric naturally falls onto a specific body (e.g., a sphere) due to gravity, as seen in Figure 2-27a. In the stamping process, a fabric, generally a fabric prepreg, is laid on the die and then pushed into the die by a punch, as seen in Figure 2-27b. Typically, the punch is an elastic body, such as silicon rubber. The holder reduces boundary irregularities during the stamping process. In the molding process, a fabric is placed on the bottom mold, and then the top mold moves downwards slowly, as illustrated in Figure 2-27c. The fabric conforms to the cavity shape created by both molds. Meanwhile, resin is injected from the top mold to consolidate the fabric into a composite part. Although details differ, common simulation issues exist among the processes, such as how to represent the fabric and the rigid or elastic body, and how to model the

contacts between fabric and body. Correct modeling of these behaviors leads to an accurate prediction of the fabric deformability and micro- and macro- geometry of fabric reinforced composite.

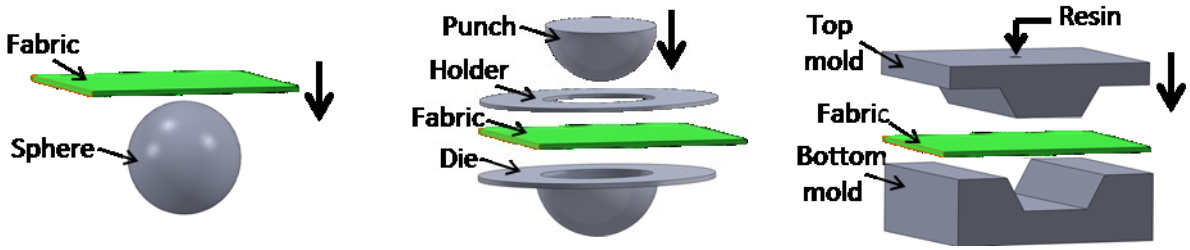

(a) Draping (b) Stamping (c) Molding

Figure 2-27 Common Fabric Deformation Processes

Research focusing on the simulation of the fabric deformation process can be categorized into two primary groups [51]: geometric and mechanical models. Both models are discussed in this section.

2.3.1 Geometric Model

The geometric model, also called the fishnet model, describes the fabric by straight segments connected with pin joints, as seen in Figure 2-28. The rigid body is discretized into three- or four-node elements. Nodes of fabric are geometrically mapped to nodes of the rigid body accordingly.

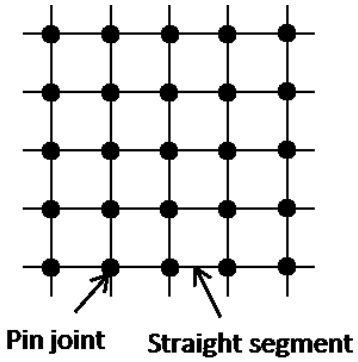

Figure 2-28 Fabric Geometric Model

Basic mapping steps can be summarized as follows [52][53]:

1) Discretize the fabric into pin-connected straight segments and discretize the body surface into three- or four-node elements;
2) Choose initial points on both fabric and body surface;
3) Choose two perpendicular constrained lines passing the initial point on the fabric and map them onto the body surface;
4) Map all other points on fabric to the body surface according to geometric relations with constrained lines.

A deformed fabric after the mapping process is illustrated in Figure 2-29.

Figure 2-29 Fabric Geometrically Mapped to a Sphere

The geometric model was introduced by Mack and Taylor [54] in the 1960s. In their model, woven cloth was assumed to be an assembly of inextensible yarns, and the yarn crossing was simulated as a pivoting joint where no slippage occurs. Yarn segment between the joints was a straight line. The square unit cell was deformed into a rhombus under the shear force, as seen in Figure 2-30.

This geometric model was later tested and adopted by Potter [55] in the late 1970s, and was also employed by Robertson et al. [56] in the 1980s.

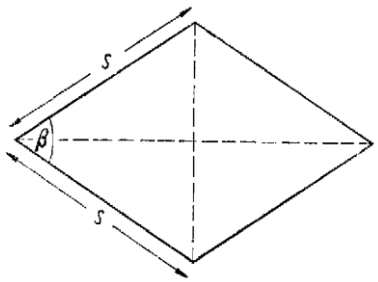

Figure 2-30 Rhombus Model of Deformed Unit Cell [54]

In the 1990s, VanWest et al. [52] used the geometric model to predict fabric wrinkling and bridging, as seen in Figure 2-31. Two perpendicular constrained yarns served as mapping references. Wrinkling was defined as an excess of fabric to cover the body surface. Bridging was defined as a situation in which fabric cannot deform sufficiently to the surface concavity. Both phenomena occurred when shear deformation was higher than the locking limit.

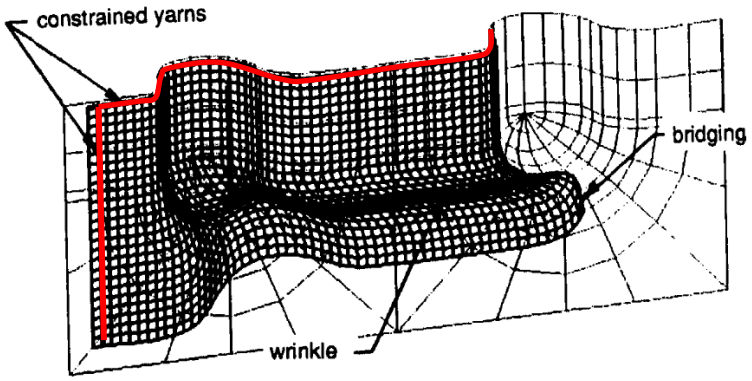

Figure 2-31 Draping Model with Bridging and Wrinkle [52]

The geometric model predicts fabric deformability in a fast and fairly efficient way and has been adopted by some commercial software codes, such as PAM-QuickForm [57] and FiberSIM [58]. However, this model is purely geometric and cannot reflect the mechanical behaviors during the forming process.

2.3.2 Mechanical Model

The mechanical model defines the fabric using finite elements and solves the fabric deformation process using implicit/explicit finite element methods. Based on fabric representation, mechanical model can be classified into three major models: continuous, bi-component, and discrete models, as seen in Figure 2-32. The continuous model considers the entire fabric as a homogenized material, usually expressed by finite shell or membrane elements. The bi-component model describes the fabric using two types of elements: shell/membrane and truss/beam. The discrete model considers the fabric to be heterogenized and models each yarn individually using finite spring, truss, shell, or solid element.

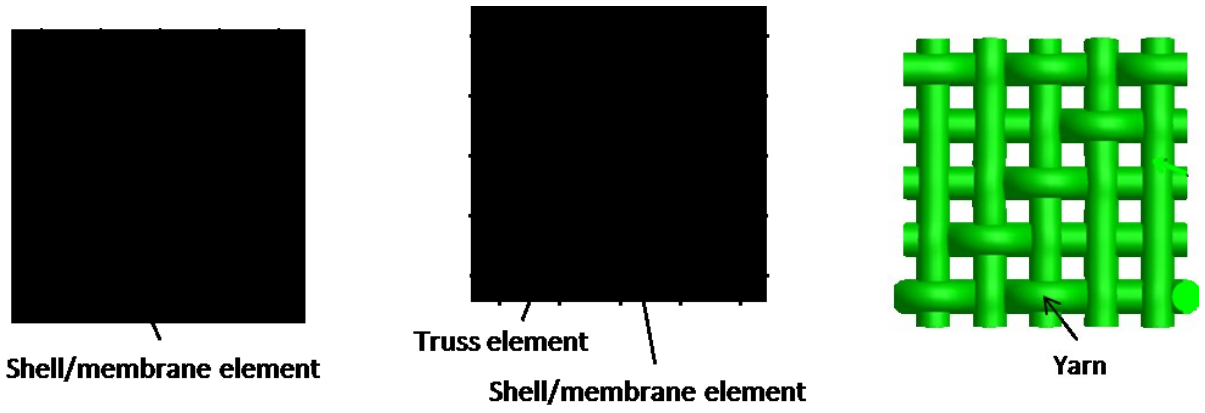

Figure 2-32 Fabric Mechanical Models: Continuous, Bi-component, and Discrete

2.3.2.1 Fabric in Continuous Model

The continuous approach describes the fabric as a continuum using finite shell or membrane elements.

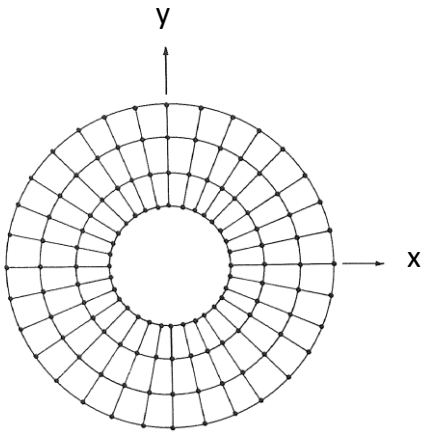

Figure 2-33 Finite-element Mesh of an Annulus Fabric [59]

In the early 1990s, Collier et al. [59] used the four-node shell element with orthotropic properties to model fabric in the draping process. Figure 2-33 shows an annulus shape fabric in the x-y plane. All nodes on the inner ring are fixed and all other nodes are free to move. External force was provided by gravity of the fabric. Effects of tensile modulus, shear modulus and

Poisson's ratio were investigated. A non-linear finite element method, coupled with orthotropic properties, was employed to predict fabric draping behavior.

In the mid-1990s, Eischen et al. [60] developed a computer tool to simulate different modes of fabric deformation. Fabric was modeled by the finite shell element by addressing both linear and nonlinear elastic isotropic material properties. Contact between fabric and rigid surface was modeled by the spring element. As demonstrated in Figure 2-34, numerical simulations of various fabric deformation behaviors were conducted: draping over a block, hanging over a rod diagonally, and folding diagonally.

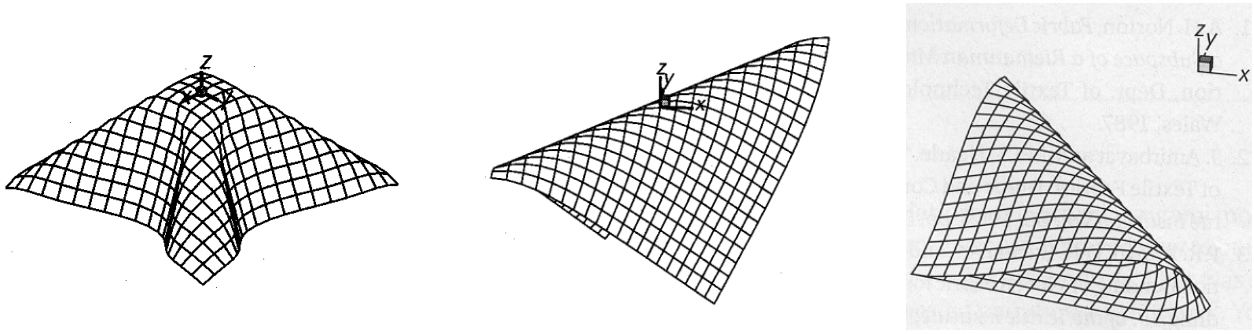

(a) Draping over a block (b) Hanging over a rod diagonally (c) Folding diagonally

Figure 2-34 Simulation of Different Fabric Deformation Behaviors [60]

In 2000, Lekakou et al. [61] modeled fabric using a four-node shell element with linear elastic anisotropic properties in the stamping process. The numerical model shown in Figure 2-35 includes a rigid punch, a holder, a fabric, and a die. The punch, holder, and die were modeled using 3-D rigid surface elements. A parameter study was conducted to evaluate effects of friction confident, punch speed, mesh size, time step, tensile and shear moduli, and holding force. Updated material behavior law with consideration of fiber direction evolution was also studied [62].

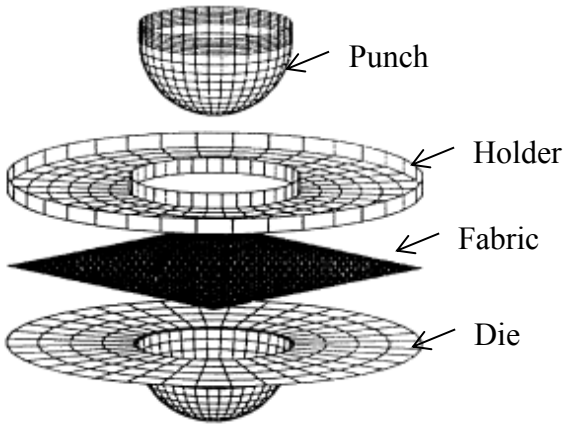

Figure 2-35 Finite Element Model for Stamping Simulation [61]

2.3.2.2 Fabric in Bi-component Model

In a bi-component model, two types of finite elements are typically adopted: shell/membrane and truss/beam elements.

In 2001, Cherouat et al. [63] developed a bi-component model to simulate the deformation of fabric prepreg. The membrane element represents the resin with assigned isotropic viscoelastic property and the truss element represents the yarns with assigned isotropic elastic nonlinear property. Weft and warp yarns were coupled kinematically with resin and hence no sliding occurred at the connecting points, as shown in Figure 2-36. Three types of fabric deformations were simulated: layering-up shaping, draping, and deep drawing shaping processes. Forming parameters examined included initial shape of fabric, fiber orientation, and resin viscosity. An adaptive remeshing technique with local refinement and coarsening was also employed in order to incorporate large deformation of fibers [64].

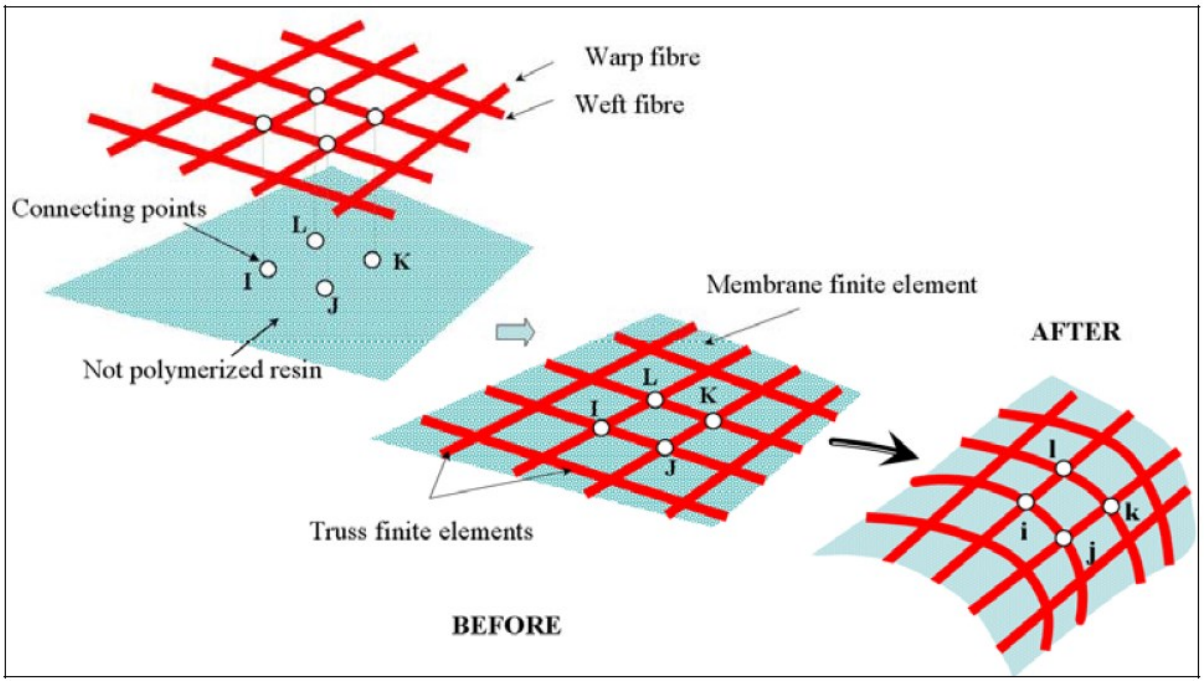

Figure 2-36 Schematics of Fabric Prepreg [64]

In 2001, Averill et al. [65] developed a bi-component model that incorporated inter-yarn sliding and inter-yarn jamming. The truss element modeled yarns, and the shell element represented a fictional transition medium. The checkboard model of a $\pm 45^0$ plain weave fabric was studied. As seen in Figure 2-37a, the unit cell was comprised of four four-node shell elements and four two-node truss elements. "I" and "II" denote two types of sub-regions of the checkboard. The four truss elements were independent of each other and did not share any nodes. Connectivity was formed only by the shell elements and hence yarn sliding was accounted. Two types of yarn-to-shell element connectivity were thus formed for the entire fabric, as seen in Figure 2-37b.

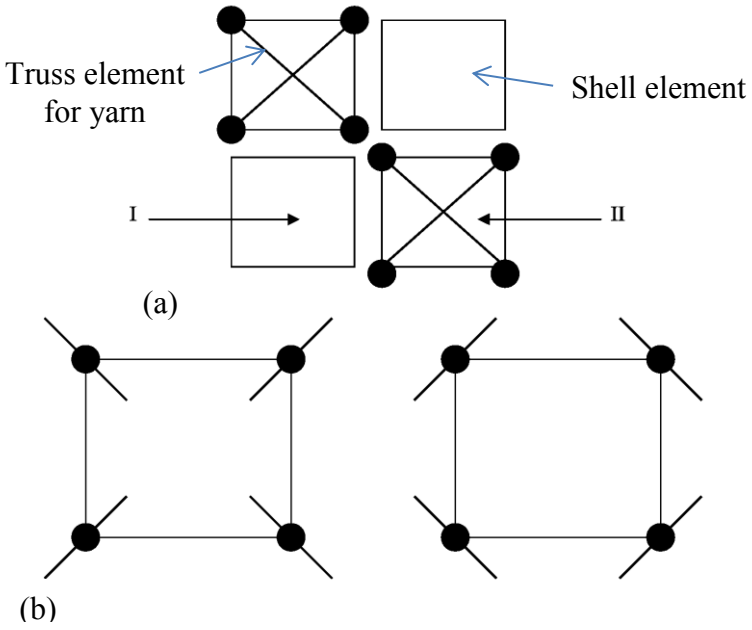

Figure 2-37 Checkboard Model: (a) Unit Cell; (b) Element Connectivities [65]

Other research works on fabric deformation using the bi-component model can be found in literatures [66]-[68].

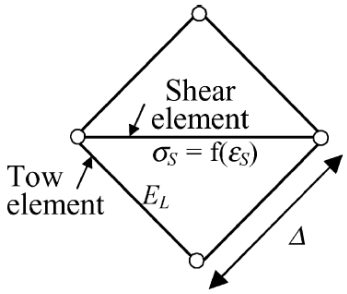

Figure 2-38 Unit Cell Bi-component Model [69]

Other research works using one kind of finite element but with two different properties assigned can be found in literatures [69]-[71]. One example is shown in Figure 2-38. In this unit cell, the four outer elements represented tows/yarns and the diagonal elements modeled shear effect. E_L denotes yarn longitudinal modulus, and σ_s defines shear stress which is a function of

shear strain ε_s. Both tow and shear elements were implemented with the truss element but with different assigned stiffness.

2.3.2.3 Fabric in Discrete Model

Primary disadvantages of continuous and bi-component models include their inability to model yarn-to-yarn interaction, which is significant in the fabric deformation process. In the discrete model, each individual yarn is identified and modeled by finite element representation. External forces are applied to each yarn and yarn-to-yarn interactions can be modeled.

Boisse et al. [51][75] developed a discrete model based on their previous semi-discrete model [72]-[74]. Figure 2-39a shows the unit cell model of an undeformed plain weave fabric. Each yarn was modeled by a set of finite shell elements, and tensile force can be directly applied to each yarn. Yarn-to-yarn contact and yarn-to-yarn sliding were also taken into account. In this case, in-plane shear behavior was naturally reflected. Figure 2-39b shows the simulation result of a quarter of the deformed fabric under the stamping process.

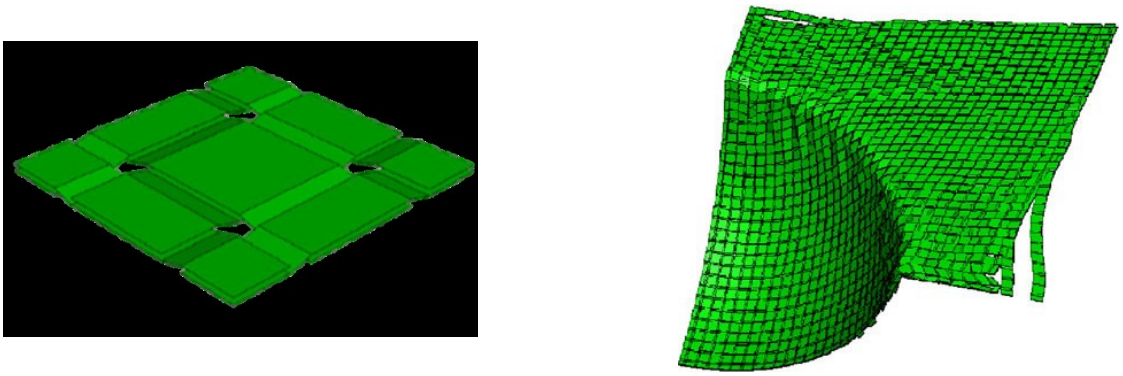

(a) Undeformed unit cell (b) A quarter of the deformed fabric

Figure 2-39 Discrete Model (Shell Element) for Stamping [51]

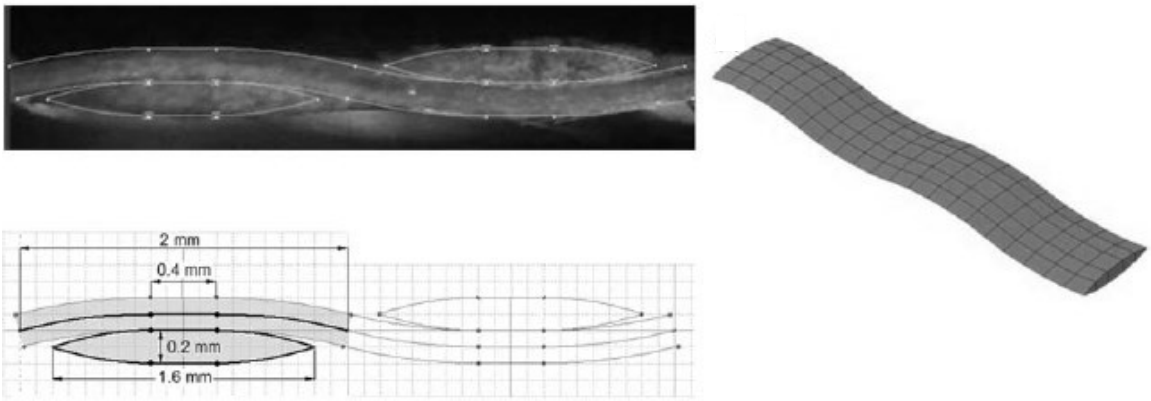

(a) unit cell and yarn models

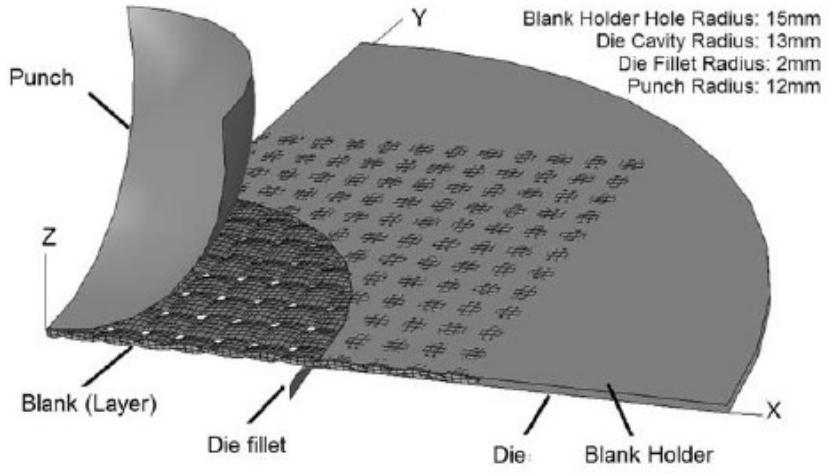

(b) Initial settings of stamping process

Figure 2-40 Finite Element Model for Stamping [76]

Most recently, Tavana et al. [76] described fabric and yarn models based on experimental investigations in order to simulate the damping process. Figure 2-40a shows microscopic images and numerical models of unit cell and yarn. Yarn was expressed by linear eight-node brick elements and linear six-node triangular prism elements with assigned transversely isotropic elastic properties. Figure 2-40b demonstrates the initial finite element model for the stamping

process. Only a quarter of the fabric was modeled. All forming tools, including the punch, die and blank holder, were described as rigid surfaces.

Wang et al. [1]-[10] developed a sub-yarn approach to model fabric micro-geometry, as introduced in Section 2.1.2.2.1. Figure 2-41 shows a plain weave fabric, in which a yarn is represented by 19 digital fibers. It is feasible to simulate the deformation process of fiber-level fabric with modern computer power. Details are explained in Chapter 5.

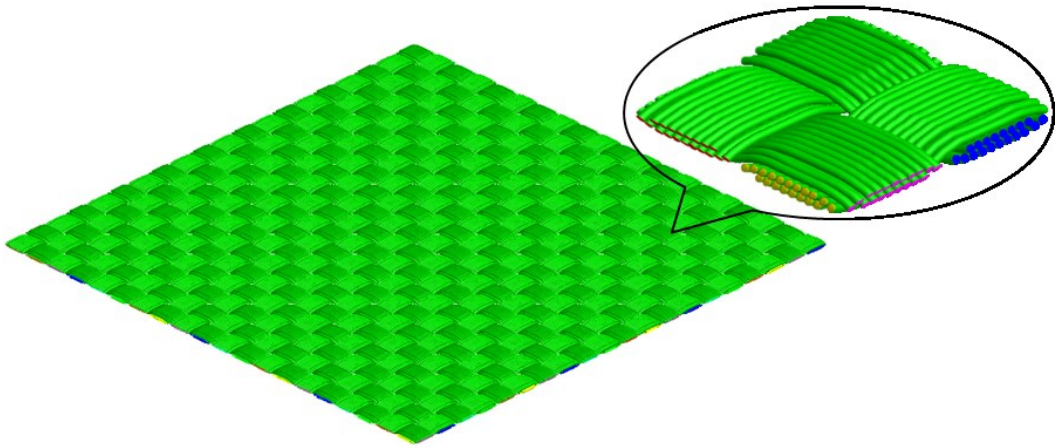

Figure 2-41 Fiber-level Fabric

2.4 Remarks

This chapter provides an overview of simulating micro- and macro-geometry of fabric and fabric reinforced composite, including fabric micro-geometry, near-net shape fabric manufacturing, and fabric deformation process.

In simulation of fabric micro-geometry, woven structures are highlighted. Fabric structure modeling methods are then stated by both yarn-level and fiber-level analyses. At the yarn-level analysis, yarn cross-section definition is highly dependent on empirical research or experimental

observation. A constant yarn cross-section assumption may create yarn-to-yarn interference and a variable yarn cross-section shape would be hardly retrieved from actual structures. At the fiber-level analysis, yarn shape is defined by fiber paths and fiber arrangements on the yarn cross-section. The fiber-level DEA has successfully demonstrated its capability for estimating fabric micro-geometry. It models a yarn as an assembly of digital fibers and each fiber as a frictionless pin-jointed digital chain. Related theories are further discussed in Chapter 3.

3-D near-net shape manufacturing has become an attractive technology in making complex composite parts. This technology saves labor costs for surfacing trimming and also guarantees mechanical properties of the composite product. However, numerical simulations of near-net shape manufacturing and relevant fabric micro-geometry rarely occur. The ability of DEA in simulating near-net shape fabric is discussed in Chapter 4.

Existing research in regard to estimating fabric reinforced composite and the corresponding fabric deformation process can be classified into two groups: geometric model and mechanical model. The geometric model describes fabric using the pin-jointed fishnet model and geometrically maps the fabric to an elastic/rigid body surface. This model is efficient but ignores mechanical behaviors. The mechanical model describes fabric using finite elements and mechanically simulates the fabric deformation process. The mechanical continuous model uses finite shell or membrane element to represent fabric. The mechanical bi-component model uses a combination of finite shell/membrane element and truss/beam element to model fabric. The mechanical discrete model incorporates the textile weaving pattern and describes each yarn or fiber individually. In the discrete model, yarn-to-yarn interactions and even fiber-to-fiber interactions can be gracefully reflected. Modeling fabric deformability at the fiber-level produces

the most accurate results. The DEA are adopted and the relative theories are detailed in Chapter 5.

Chapter 3 - 3-D Woven Fabric Unit Cell Micro-geometry

Fabric micro-geometry is determined by textile weaving mechanics. A dynamic DEA with periodic boundary conditions is developed to determine 3-D woven fabric unit cell micro-geometry.

Previously, two numerical procedures using DEA simulation were developed to determine textile fabric geometry. In one procedure, the textile process is simulated step-by-step as a quasi-static process, thus consuming a great amount of computer resources. In the other procedure, fabric micro-geometry is derived through a static relaxation process. In static simulation, the global stiffness matrix must be solved in each simulation step. Fibers and yarns are so flexible that the global stiffness matrix is either singular or ill-conditioned. Special treatment must be added to improve the matrix condition, thus slowing convergent rates. During simulation, new contact elements are created and some old contact elements are removed. Thus, connectivity must be re-established between nodes during the simulation. Building a periodic boundary zone into quasi-static simulation would be a tedious procedure. It would be, at best, difficult to use a desktop PC to generate a complex 3-D unit-cell with a fine mesh.

The dynamic relaxation process does not require the establishment of a global stiffness matrix, thus saving a vast amount of computer memory space and avoiding the problem of ill-conditioned stiffness matrix. Introduction of the periodic boundary condition reduces the necessary material domain to a single unit cell plus a surrounding boundary zone. This approach generates high quality fiber- and yarn-level micro-geometries.

This chapter contains four sections: 1) Unit cell and yarn topologies, 2) Dynamic relaxation with periodic boundary conditions, 3) Yarn-level micro-geometry, and 4) Numerical results validation. Corresponding research work has been published in references [1][6][9].

3.1 Unit Cell and Yarn Topologies

3.1.1 Unit Cell Topology

Fabric micro-geometry is determined by textile process kinematics and kinetics. Kinematics defines fabric topology, and kinetics produces fabric detailed micro-geometry. Fabric topology relates to an essential weaving pattern in a fabric. Detailed micro-geometry concerns yarn paths and yarn cross-section shapes, as well as fiber arrangements within yarns.

In a uniform fabric, the unit cell can be defined. A 3-D layer-to-layer fabric is shown in Figure 3-1a, including three repeated unit cells, each with two columns of wefts. Warps are located on two planes called warp sections. Two weaving diagrams, shown in Figure 3-1b, represent warp patterns on these two warp sections, respectively. The unit cell topology of this 3-D woven fabric is characterized by the weft pattern matrix, denoted by $\boldsymbol{W_e}$, and the warp pattern matrices, denoted by $\boldsymbol{W_a}$.

The dimension of $\boldsymbol{W_e}$ is determined by the total number of weft layers and the total number of weft columns. As shown in Figure 3-1a, weft yarns are arranged in 10 layers and 2 columns. As such, there are 10 rows and 2 columns in weft pattern matrix $\boldsymbol{W_e}$. Each numeral in $\boldsymbol{W_e}$ represents the yarn type ID of a weft yarn in the corresponding locations. If no weft yarn is present in a location, “0” is filled into the corresponding location of the matrix. In the presented example, all wefts are made of the same type of yarn with the type ID of “1”. Therefore, all components in the matrix are defined as “1”. The weft pattern matrix defines the weft yarn

location and the weft yarn type ID. Yarn properties are defined in each yarn type: yarn cross-section area, fiber longitudinal and transverse moduli, and fiber density.

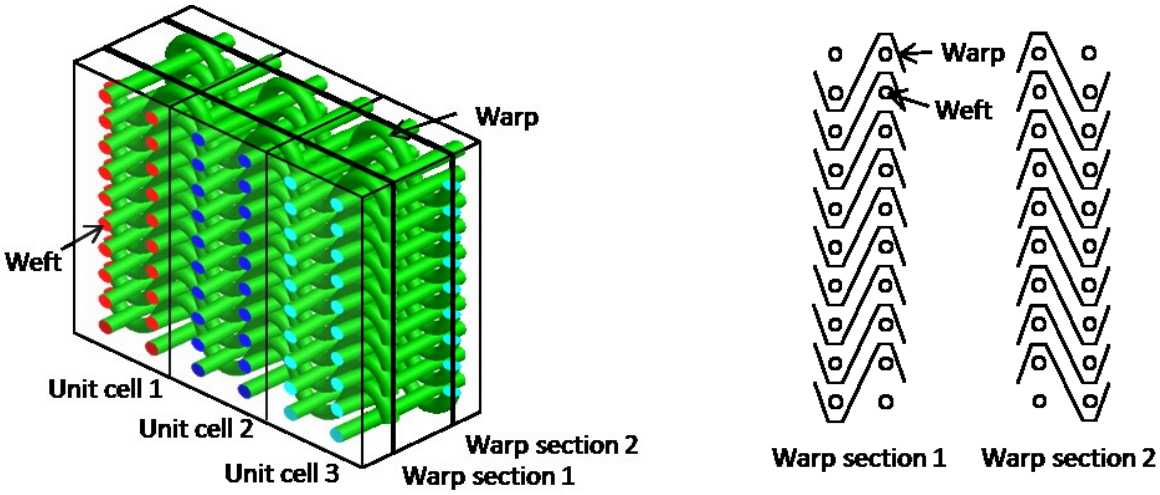

(a) 3-D layer-to-layer woven fabric (b) Weaving diagrams

Figure 3-1 Weaving Pattern of a 3-D Woven Fabric

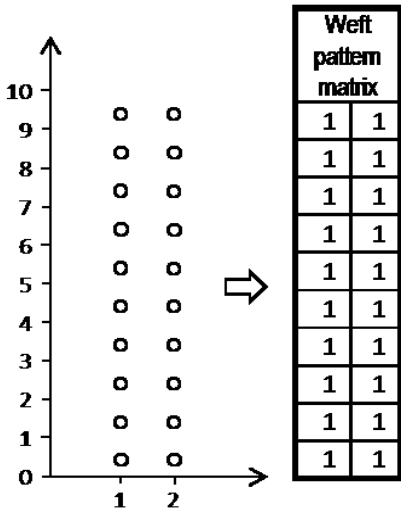

(a) Weft pattern matrix

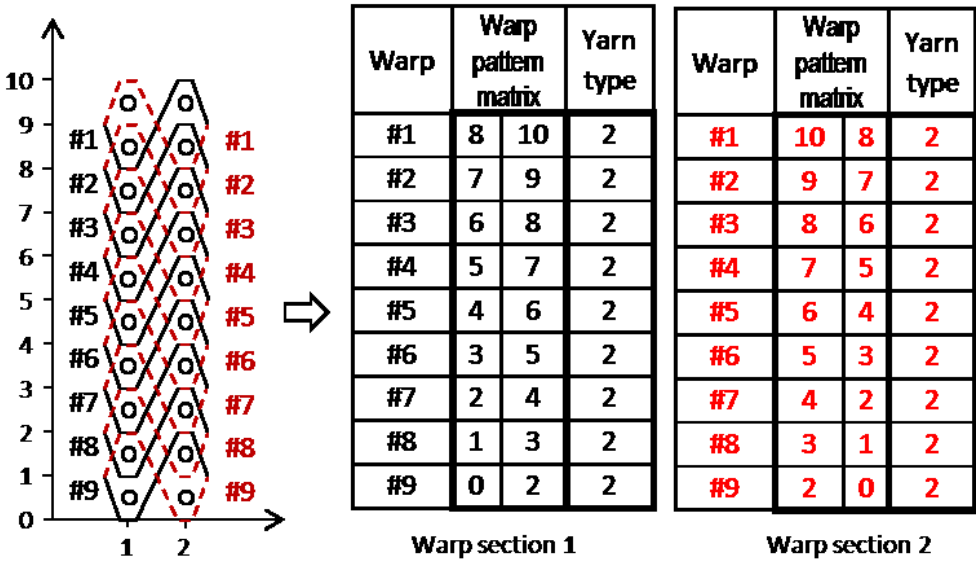

Warp	Warp pattern matrix		Yarn type
#1	8	10	2
#2	7	9	2
#3	6	8	2
#4	5	7	2
#5	4	6	2
#6	3	5	2
#7	2	4	2
#8	1	3	2
#9	0	2	2

Warp section 1

Warp	Warp pattern matrix		Yarn type
#1	10	8	2
#2	9	7	2
#3	8	6	2
#4	7	5	2
#5	6	4	2
#6	5	3	2
#7	4	2	2
#8	3	1	2
#9	2	0	2

Warp section 2

(b) Warp pattern matrices

Figure 3-2 Weft Pattern Matrix and Warp Pattern Matrices

Definition of the warp pattern matrix $\boldsymbol{W_a}$ is shown in Figure 3-2b. The picture on the left shows warp patterns. Warps in Section 1 are represented by solid black lines, and warps in Section 2 are represented by red dashed lines. In each section, each warp yarn is assigned a local warp ID. Warp ID numbers of Section 1 are in black and warp ID numbers of Section 2 are in red. The two tables on the right are the warp pattern matrices and yarn type ID vectors for Section 1 and Section 2, respectively. The dimension of the warp pattern matrix $\boldsymbol{W_a}$ is determined by the total number of warps in that section and the total number of weft columns in the unit cell. Nine warps are present for each warp-section and two weft columns are present in the unit cell. As such, both warp pattern matrices have nine rows and two columns. Each numeral in the matrix represents the interlacing location of the corresponding warp in the corresponding column. Because the warp pattern matrix does not include the yarn type ID

number, an additional yarn type ID vector is used to store the yarn type ID of each warp in the section.

Interlacing locations of warps are defined by integers. Refer to the picture on the left of Figure 3-2b. In warp Section 1, warp #1 is above the 8th weft layer and below the 9th weft layer in the first weft column. The corresponding interlacing location is thus defined by integer "8". In the second weft column, warp #1 is above the 10th weft layer, therefore the interlacing location is defined as "10". Interlacing locations of warp #1 are filled in the first row of warp pattern matrix $\boldsymbol{W_a}$. As such, $\boldsymbol{W_a}(1, 1) = 8$ and $\boldsymbol{W_a}(1, 2) = 10$, as shown in the first table of Figure 3-2. Similarly, interlacing locations of warps #2, #3,…, #9 are defined and filled in the 2nd, 3rd,…, 9th rows of $\boldsymbol{W_a}$. The warp pattern matrix for Section 1 is thus generated. Likewise the warp section matrix for Section 2 is defined. Key points of warp yarns can be derived based upon the warp pattern matrix.

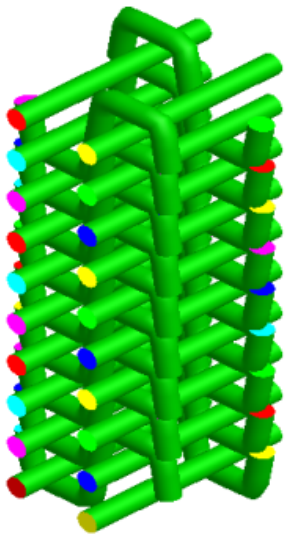

Figure 3-3 Unit Cell Topology Generated by DFMA

Unit cell topology can then be generated by DFMA based upon information provided by the weft pattern matrix and warp pattern matrices. The unit cell topology of this example fabric is shown in Figure 3-3.

3.1.2 Yarn/tow Structure and Digital Element Mesh

The digital element mesh is created through two processes: yarn discretization and fiber discretization. In yarn discretization, each yarn is split into multiple digital fibers. In fiber discretization, each digital fiber is divided into many rod elements.

Two types of yarn micro-structures include plain and twisted. A tow consists of either a single yarn or multiple yarns. A multi-yarn tow is typically formed through a twisting process. Yarn/tow structure is created through the digital element meshing process in which each tow is split into yarn(s) and each yarn is split into multiple digital fibers.

3.1.2.1 Yarn discretization

If a plain yarn is discretized into multiple digital fibers, all fibers within the yarn are parallel to each other and parallel to the original yarn centroid path. If a twisted yarn is discretized, all fibers rotate along the original yarn path with a defined twist rate.

One procedure used to determine fiber paths within a yarn is shown in Figure 3-4 and Figure 3-5.

In the first step of the procedure, the yarn path is divided into iso-length segments connected by nodes as shown in Figure 3-4. For simplicity, only four segments are shown in the picture. The yarn path is represented by an approximate broken line $\overline{C_1C_2C_3C_4}$. S_1, S_2, S_3, and S_4 are yarn cross-sections perpendicular to the yarn path. These cross-sections are assumed to be circular initially and will deform during the relaxation process. $\mathbf{t}_1$, $\mathbf{t}_2$, $\mathbf{t}_3$, and $\mathbf{t}_4$ are unit tangential vectors of the yarn path at nodes C_1, C_2, C_3, and C_4.

The second step of the procedure is to define coordinates on each cross-section. First, an arbitrary point, denoted as N_1, is located at the circumference of cross-section S_1. Then, a line is drawn parallel to $\overline{C_1C_2}$ from point N_1. The line intersects S_2 at a point denoted as N_2. $\overline{N_1N_2}$ is parallel to $\overline{C_1C_2}$. Similarly, $\overline{N_2N_3}$ and $\overline{N_3N_4}$ can be drawn, which are parallel to $\overline{C_2C_3}$ and $\overline{C_3C_4}$, respectively. Thus, a broken line $\overline{N_1N_2N_3N_4}$, which is parallel to $\overline{C_1C_2C_3C_4}$, is generated. The distance between $\overline{N_1N_2N_3N_4}$ to the yarn path $\overline{C_1C_2C_3C_4}$ is equal to yarn radius R. Let coordinate vectors be $\mathbf{u}_i$ and $\mathbf{v}_i$ on each cross-section. The first coordinate vector $\mathbf{u}_i$ is defined by a vector that starts from C_i and ends at N_i as shown in Figure 3-4. The second coordinate vector $\mathbf{v}_i$ should be perpendicular to both the first coordinate vector $\mathbf{u}_i$ and the yarn path tangential vector $\mathbf{t}_i$. $\mathbf{v}_i$ is defined by the cross product of $\mathbf{t}_i$ and $\mathbf{u}_i$, i.e., $\mathbf{v}_i = \mathbf{t}_i \times \mathbf{u}_i$.

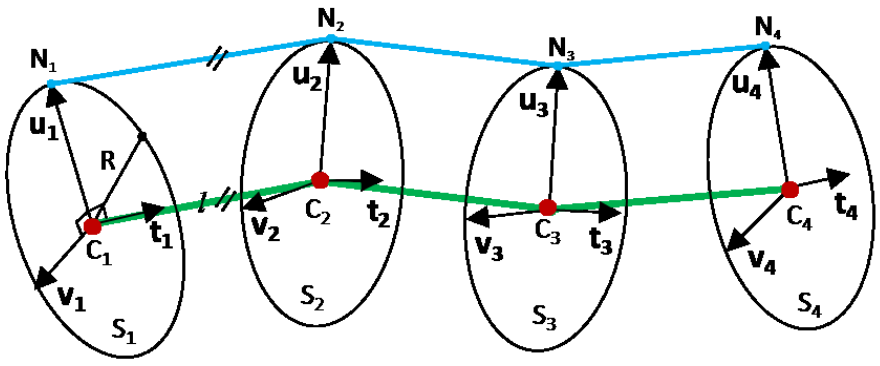

Figure 3-4 Determine Coordinate Directions on Yarn Cross-sections

The third step is to determine the fiber arrangement on each yarn cross-section.

If a tow consists of only a single plain yarn, fiber arrangements on all cross-sections of the yarn are identical in their respective coordinate systems. An example is presented in Figure 3-5a. For simplicity, only three cross-sections, S_1, S_2, and S_3, are shown and the yarn is discretized into only three fibers. Fiber cross-section areas are represented by red, green, and blue circles. As

demonstrated, the fiber arrangement on cross-sections S_1, S_2, and S_3 are identical in shape and orientation. The center of each circle is identified as the intersection point of the corresponding fiber axial path and the yarn cross-section. Intersection points of a fiber with cross-sections S_1, S_2, S_3 … are used as keypoints to generate the fiber path. As such, axial paths of all three fibers within the plain yarn are parallel to each other and parallel to the original yarn path $\overline{C_1C_2C_3\ldots\ldots}$.

If the tow consists of only a twist yarn, fiber arrangement rotates around the original yarn/tow path with a specified twist rate. An example is shown in Figure 3-5b. The fiber arrangement rotates $\Delta\theta$ around the cross-section center from cross-section S_1 to cross-section S_2, and rotates an additional $\Delta\theta$ from cross-section S_2 to cross-section S_3. $\Delta\theta$ is derived by the product of the twist rate and the yarn segment length, i.e., $\Delta\theta = T \times \Delta L$, where T denotes the twist rate and ΔL denotes the distance between two cross-sections.

If the tow consists of multiple yarns formed through a twist process, the tow is split into yarns first. Yarn arrangement within a tow can be ascertained with the same method employed to establish fiber arrangement within a twisted yarn, as described in the previous paragraph. Each yarn is then discretized into digital fibers.

Two principles are adopted during yarn/tow discretization: 1) the total cross-section area of fibers of a yarn/tow equals the original yarn cross-section area; and 2) all fibers are arranged inside the circumference of the original circular yarn/tow cross-section. As such, interference between fibers is inevitable immediately after discretization. These interferences are eliminated through numerical relaxation, discussed in the following section.

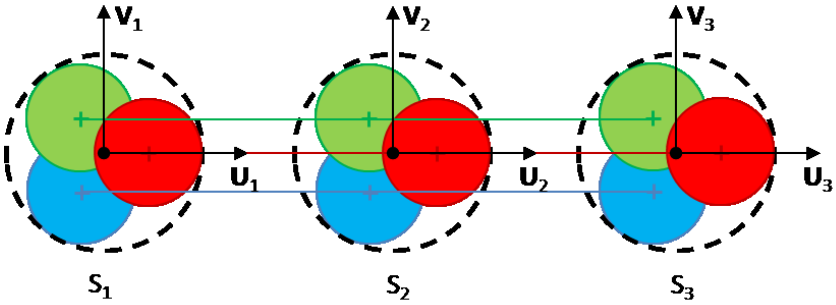

(a) Plain yarn

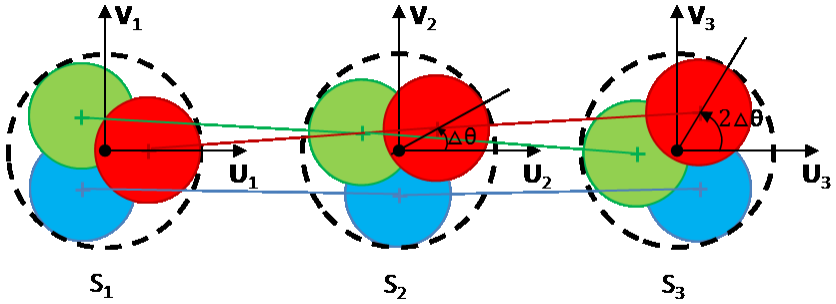

(b) Twisted yarn

Figure 3-5 Fiber Arrangement at Yarn Cross-sections

Figure 3-6 displays typical patterns of initial yarn discretization used in DEA. The yarn discretization process is replicable, which means one yarn can be split into a specific number of fibers which can be further split. Whatever the splitting process, the sum of cross-section areas of all fibers within one yarn equals the cross-section area of that yarn.

Figure 3-7 shows three different yarn structures: plain yarn, twisted yarn, and twisted tow composed of two plain yarns.

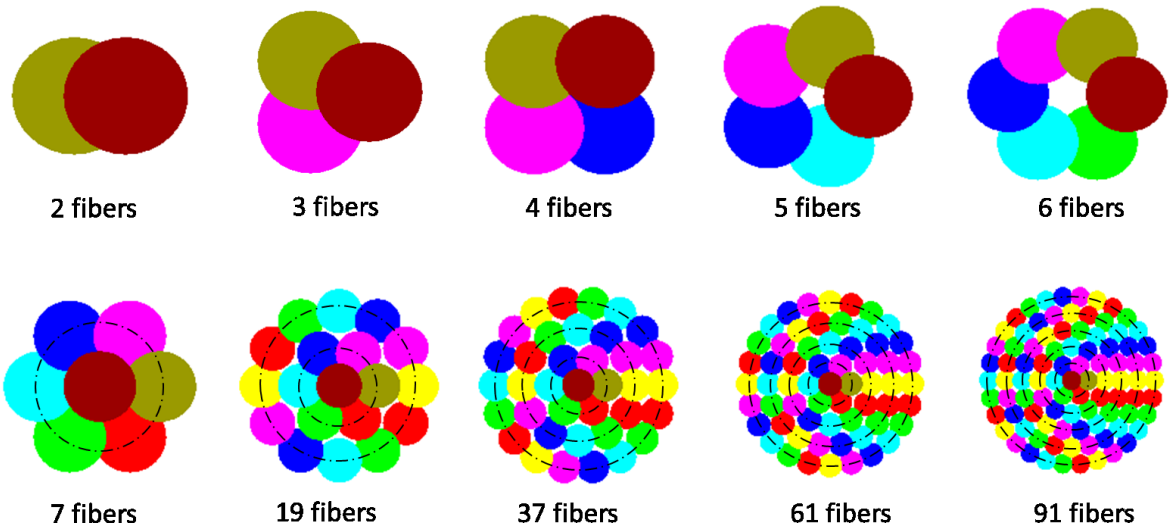

Figure 3-6 Different Yarn Discretization Patterns

(a) A plain yarn (b) A twisted yarn (c) A twisted tow

Figure 3-7 Different Yarn Structures

3.1.2.2 Fiber discretization

In order to avoid fiber-to-fiber interaction, each fiber must be discretized into a digital element chain after a yarn is discretized into multiple digital fibers. The element length is always shorter than the original fiber segments. As shown in Figure 3-8, the green dashed line is the fiber path prior to discretization, with the segment length of l_o'. The blue solid line is the fiber path subsequent to discretization, with the element length of l_o. The suggested element length ranges from 0.3 to 0.7 times the fiber diameter. The new fiber path is obtained by a linear interpolation along the original fiber path, so

$$l_o = l_1 + l_2 \tag{3.1}$$

where l_1 and l_2 are two segment lengths along the original fiber path. Element lengths along the new fiber path are slightly different from each other after element discretization, but they will be quickly unified in the simulation process. Element length adjustment is discussed in Section 3.2.5.

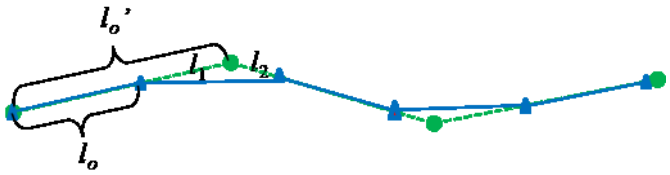

Figure 3-8 Element Discretization

Figure 3-9 displays a fiber shape before and after a new element discretization. In the left picture, the ratio of element length (l) to fiber diameter (D) is 1. In the right picture, the ratio is 0.5.

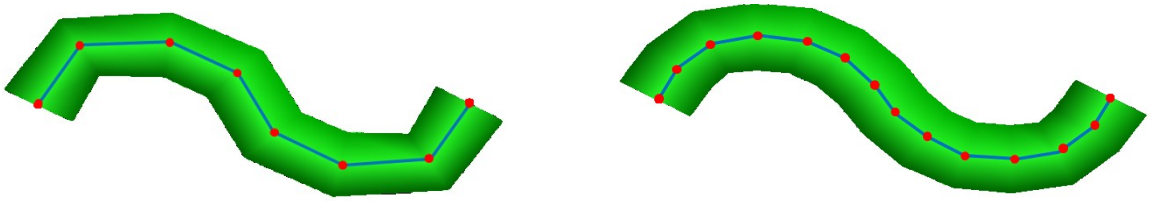

(a) A fiber with $l/D = 1$ (b) A fiber with $l/D = 0.5$

Figure 3-9 Fiber Before and After Element Discretization

3.2 Dynamic Relaxation with Periodic Boundary Conditions

As discussed in Section 2.1.2.2.1, the solver of the DEA has employed quasi-static and static procedures. Major obstacles of these procedures include computer resources and computation speed. In this section, the dynamic relaxation process with periodic boundary conditions is explained.

3.2.1 Nodal Force Calculation

Four types of force are applied to each node: tension induced force, fiber-to-fiber contact induced force, damping force, and bending induced force. The first two forces have been introduced in previous literatures [3]-[5] and are reprised in this section for an integral view of DEA. The damping force is added to the dynamic relaxation in order to remove fabric kinetic energy during the simulation process. Because yarn bending stiffness is much smaller than either axial stiffness or contact stiffness, the bending induced nodal force is much smaller than the tension induced nodal force or inter-fiber contact induced nodal force. For this reason, bending induced force does not affect the final results of numerical simulation. In most numerical simulations, the bending induced nodal force is neglected. However, the bending moment induced nodal force needs to be calculated if stiffer metal wires are embedded in the fabric.

3.2.1.1 Tension induced nodal force

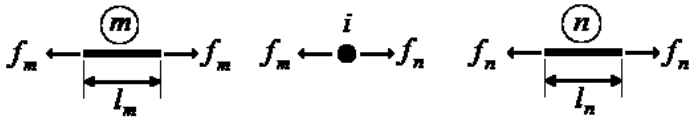

Figure 3-10 Tension Induced Nodal Force

Referring to Figure 3-10, node *i* is adjacent to two rod elements: element *m* and element *n*. The tensions of these two elements are

$$\overrightarrow{f_m} = E_L A \frac{\overrightarrow{l_m} - \overrightarrow{l_o}}{l_o}$$
$$\overrightarrow{f_n} = E_L A \frac{\overrightarrow{l_n} - \overrightarrow{l_o}}{l_o} \tag{3.2}$$

where E_L is the digital fiber longitudinal modulus, A is the fiber cross-section area, l_m and l_n are lengths of element *m* and element *n* at the simulation step. The tension induced force applied to node *i* is

$$\vec{F_i} = -\overrightarrow{f_m} + \overrightarrow{f_n} \tag{3.3}$$

3.2.1.2 Fiber contact induced nodal force

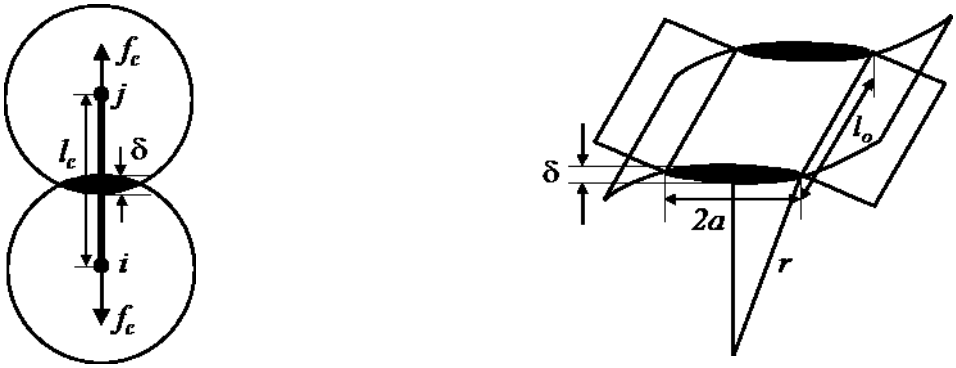

(a) Contact force (b) Contact area

Figure 3-11 Fiber Contact Induced Nodal Force

Contact force calculation is described in Figure 3-11. Hertz contact theory [77] is adopted and an elastic contact is assumed. Contact force at each time step is defined as

$$d\vec{f_c} = k_c d\vec{\delta} \tag{3.4}$$

where δ is the penetration displacement and k_c is the contact stiffness, which is defined as

$$k_c = \frac{E_T A_c}{l_c} = \frac{2E_T a l_o}{l_c} \tag{3.5}$$

where E_T is the digital fiber transverse modulus, and A_c is the contact area and is defined in Figure 3-11b, in which $2a$ and l_o denote width and length of the contact area, respectively.

Contact width $2a$ is calculated from

$$a = \sqrt{r^2 - (r - \delta/2)^2} = \sqrt{r\delta - \delta^2/4} \cong \sqrt{r\delta} \tag{3.6}$$

where r denotes fiber radius. This equation is derived with the consideration that δ is much smaller than r.

Using Equation (3.6), Equation (3.5) is then rewritten as

$$k_c = \frac{2E_T\sqrt{r\delta}\, l_o}{l_c} \tag{3.7}$$

Integrating both sides of Equation (3.4) with Equation (3.7) substituted, the contact force is then expressed by

$$\vec{f_c} = \int_0^{\delta} k_c \, d\vec{\delta} = \int_0^{\delta} \frac{2E_T\sqrt{r\delta}\, l_o}{l_c} d\vec{\delta} = \frac{4E_T\sqrt{r} l_o}{3l_c} \vec{\delta}^{3/2} \tag{3.8}$$

The nominal contact force is then described as

$$\frac{\vec{f_c}}{D} = \frac{4E_T\sqrt{D/2}\, l_o}{3l_c D} \delta^{3/2} = \frac{2\sqrt{2}E_T l_o D}{3l_c} \left(\frac{\vec{\delta}}{D}\right)^{3/2} \tag{3.9}$$

3.2.1.3 Damping induced nodal forces

The damping force applied to each node can be expressed as

$$\overrightarrow{f_i'} = -c\overrightarrow{v_i} \tag{3.10}$$

where c is the damping coefficient and v_i is the nodal velocity. The critical damping coefficient of the rod element [78] is

$$c_{cr} = 2\sqrt{k_L m} = 2\sqrt{\frac{E_L A m}{l_o}} \tag{3.11}$$

where m is the nodal mass. A non-dimensional damping ratio ς is used as the input parameter. It is defined as

$$\zeta = \frac{c}{c_{cr}} \tag{3.12}$$

The recommended damping ratio range is $0.2 \leq \varsigma \leq 1$.

The initial fabric geometry could be quite different from the minimum potential energy state fabric geometry. A damping ratio near 1 is required to remove kinetic energy quickly and prevent nodal vibrations at the start of the relaxation process. The damping ratio should subsequently be reduced gradually as the stability condition improves. The stability condition is controlled by nodal forces, nodal velocities, and total potential energy, all of which should approach minimums during the simulation. The damping ratio is automatically adjusted in the DFMA code throughout the relaxation process. The adjustment procedure is as follows

1) Calculate L^2-norm of nodal velocities as

$$\|v_i\|_2 = \sqrt{{v_{ix}}^2 + {v_{iy}}^2 + {v_{iz}}^2} \tag{3.13}$$

2) Find the maximum L^2-norm of nodal velocities, denoted by$(\|v\|_2)_{max}$.

3) If $(\|v\|_2)_{max}$ is larger than base velocity which is defined as 0.2-0.5, decrease the damping by 10%; otherwise, increase the damping by 10%.

3.2.1.4 Bending induced force

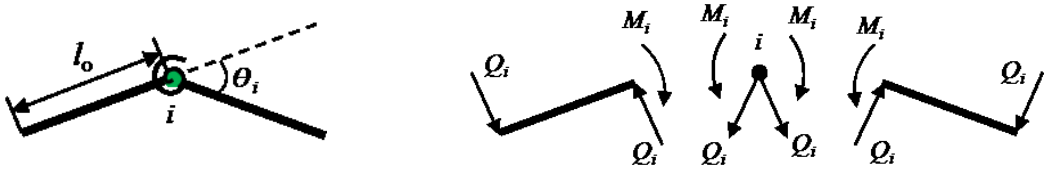

Figure 3-12 Transverse Nodal Force and Nodal Moment Relations

Refer to Figure 3-12. In order to incorporate the bending moment in the numerical simulation, node *i* is modeled as a torsional spring instead of a frictionless pin. Curvature of the fiber at node *i* can be calculated as

$$\kappa_i = \frac{\theta_i}{l_o} \tag{3.14}$$

Assume that M_i is the moment applied to the two adjacent elements. The relation of the moment M_i and angle θ_i is determined by the bending rigidity of the digital fiber. The bending rigidity of a yarn is related to the moment of inertia of the digital fiber, which can be calculated as

$$I = \frac{\pi r^4}{4}\frac{N_d}{N_a} \tag{3.15}$$

where r is the radius of digital fiber, N_d is the number of digital fibers per yarn, and N_a is the number of actual fibers per yarn. Typically, N_a is much larger than N_d. An actual yarn often consists of tens of thousands fibers. In numerical simulation, a yarn is typically split into less than 100 digital fibers.

The M_i-θ_i relation can then be derived as

$$M_i = E_L I \kappa_i = \frac{E_L I \theta_i}{l_o} \tag{3.16}$$

Nodal forces at node *i* can be derived as

$$Q_i = \frac{M_i}{l_o} = \frac{E_L I \theta_i}{{l_o}^2} \tag{3.17}$$

3.2.2 Explicit Algorithm

A central-difference explicit numerical algorithm [79] is utilized to calculate nodal accelerations, nodal velocities, and nodal displacements in the numerical simulation. It is described as

$$\begin{aligned} (a_i)_n &= \frac{(F_i)_n}{m_i} \\ (v_i)_{n+1/2} &= (v_i)_{n-1/2} + (a_i)_n \Delta t \\ (u_i)_{n+1} &= (u_i)_n + (v_i)_{n+1/2} \Delta t \end{aligned} \tag{3.18}$$

where *i* denotes the nodal number, *n* the step number, and Δt the time step. F_i, m_i, a_i, v_i, u_i denote the nodal force, the nodal mass, the nodal acceleration, the nodal velocity, and the nodal displacement, respectively. In the explicit simulation, the time step Δt must be smaller than the critical time step Δt_{cr}.

Frequencies of contact elements are always lower than those of digital elements. As such, the critical time step for the digital element is used to calculate the critical time step for the numerical process, which can be expressed as

$$\Delta t_{cr} = \frac{l_o}{s} = \frac{l_o}{\sqrt{E_L/\rho}} \tag{3.19}$$

where *s* is the propagation speed along a digital element, and ρ is the fiber density.

The magnitude of critical time step Δt_{cr} is related to the fiber axial modulus E_L. The greater the fiber axial modulus E_L, the smaller the critical time step Δt_{cr}, and the smaller the Δt_{cr}, the slower the numerical simulation. In general, the fiber axial modulus has an insignificant effect on the equilibrated fabric unit cell micro-geometry. Therefore, it is recommended that a modulus, which is much smaller than the actual fiber modulus, is used in the relaxation process. Fiber modulus used in simulation ranges 1% - 1‰ of that of actual fiber.

3.2.3 Periodic Boundary Conditions

A periodic boundary condition is employed in the DEA dynamic relaxation. The fabric unit cell is a non-continuum domain. During numerical relaxation, interior nodes within the unit cell may move to the boundary and boundary nodes may move to the interior. Furthermore, the boundary of the unit cell may change shape, as shown in Figure 3-13a. The two pictures on the left side represent the initial micro-geometry of an orthogonal woven fabric unit cell and the two pictures on the right side represent the micro-geometry after relaxation. The top two pictures are isometric views and the bottom two pictures are side views. Dashed rectangles in the side views represent the initial unit cell boundary. Side views show that subsequent to relaxation some fibers move outside the left boundary. These views also show empty spaces inside the right side of the boundary, which should be filled by fibers from neighboring cells. In order to calculate nodal force in the vicinity of the boundary, nodal locations from the neighboring unit cells must be known. As such, an external boundary zone must be added based upon the periodic principle, as shown in Figure 3-13b. The top picture is the side view of the unit cell only and the bottom picture is the side view of the unit cell with the periodic boundary zone. Two internal boundary regions are defined in the top picture, L, on the left and, R, on the right. Two external boundary regions are added to the unit cell in the bottom picture, L' and R'. These are images of regions L

and R, respectively. Region L' fits into region R and region R' fits into region L. Region L' belongs to the neighboring unit cell on the right side and region R' belongs to the neighboring unit cell on the left side.

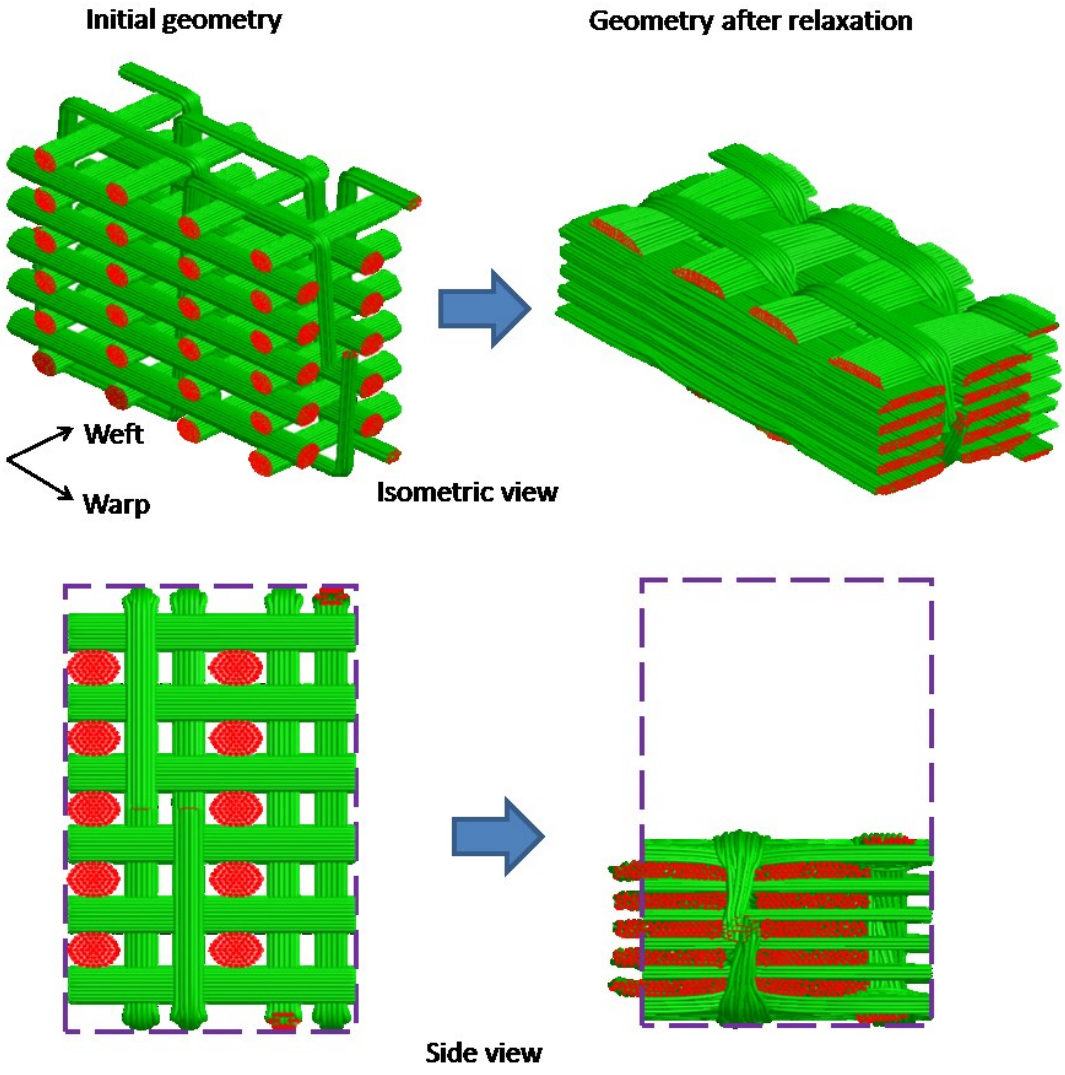

(a) Geometry change under dynamic relaxation

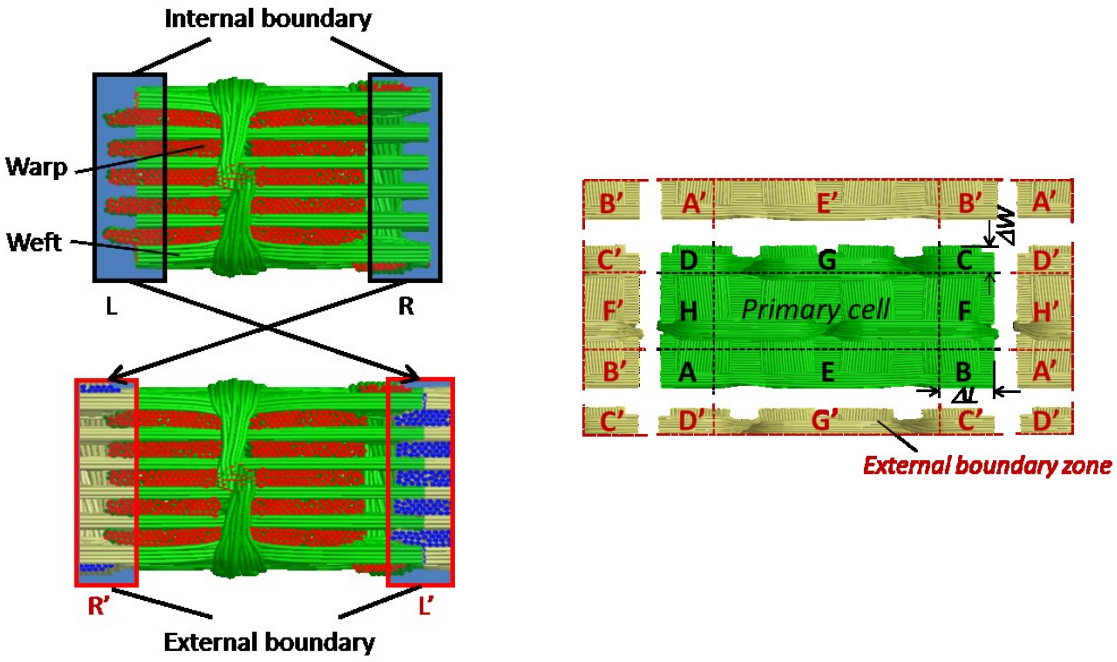

(b) Side view (c) Top view

Figure 3-13 Periodic Boundary Condition

The top view of the mapping process is shown in Figure 3-13c. The green region is the unit cell and the brown region is the added periodic boundary. The boundary of the unit cell is divided into eight blocks: A, B, C, D, E, F, G, and H. During the relaxation process, the renewed nodal locations inside the unit cell are calculated. Then a mapping process is adopted to determine the renewed nodal locations in the surrounding periodic boundary zone, i.e., the nodal positions in the brown area. The surrounding boundary zone is divided into 16 blocks: 3 A' blocks, 3 B' blocks, 3 C' blocks, 3 D' blocks, and E', F', G', and H' blocks. Fiber micro-geometry in blocks A', B', C', D', E', F', G', and H' is identical to blocks A, B, C, D, E, F, G and H, respectively.

The mapping process is conducted on the x-y plane by following

$$x' = x + L$$
$$y' = y + W \tag{3.20}$$

where x' and y' denote nodal coordinates in external boundary zone, x and y denote nodal coordinates in internal boundary zone, and L and W denote unit cell length and width, respectively. The mapping length and mapping width, denoted by ΔW and ΔL in Figure 3-13c, respectively, are defined as approximately the distance between weft columns and the distance between warp sections, respectively.

3.2.4 Contact Search

In DEA simulation, 80-90% of computing time is used to search contacts between nodes. In order to reduce computing time, it is critical to establish an efficient algorithm for contact search.

The search includes two processes. In the first process, the material domain is divided into many cubes as shown in Figure 3-14a. The size of these cubes, denoted as "*a*" in the picture, ranges from 1.2 to 1.5 times the fiber diameter. As such, it is only possible for each node to contact nodes in the same cube and nodes in the adjacent 26 cubes as shown in Figure 3-14b. If the distance between two nodes is smaller than the cubic size "*a*", they are considered as a contact pair, expressed as (n_1, n_2). "n_1" is called "contacting-node" and "n_2" is called "contacted-node". Each contact would be searched twice, as (n_1, n_2) and (n_2, n_1), if the search for contacted-nodes were conducted in all 27 cubes. To avoid double counting, a forward search algorithm is applied. For contacting node *i* in cube *A*, the paired "contacted-nodes" must be either inside the 13 cubes marked "×" or inside cube *A* as shown in Figure 3-14b. Therefore, the search is first conducted in the 13 cubes marked "×". Then, the search continues inside cube *A* for which a forward search algorithm is also designed. Assume that both node *i* and node *j* belong to cube *A*

and $j > i$. The contact pair (i, j) is accepted and the contact pair (j, i) is rejected. In addition, the contacting node and the contacted-node must belong to two different fibers.

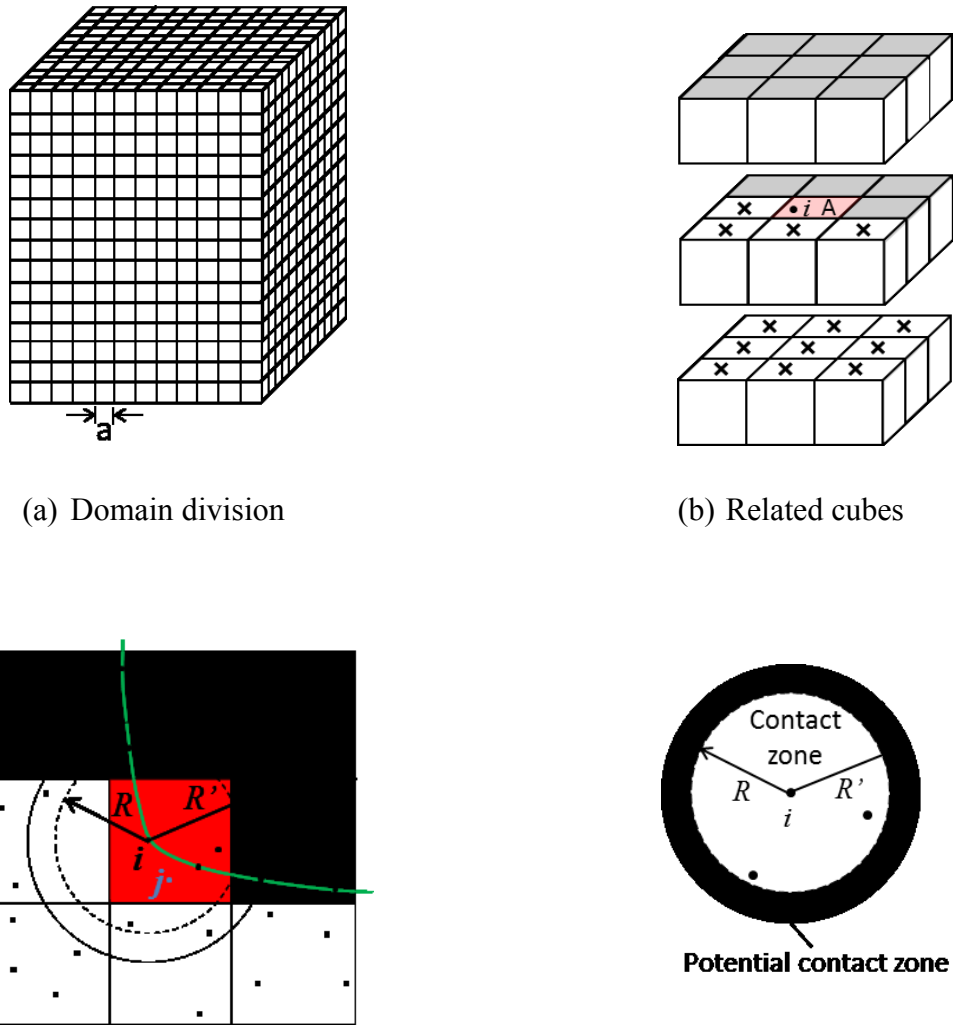

(a) Domain division

(b) Related cubes

(c) Contact pair search

(d) Contact zone

Figure 3-14 Contact Search

The contact search is a time consuming process. In order to further improve code efficiency, the search for contacts is typically conducted every 50-100 simulation steps. Nodes in a contact pair are not necessarily in contact at the step that the search is conducted, but they might be in

contact in the next 50-100 simulation steps. Refer to Figure 3-14c. The green curve represents a fiber. For node *i,* all paired contacted-nodes are located inside the solid circle with node *i* as the center. The radius of the solid circle *R'* is equal to the cubic size *a*, i.e., *R'* = *a*. A dashed circle is located inside the solid circle and the radius of the dashed circle *R* is equal to the digital fiber diameter. Nodes inside the dashed circle are in contact with node *i* at the step that the search is conducted. Therefore, the area surrounded by the dashed circle is defined as the contact zone of node *i*. Nodes between the dashed circle and the solid circle are not in contact by node *i* at the step the search is conducted, but would be in contact in the ensuing simulation steps. As such, the area between the dashed circle and the solid circle is defined as the potential contact zone. Each node has a contact zone and a potential contact zone. In general, 2 to 10 contacted-nodes are located inside the contact or potential contact zones for a specific node, as shown in Figure 3-14d.

The second process of the search is conducted in every simulation step. This process checks the distance from every node to any other node located within its contact and potential contact zones. If the distance is smaller than the fiber diameter, contact occurs. The contact force is calculated as described in Section 3.2.1.2.

3.2.5 Element Length Adjustment

An initial tension is applied on each yarn to deform the fabric. Yarn tensions gradually decrease or even vanish during the relaxation. Simulation becomes less efficient or even stop. Therefore, a proper yarn tension must be maintained. During the simulation, the assumed original element length within a yarn must be adjusted to maintain the assumed yarn tension, which is thus named "targeted yarn tension" in DEA simulation. The adjustment procedure can be divided into the following sub-steps:

1) Determine the average stress of each yarn. The average yarn stress is calculated as

$$\bar{\sigma} = \frac{\sum_{i=1}^{N} E_L (\frac{\Delta l_o}{l_o})_i}{N_e} \tag{3.21}$$

where N_e is the total number of elements within the yarn.

2) Yarn tension can then be calculated as

$$F_y = A_y \bar{\sigma} \tag{3.22}$$

where A_y is the yarn cross-section area.

3) If yarn tension F_y differs from the targeted yarn tension F_t , the original element length will be modified. The adjusted element strain is

$$\Delta\varepsilon = \frac{F_y - F_t}{A_y E_L} \tag{3.23}$$

The original element length should be modified as

$$l_o' = l_o(1 + \Delta\varepsilon) \tag{3.24}$$

The adjusted original element length will be used in the ensuing simulation step. By adjusting the original element length, the yarn tension approximates the target tension in the entire relaxation process.

3.2.6 Numerical Procedure

The numerical procedure of the dynamic relaxation is shown in Figure 3-15. Input data includes yarn properties, unit cell dimension, weft pattern matrix, and warp pattern matrices. The unit cell topology is determined based upon the input data. Digital element mesh is then generated by two processes: yarn discretization and fiber discretization. The following step is to define targeted yarn tensions, size of the periodic boundary zone, and simulation parameters, such as time step, damping coefficient, and so on. Numerical simulation then starts. Each simulation step includes four actions: 1) search contacts between fibers; 2) calculate nodal forces;

3) calculate nodal accelerations, velocities, and displacements within the unit cell; and 4) renew nodal displacements inside the external boundary zone through a mapping process based upon a periodic principle. Numerical simulation continues until nodal forces vanish, i.e., potential energy approaches a minimum state.

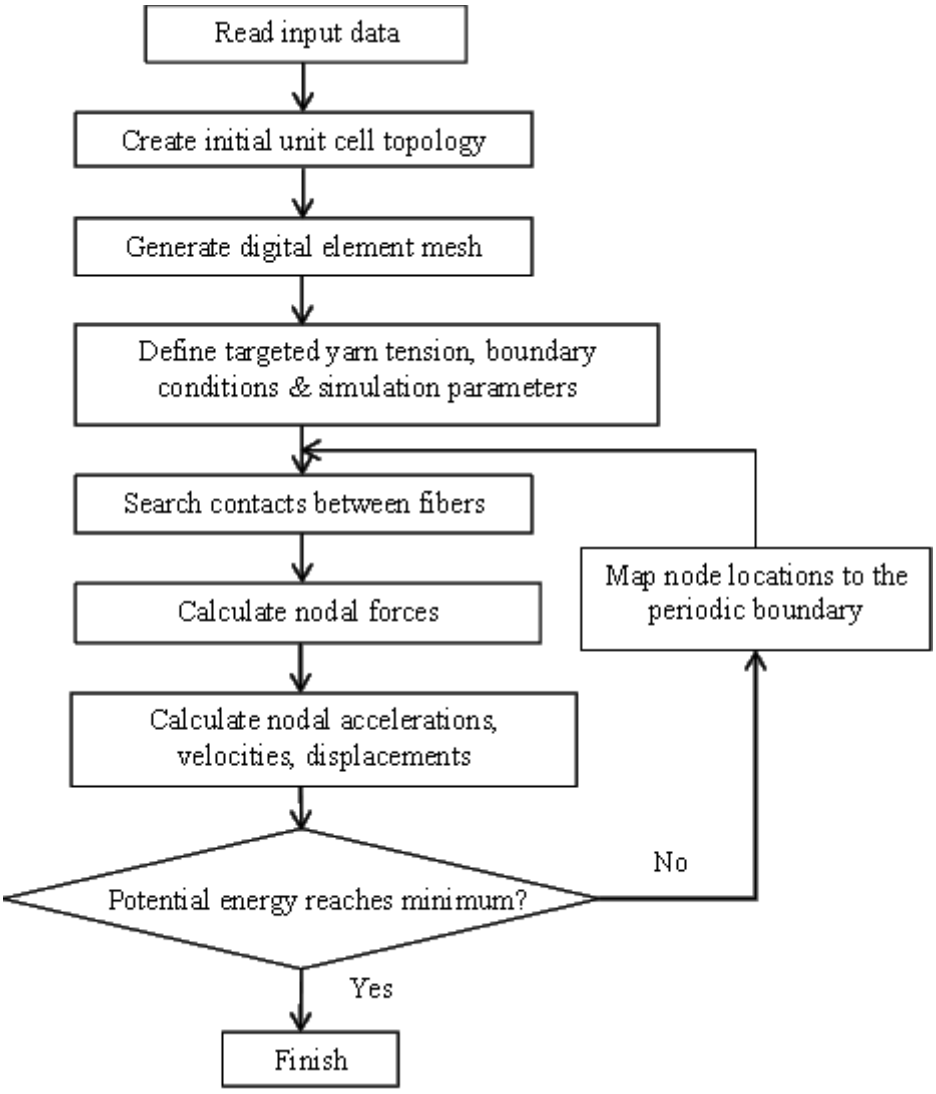

Figure 3-15 Flowchart of the Numerical Procedure

3.2.7 Multi-level Dynamic Relaxation

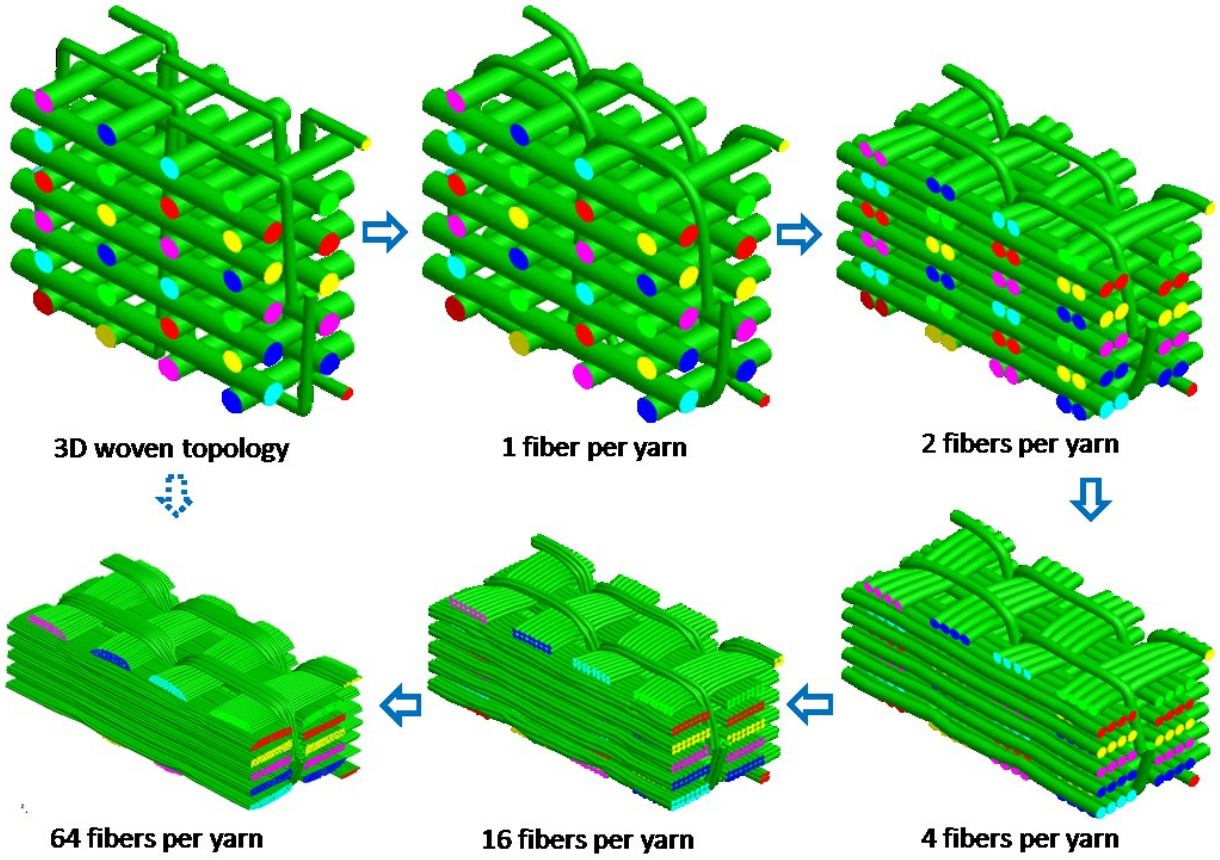

Figure 3-16 Multi-step Simulation

Accuracy of the unit cell micro-geometry is related to the digital element mesh used in the numerical simulation. The finer the mesh, the more accurate the result. A multi-step, multi-level digital element mesh relaxation process is used. An example of multi-step, multi-level simulation is shown in Figure 3-16. The first picture is the unit cell topology. The first step of relaxation is performed with each yarn consisting of one digital fiber. The simulation result is shown in the second picture. Subsequently, each yarn is split into two finer fibers. The second step of relaxation is then conducted and the result is shown in the third picture. The process continues

and each yarn is split into more and more digital fibers with the total fiber area unchanged. The derived micro-geometry becomes increasingly accurate. In the final step of discretization, each yarn consists of 64 digital fibers. A high quality micro-geometry is obtained. Significant computing time is saved by using multi-level relaxation compared to single-level relaxation with a fine element mesh.

3.3 Yarn-level Micro-geometry

DEA simulations generate digital fiber-level micro-geometries, which can be used for fabric mechanics analysis. However, most textile composite FEM analyses are based upon yarn-level micro-geometry. For this reason, it is necessary to transfer fiber-level geometry into yarn-level geometry.

The first step to derive a yarn-level micro-geometry is to determine the yarn axis and the yarn cross-section planes with coordinate vectors. The yarn axis is determined by the geometric center of all fiber axes of the yarn. Yarn cross-section planes are then defined and these planes are perpendicular to the yarn axis. Using an approach similar to one described in Section 3.1.2.1, the coordinate system of each cross-section can be defined. The next step is to generate a yarn cross-section profile with a smooth perimeter.

One example of fiber distribution on a yarn cross-section is shown in Figure 3-17. Small blue circles represent fibers. The yarn cross-section profile perimeter is determined through two sub-steps. During the first sub-step, a “roughness roller” rolls counterclockwise on the yarn cross-section, as shown in Figure 3-17a. The locus of the center of the roughness roller is the closed green curve. During the second sub-step, the roughness roller rolls on the inner side of the green curve, as shown in Figure 3-17b. The locus of the center of the roughness roller center is the red

curve, which is defined as the yarn cross-section profile perimeter. In general, the radius of the roller should be 5 to 20 times larger than the fiber radius. The size of the roller affects the smoothness of the generated profile perimeter. As such, it is named as "roughness roller". The larger the roughness roller, the smoother the yarn cross-section profile perimeter.

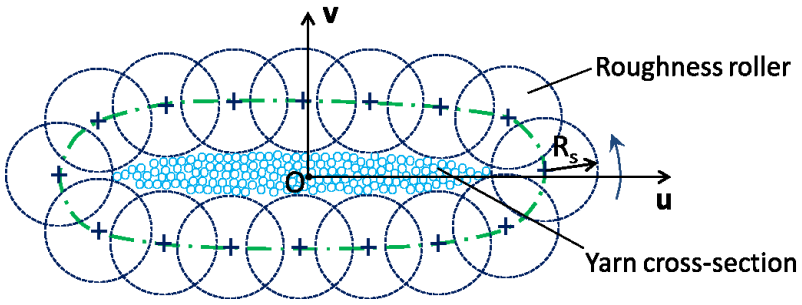

(a) Sub-step 1

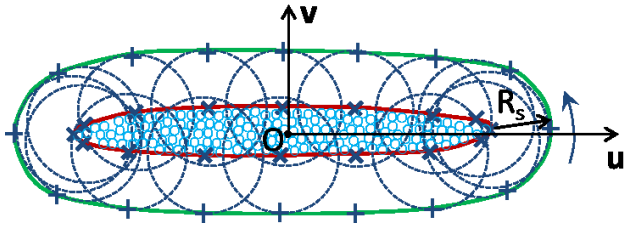

(b) Sub-step 2

Figure 3-17 Generate Yarn Cross-section Profile Perimeter

The yarn's cross-section profile is the outer envelope of its fibers. In order to create yarn surface, corresponding points on the perimeters of two neighboring yarn cross-sections are connected. Refer to Figure 3-18. $\mathbf{u}_i$-$\mathbf{v}_i$ and $\mathbf{u}_{i+1}$-$\mathbf{v}_{i+1}$ denote two neighboring yarn cross-section planes. O_i and O_{i+1} are centers of the two neighboring cross-sections, respectively. $P_{i,j}$ and $P_{i,j+1}$ are two adjacent points on plane $\mathbf{u}_i$-$\mathbf{v}_i$, and $P_{i+1,j+1}$ and $P_{i+1,j}$ are two adjacent points on plane $\mathbf{u}_{i+1}$-$\mathbf{v}_{i+1}$. By connecting these points, a four-node element, $P_{i,j}$-$P_{i,j+1}$-$P_{i+1,j+1}$-$P_{i+1,j}$ or two three-

node elements, $P_{i,j}$-$P_{i,j+1}$- $P_{i+1,j}$ and $P_{i,j+1}$-$P_{i+1,j+1}$-$P_{i+1,j}$ can be created. In most cases, two neighboring yarn cross-sections are not parallel to each other, so nodes of a four-node element are not on the same plane, which will cause problems in creation of the solid yarn model. Hence, three-node elements of yarn surface are recommended. In addition, because the fiber area fraction within a yarn cross-section could vary along the yarn's path, the yarn cross-section area may vary slightly.

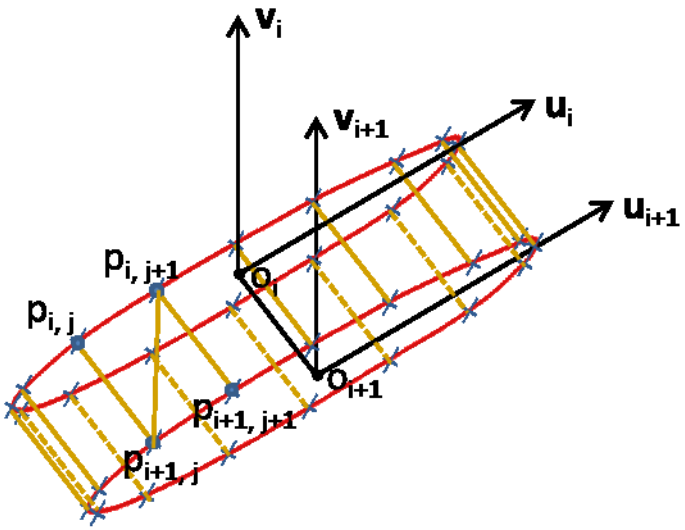

Figure 3-18 Yarn Surface Description

In the fiber-level micro-geometry generated by DEA simulation, no interference occurs between fibers. Elements of yarn surface are numerically created based on fiber arrangements within that yarn only. Intersection could occur between these elements from two interlacing yarns. In order to eliminate interferences between these yarns, the fiber-to-fiber contact element length is increased by a factor, defined as the gap factor, if the two fibers in contact belong to different yarns. As a consequence, a gap is produced between two neighboring yarns in the fiber-

level micro-geometry as shown in Figure 3-19a. The suggested gap factor ranges from 0.2 to 0.5. As such, interferences between yarns are eliminated, as shown in Figure 3-19b.

(a) Fiber-level view (b) Yarn-level view

Figure 3-19 Gap Between Two Contacting Yarns

Figure 3-20 shows a yarn-level micro-geometry of a 3-D orthogonal woven fabric unit cell. The yarn-level geometry created by DFMA can be read by commercial FEM codes, such as ANSYS, SolidWorks and MSC Marc [23].

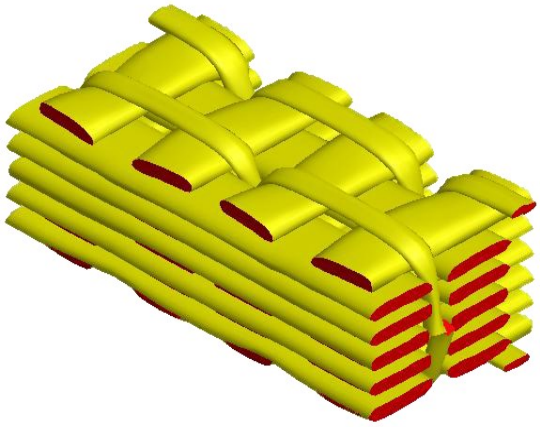

Figure 3-20 Yarn-level Geometry of Fabric Unit Cell

3.4 Numerical Results Validation

Numerical results are compared with experimental results in regard to: fabric thickness, fiber volume fraction, and fabric micro-geometry.

Thickness is measured using digital clipers or gauges on dry fabrics. Several locations are normally chosen and an average fabric thickness is reached.

Fiber volume fraction is defined as

$$v_f = \frac{V_F}{V_C} = \frac{W_F/\rho}{LWH} \tag{3.25}$$

where V_F defines the total volume of fibers and V_C the volume of composite. Total volume of fibers is defined by the division of the total weight of fibers W_F to fiber density ρ. The shape of a composite unit cell is assumed as a cuboid and the volume is defined by the multiplications of length L, width W, and height H of the unit cell.

In oder to investigate the fabric micro-structure, the surface of the dry fabric or the composite is first observed using a microscope. Then, the composite specimen is sliced and interior micro-structures are observed.

3.4.1 Two Samples of Fabrics

Two samples are selected for numerical and experimental results comparisons: 3-D woven angle interlock fabric and 3-D woven orthogonal fabric with twisted yarns. Both samples are provided by Materials Research & Design, Inc. (MR&D) [22].

The first sample is woven from Nicalon CG yarns. The corresponding yarn denier number is 1800 g/9000m. The fiber density is 2550 kg/m^3. The second sample is woven from S-glass yarns. Wefts and warp stuffers are made of 250 S-glass yarns and warp weavers are made of 1250 S-glass yarns. The yarn denier numbers of both glass yarns are 17874 g/9000m and 3575 g/9000m, respectively. The fiber density is 2460 kg/m^3. However, it was found that the actual yarn denier number was greater than that defined in the datasheet. The reason for this discrepancy probably relates to the sizing process. The yarn's denier number affects the calculation of the yarn's cross-section area, which, in turn, affects fabric thickness in numerical simulation. Therefore, the first

step of the experimental research was to measure the actual denier number using an analytical balance. The measured yarn denier numbers for Nicalon CG yarn, 250 S-glass yarn, and 1250 S-glass yarn are 1988, 18926, and 3697 g/9000m respectively. The measured denier numbers are used to calculate the yarn cross-section area in numerical simulation.

Figure 3-21a shows the weaving pattern of a 3-D angle-interlocking fabric. The solid ellipses and broken lines represent wefts and weavers, respectively. The unit cell has 68 weft yarns (17 columns and 4 layers) and 9 weaver yarns. Fabric micro-geometry after simulation is displayed in Figure 3-21b, where each weft yarn and warp yarn respectively consists of 24 and 12 digital fibers. The black dashed lines on the fabric surface mark the unit cell domain.

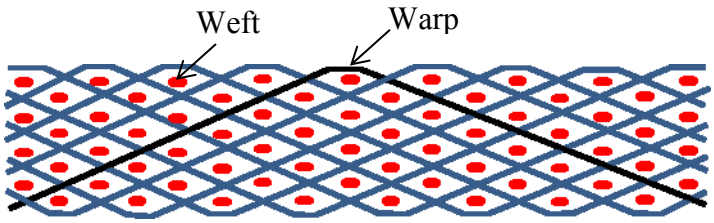

(a) Weaving pattern

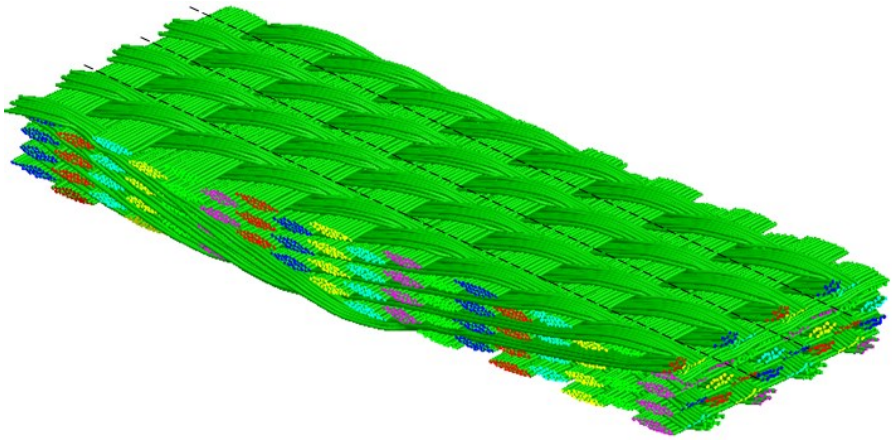

(b) Detailed geometry

Figure 3-21 Sample 1: 3-D Woven Angle Interlock Fabric

Figure 3-22a depicts the weaving pattern of a 3-D woven orthogonal fabric. Solid ellipses, straight lines, and broken lines describe the wefts, warp stuffers, and warp weavers, respectively. The picture on the left depicts the weaving pattern at warp sections 1 and 2, and the picture on the right depicts the weaving pattern at warp sections 3 and 4. Warp stuffers and warp stuffers are in different sections. Warp stuffers are in sections 2 and 4, and warp weavers are in warp sections 1 and 3. Each unit cell contains 14 wefts (2 columns and 7 layers), 12 warp stuffers, and 6 warp weavers. In DEA simulation, a twist yarn is represented by 19 digital fibers. Corresponding fabric micro-geometry is shown in Figure 3-22b. Black dashed lines on the fabric surface mark the unit cell domain.

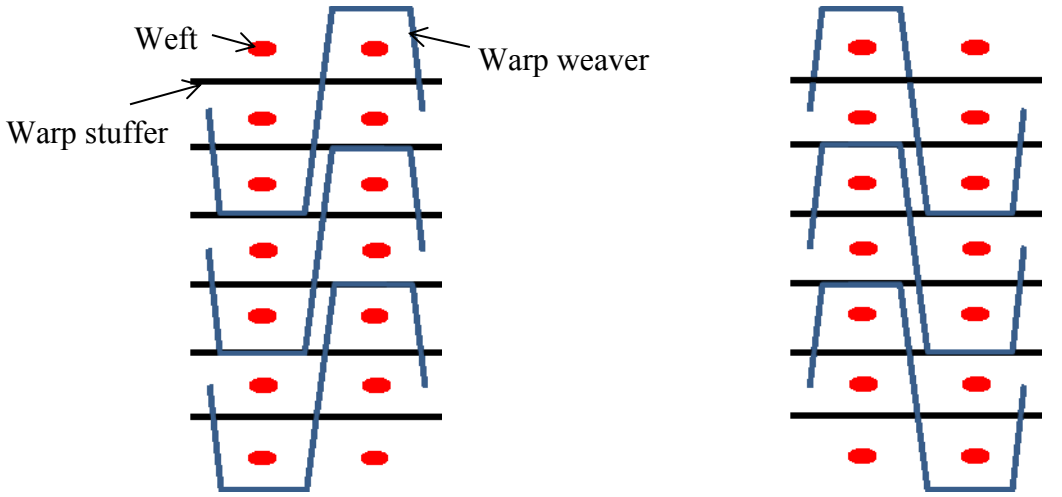

Warp sections 1 and 2 Warp sections 3 and 4

(a) Weaving pattern

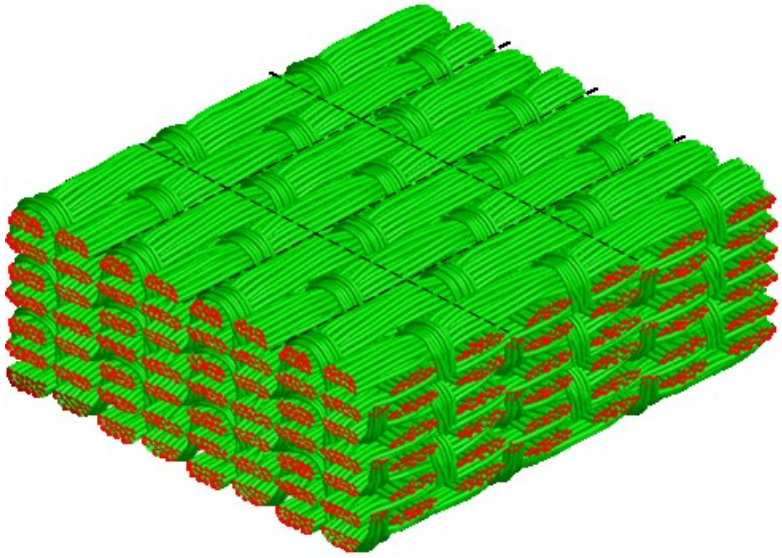

(b) Detailed geometry

Figure 3-22 Sample 2: 3-D Woven Orthognal Fabric with Twisted Yarns

3.4.2 Comparison with Experimental Results

Microscopic pictures of the first sample are provided by MR&D and the experiments of the second sample are conducted at Kansas State University Composites Lab.

Comparisons of fabric thicknesses are listed in Table 3-1. For the first sample, thickness obtained from the numerical simulation is nearly 10% smaller than thickness from the experimental measurement. This is because the actual fabric micro-geometry is affected by many effects, such as the weaving speed, beat-up speed, and yarn tension. Hence, the micro-geometry of the actual fabric may not be the one that reaches the minimum potential energy state. For the second sample, fabric thickness derived from numerical simulation is only slightly (1.71%) thinner than that of the actual fabric. This is because twist rate plays a more important role than weaving kinetics to determine fabric thickness. Thus, the cross-section deformation of twisted yarn is more restrictive than that of plain yarn.

Table 3-1 Comparison of Fabric Thicknesses

	Experimental results (m)	**Numerical results (m)**	**Discrepancy**
Sample 1	0.00310	0.00274	-11.61%
Sample 2	0.00879	0.00864	-1.71%

Comparisons of fiber volume fractions are listed in Table 3-2. It shows that the simulation result is 5~10% larger than the experimental measurement. This may be because thickness from the numerical simulation is smaller than that of the experimental measurement, while other parameters are correspondingly equal. Refer to the calculation of fiber volume fraction in Equation (3.25).

Table 3-2 Comparison of Fiber Volume Fractions

	Experimental results (%)	**Numerical results (%)**	**Discrepancy**
Sample 1	39.12	42.15	7.75%
Sample 2	48.04	51.9	8.03%

Micro-structures of numerical results are also compared with microscopic images, as displayed in Figure 3-23 and Figure 3-24.

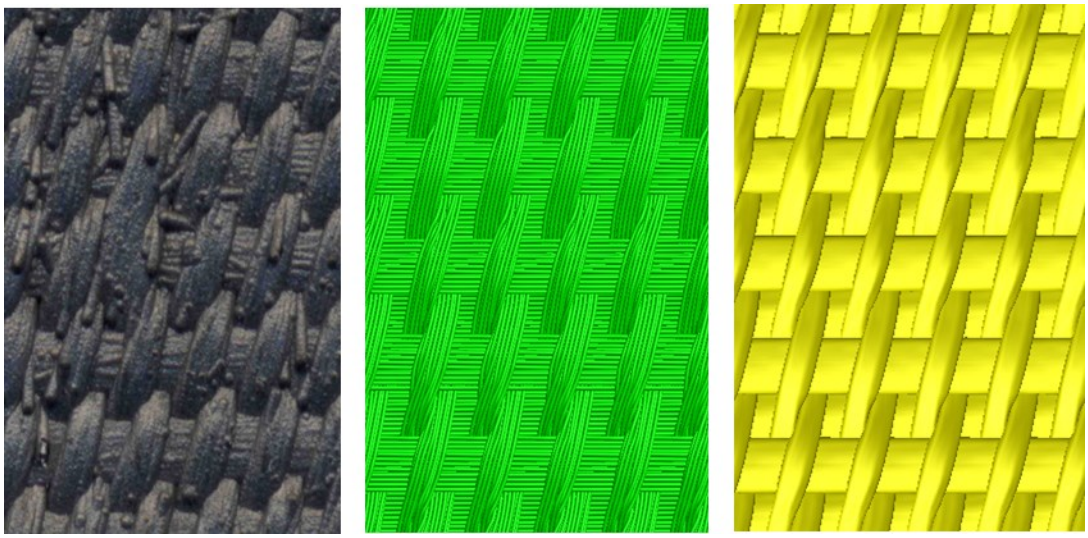

(a) Fabric surface pattern comparison

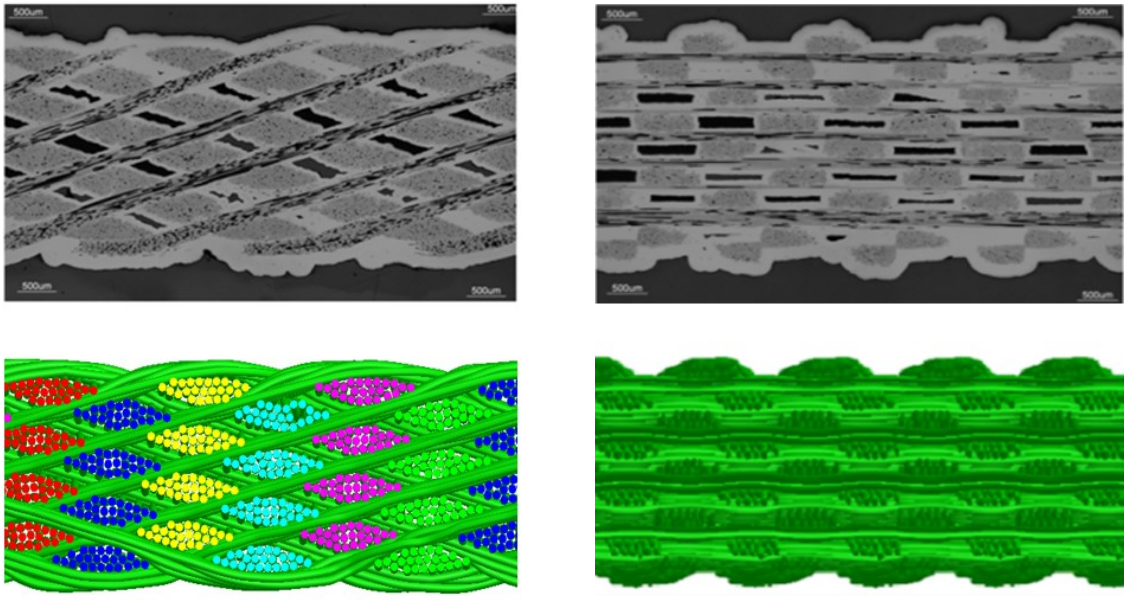

(b) Warp section comparison (c) Weft section comparison

Figure 3-23 Fabric Micro-structure Comparison of Sample 1

For the first sample, micro-structure comparisons are shown in Figure 3-23. The surface appearance comparison is shown in Figure 3-23a. The first picture is the microscopic image of the fabric, the middle picture is a fiber-level surface pattern derived by numerical simulation, and the third picture is a yarn-level microstructure. Microscopic images of the fabric's interior cross-sections are then compared to numerical results in Figure 3-23b and Figure 3-23c. Figure 3-23b shows warp-direction cross-sections and Figure 3-23c shows weft direction cross-sections. The two pictures in the upper positions are microscopic images, and the two pictures in the lower positions are derived from numerical simulations. Desirable visual agreement is reached between exprimental and numerical results.

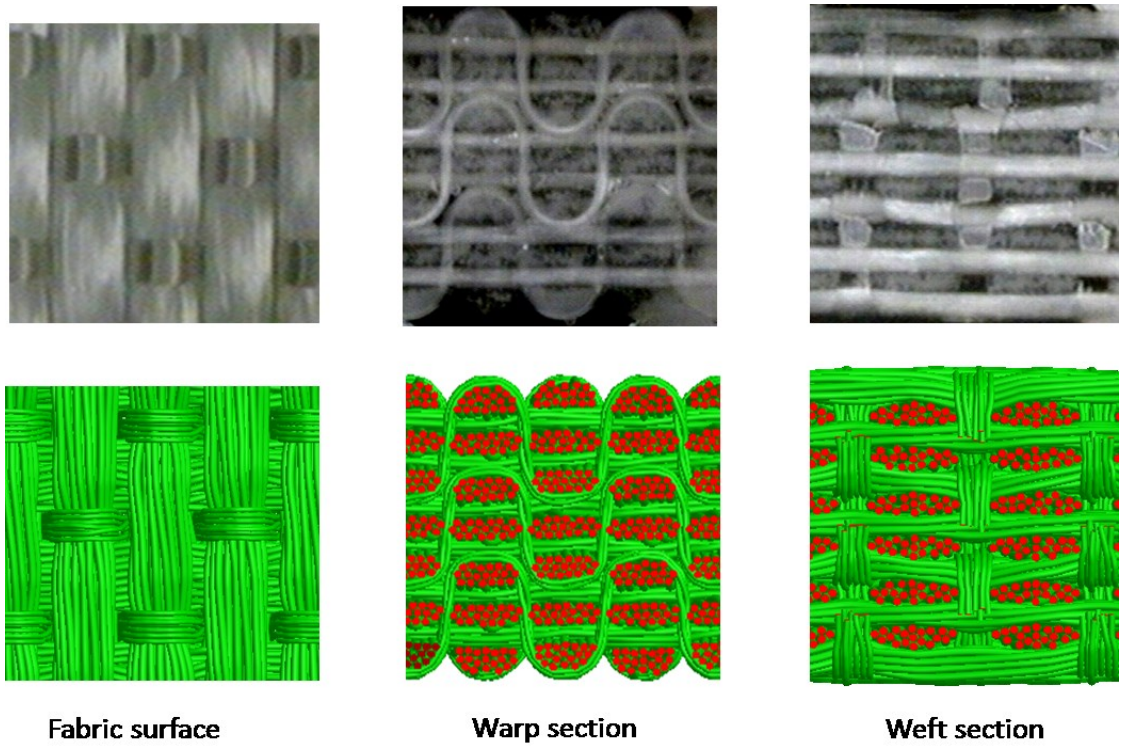

Figure 3-24 Fabric Micro-structure Comparison of Sample 2

For the second sample, micro-structure comparisons are shown in Figure 3-24. The top pictures are experimental investigations, and the bottom pictures are numerical simulations. Micro-structures are compared in three different views: fabric surface, warp section, and weft section. Good visual agreements between experimental results and numerical results are also achieved.

3.5 Remarks

A dynamic DEA with periodic boundary conditions is presented to determine 3-D woven textile micro-geometries. DEA generates fabric micro-geometry from the unit cell topology to unit cell detailed geometry. Both fiber- and yarn-level micro-geometries of various 3-D woven fabrics with complex patterns can be derived using a PC.

Unit cell topology is established based on weft pattern matrix and warp pattern matrices with yarn properties assigned. Different yarn discretization patterns are provided, from 2 fibers per yarn to 91 fibers per yarn. Different yarn/tow structures are generated, including plain yarn, twisted yarn, and twisted tow.

An explicit algorithm with a periodic boundary condition is introduced. Nodal forces existing in DEA simulation are tensile force, fiber-to-fiber contact force, damping force, and bending force. A central difference algorithm is adopted to calculate nodal forces, accelerations, velocities, and displacements within the unit cell. Renewed nodal displacements within the unit cell are then mapped to the external boundary zone based on the periodic principle. An efficient contact search algorithm is proposed to reduce the calculation time. A multi-level dynamic relaxation procedure is also implemented in order to save even more computer resources. A

yarn-level unit cell micro-geometry is created, which is also able to be read by commercial software for further analysis.

Two samples are provided to compare numerical simulations and actual fabrics: 3-D woven angle interlock fabric and 3-D woven orthogonal fabric with twisted yarns. Comparisons are made on three aspects: fabric thickness, fiber volume fraction, and fabric micro-structure. Good agreements are reached between numerical and experimental results.

Chapter 4 - 3-D Woven Near-Net Shape Fabric Component

Near-net shape manufacturing technology can yield a component whose shape is near to the net-shape product. It has become an appealing technology in the composite industry and has been employed in making various complex 3-D composite products. The major advantage of this technology is that it guarantees product inherent toughness with minimum debulking treatment on the composite reinforcement. For example, in making a turbine blade, the traditional way is laminating a number of layers of 2-D composites with different shapes. This will take laborious work to make the laminates, and even worse, it will cause the product with high possibility of delamination failure. If a conventional 3-D weaving technology is adopted to create a uniform composite preform with unit cell feature, then a significant amount of work will be required to remove extra portions, and even worse, the inherent toughness of the structure will be undermined. As such, the near-net shape fabric weaving technology will be an excellent choice.

Near-net shape technology creates a single fabric component with complex structure. At the macro-scale, the fabric shows a shape near to the final composite component. At the micro-scale, complex yarn-to-yarn interactions are presented and yarn shape is described by fiber arrangements in each yarn. In order to accurately reflect the fabric geometry, a full field relaxation is required in simulation of the near-net shape fabric. A powerful data and memory management, parallel processing, is conducted to handle the relatively great amount of memory.

This chapter contains two sections: 1) Full-field fabric relaxation, and 2) Comparison with experimental results. Corresponding research work has been published in reference [10].

4.1 Full-field Fabric Relaxation

Figure 4-1 shows a numerical model of a net-shape composite component. The composite component has a complex structure and its preform is made by 3-D woven near-net shape manufacturing. The 3-D near-net shape fabric is woven as a single component and needs a full-field simulation.

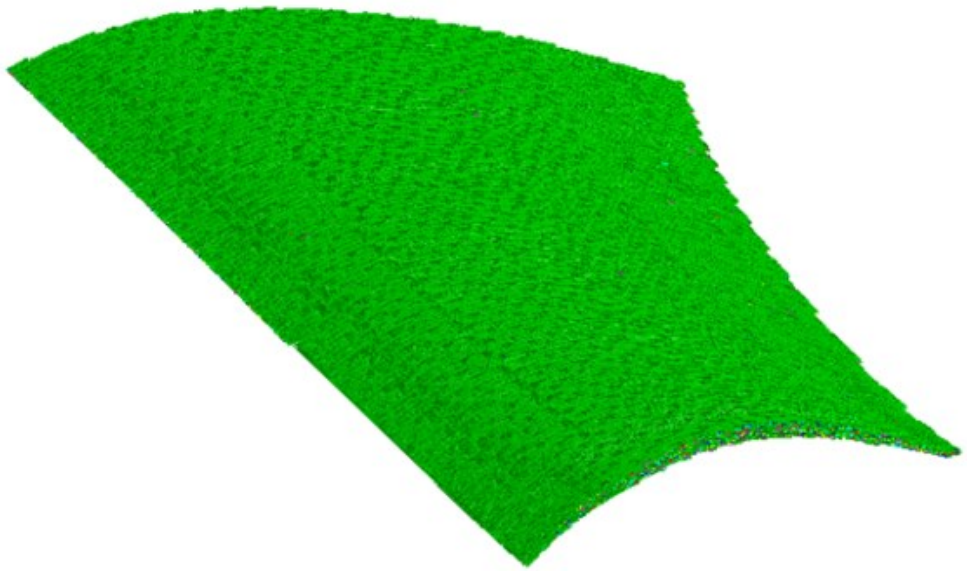

Figure 4-1 3-D Woven Net Shape Composite Component

In the DEA, to model a uniform fabric with unit cell feature, one only needs to simulate its unit cell with periodic boundary conditions and make structural copies of unit cell. To model a near-net shape fabric, a full-field simulation is required and other theories used in simulation of fabric unit cell are used except the periodic boundary condition.

A full-field relaxation models the entire fabric at the fiber level and uses much more memory than the availability of a general personal computer. As such, a powerful simulation management, the parallel processing, is adopted.

4.1.1 Boundary Conditions

A fabric is often woven as a single component from a dynamic weaving process [6]. Three actions are present in a typical weaving process: weft insertion, beating up, and warp weaving. Refer to Figure 4-2. In weft insertion, the shuttle takes a weft yarn and moves across the weaving loom back and forth. In beating up action, the reed beats the inserted weft against the newly formed fabric. In the ensuing weaving action, warps move either upward or downward to create a fabric with a specific pattern. A schematic of the resulting fabric is shown in the left portion of Figure 4-2.

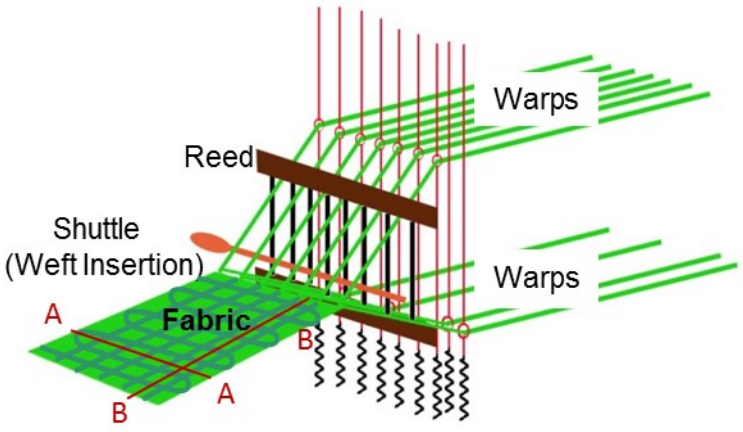

Figure 4-2 3-D Weaving Loom [6]

In simulation of the 3-D woven near-net shape fabric, boundary conditions that respect the actual weaving physics need to be applied. In reality, weft yarns are connected to be a global single yarn. Hence, all fibers in the global yarn are also internally connected. In numerical simulation, digital weft yarns are connected but only a portion of digital fibers of each weft yarn are connected in order to eliminate irregularities at connecting ends. A view of A-A from the fabric described in Figure 4-2 is displayed in Figure 4-3a. Only fibers marked with dashed centerlines in weft yarns are connected. The arrows indicate directions of weft insertion in the weaving action. During the relaxation process, fibers move toward the direction where the minimum potential energy can be reached. Consequently, weft connections are also able to keep warps running out of the fabric domain. A view of B-B from the fabric described in Figure 4-2 is described in Figure 4-3b. Similarly, warps ends are open and wefts tend to move laterally. Since fiber-to-fiber frictions are not considered, those wefts may also move out of the fabric domain. Thus, virtual boundary walls are set at both ends of warps to block the weft lateral movements.

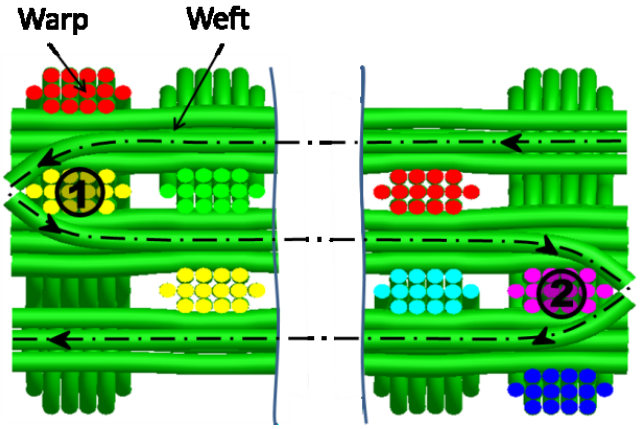

(a) Side view (A-A)

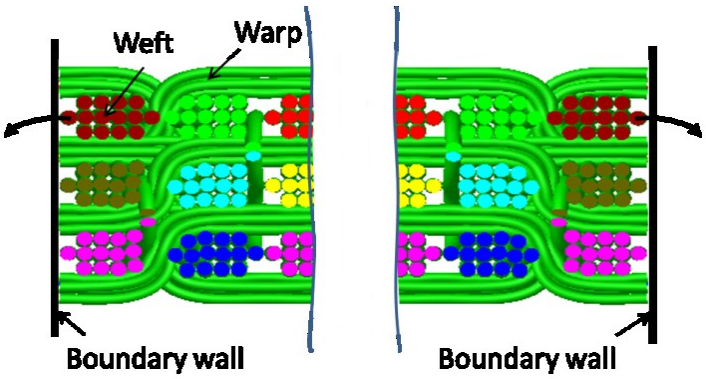

(b) Front view (B-B)

Figure 4-3 Boundary Conditions

4.1.2 Parallel Processing

Parallel processing conducts numerical simulation by simultaneously using multiple cores or processors. Each core is responsible for a portion of the entire simulation and communicates with neighboring cores at the end of calculation at each simulation step. In genearal, calculation speed increases as the number of processors increases. However, a linear speed up may not be present. Hence, optimal numbers of processors are also studied for parallel calculation.

4.1.2.1 Data Management Principle

In the DEA, data of a fabric include nodal force, nodal acceleration, nodal displacement, etc. Parallel processing starts with distributing the fabric data into a number of sections. The number of sections equals the number of processors used for calculation. The width of each section depends on the size of data it contains. Data distribution ensures each section contains approximate data size so that corresponding calculation time is approximately equal. Data distribution is a one dimensional split, either in x direction or y direction. For fabric with a fairly uniform shape, an equal width for each section is assigned.

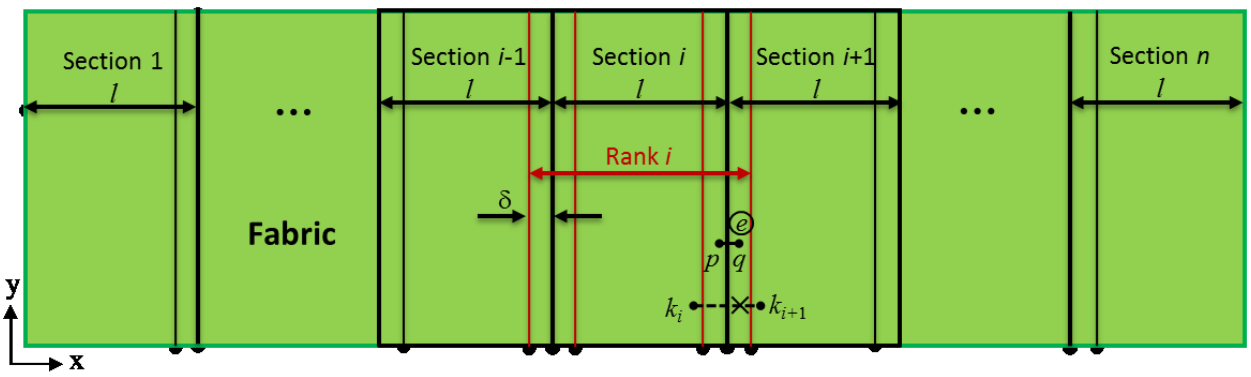

(a) Data distribution

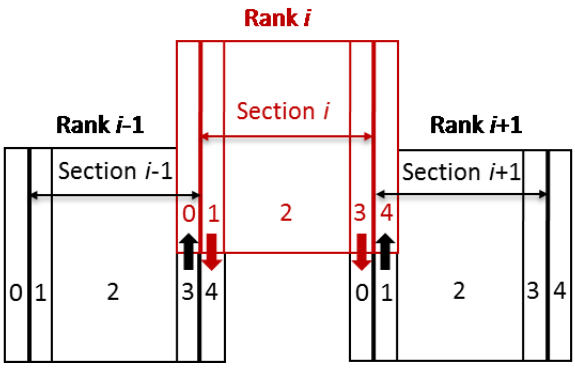

(b) Data exchange

Figure 4-4 Data Management

Refer to Figure 4-4a. Data of fabric are split into *n* sections in x direction with each section's width of *l*. Each section does not share any data with its adjacent sections. A medium of communication must be established among those sections.

Fabric is a non-continuum domain during simulation. An element could cross over the section. For example, the element ⓔ is constructed by node *p* and node *q*, while the former node is in section *i* and the latter is in section *i*+1. In order to calculate the information of node *p*, e.g., tensile force, node *q* at the other end of element ⓔ should be able to be accessed. As such, two strips are split out at both ends of each section to provide additional information for neighboring

sections to reach. Strip width, noted by δ, ranges 1~3 times of element length. Each section and two strips from neighboring sections then construct one rank. For sections at both ends of the fabric domain, section 1 and section *n*, their corresponding ranks are one section and only one strip. During the simulation, nodes always move and may move in and out of the same rank. For example, node *k* moves from rank *i* to rank *i*+1 after a period of simulation steps. Node *i*'s information will be lost if it is still treated as in rank *i*. Consequently, data redistribution is required. Since redistribution takes considerable time, it is conducted at every 50~100 steps, depending on the speeds of nodal movements.

Data of each rank is under the management of each processor. Refer to Figure 4-4b. Each rank consists of five blocks. Blocks 1, 2, and 3 contain the same data with corresponding section and blocks 0 and 4 contain the same data with two corresponding strips beyond that section. At each simulation step, blocks 1, 2, and 3 conduct calculations of nodal force, nodal acceleration, nodal displacement, etc., and then send the results in blocks 1 and 3 at current rank into blocks 4 and 0 at neighboring ranks, respectively. Thus, data at the boundaries of each section can be calculated.

4.1.2.2 Computation Evaluation

Numerical simulation of the full-field fabric is performed on an IBM parallel cluster. The cluster has 1 head node and 12 compute nodes. The head node is IBM System ×3650 M3 with 2TB disk usable and Intel Xeon Processor ×5650. The compute node is IBM System ×3755 M3 with 48 cores, 128 GB RAM, and AMD Opteron Processor Model 6172. The cluster has a total of 576 compute cores with 1.5TB RAM.

Different numbers of fibers per yarn are studied in modeling the fabric: 1, 7, and 14. The numbers of nodes for these three representations of fabric are 1 million, 12 million, and 34

million. Meanwhile, different numbers of processors are used in order to find the most efficient calculation. Calculation time of 100 simulation steps is studied. Refer to Table 4-1. For each type of fabric representation, when the number of processors increases, calculation time decreases accordingly. When the number of processors is more than 96, the decreasing speed of time is considerably slow. For fabric with 14 fibers per yarn, calculation time is absent by using two and four processors because the memory needed is too large to handle by using a small number of processors.

Table 4-1 Computation Time on Parallel Cluster

Processors	**Time (min, 100 steps)**		
	1 fiber/yarn (1 million nodes)	**7 fibers/yarn (12 million nodes)**	**14 fibers/yarn (34 million nodes)**
2	1.21	28.81	N/A
4	0.60	14.52	N/A
8	0.31	7.49	40.03
16	0.17	3.78	17.88
32	0.10	2.11	10.49
64	0.07	1.28	5.21
96	0.055	0.9	3.5
104	0.052	0.86	3.51
128	0.05	0.83	3.51

Relation of time and processor and relation of time and fibers/yarn are also drawn in Figure 4-5 and Figure 4-6. In Figure 4-5, the horizontal axis describes the number of running processors,

and the vertical axis describes the corresponding time taken for every 100 simulation steps, expressed as a logarithmic function. Linear or nearly linear speed up can be found when the number of processors is less than 96 processors. Beyond that, the speed up distinctly decreases. Hence, the number of processors around 96 can be selected for simulation of all these types of fabrics. In Figure 4-6, the horizontal axis describes the number of fibers per yarn, and the vertical axis describes the corresponding time taken for every 100 simulation steps, expressed as a logarithmic function. As the number of fibers per yarn increases, simulation time also increases and increasing slopes for all processors are approximate.

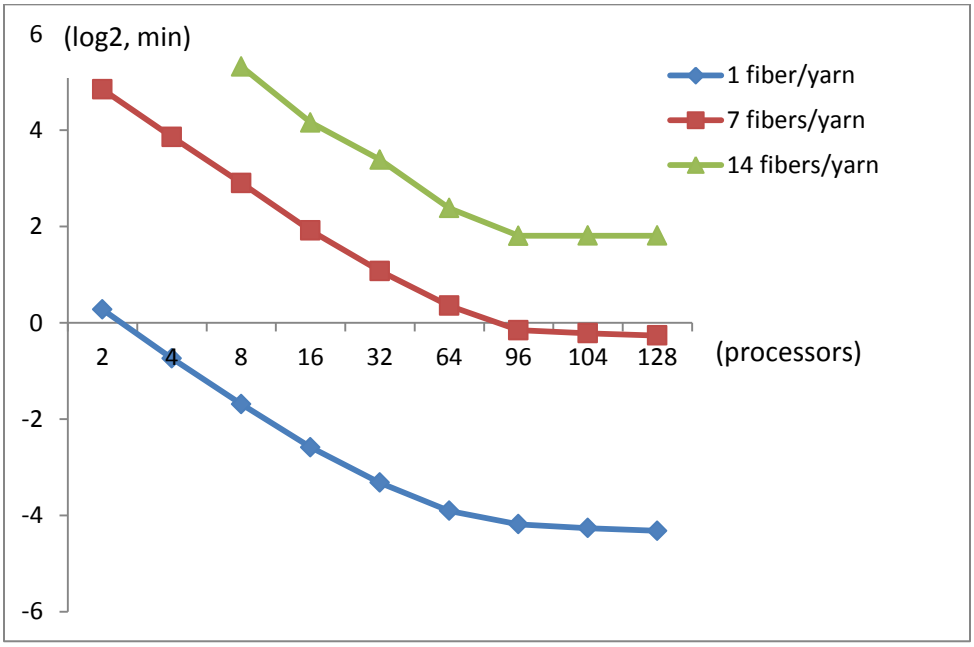

Figure 4-5 Computation Time Speed Up: Time vs. Processors

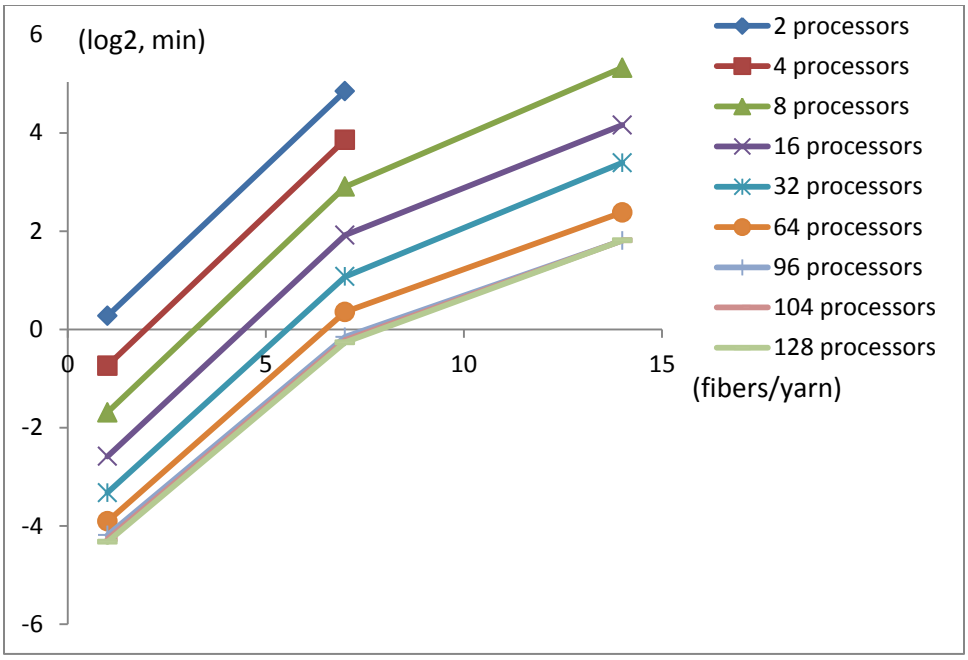

Figure 4-6 Computation Time Speed up: Time vs. Fibers/Yarn

4.1.2.3 Post-processor

After the simulation completes on parallel cluster, a post-processor is developed to transfer the data from the cluster to PC. The post-processor collects simulation results and performs a further partition process. The number of processors used in post-processor is much less than the number of processors used in simulation, and it also determines the number of fabric sections to display on PC.

Two ways of partitioning fabric data by post-processor exist, depending on whether or not a further digital element mesh is necessary. Referring to Figure 4-7, the first one illustrates partition by section and the second illustrates partition by rank. If no further digital element mesh is required, then the first partition is adopted, which will break the integrity of a weft yarn and divide one fiber into many segments, with some segments in the current section and others in the neighboring section. If the digital element mesh is further needed, then the second partition is

adopted. In order to keep every warp yarn monolithic, additional data will be provided beyond that section. Those data are in located in a strip with the width of δ, which is approximately the width of the weft column. As such, warp yarns will be cut by sections and weft yarns by ranks.

After the partition is complete, fabric can be displayed on PC either as a whole piece or section by section.

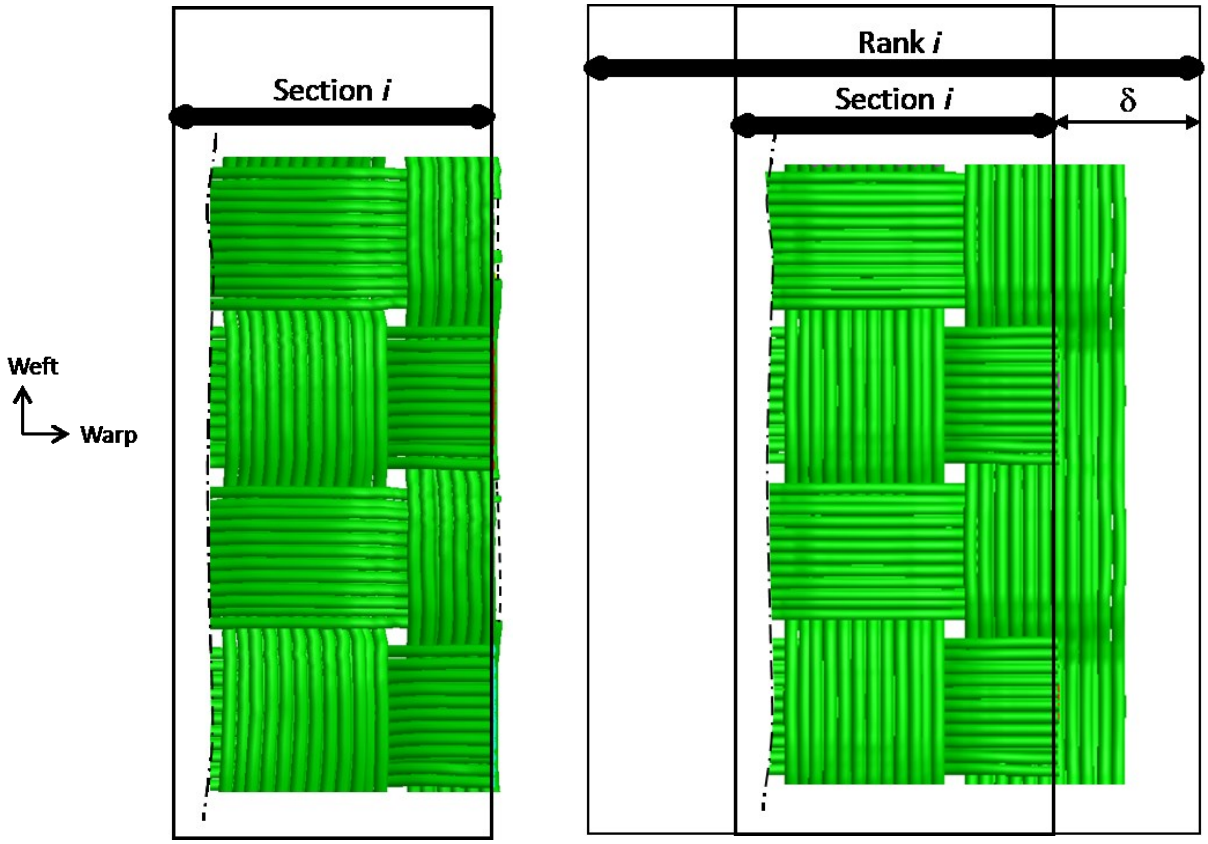

(a) Partition by section (b) Partition by rank

Figure 4-7 Partition of Fabric by Post-processor

4.2 Comparison with Experimental Results

Full-field numerical simulation of the near-net shape fabric is shown in Figure 4-8. Numerical results will be compared with experimental results in two aspects: fabric thickness and micro-structures. In modeling the fabric, 14 fibers per yarn are adopted. Experiments are conducted by Albany Engineered Composites, Inc.

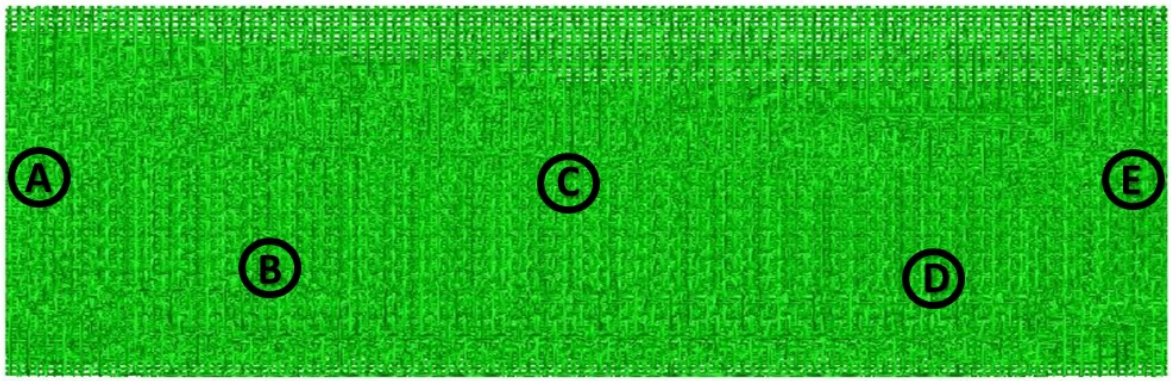

Figure 4-8 3-D Woven Near-net Shape Fabric

Several typical locations are picked for thickness verification, as seen by A, B, C, D, and E in the picture. In the experimental measurement, a standard thickness gauge is used and two different pressures are applied, 10 oz/in^2 and 32 oz/in^2. Results of comparisons are listed in Figure 4-9. The green, red, and blue bars describe numerical results free of pressure, experimental results with the pressure of 10 oz/in^2, and experimental results with the pressure of 32 oz/in^2, respectively. Thicknesses under the pressure of 32 oz/in^2 are 10~15% smaller than those under the pressure of 10 oz/in^2. The latter are also 5~10% smaller than numerical thicknesses, which are obtained without any pressure applied.

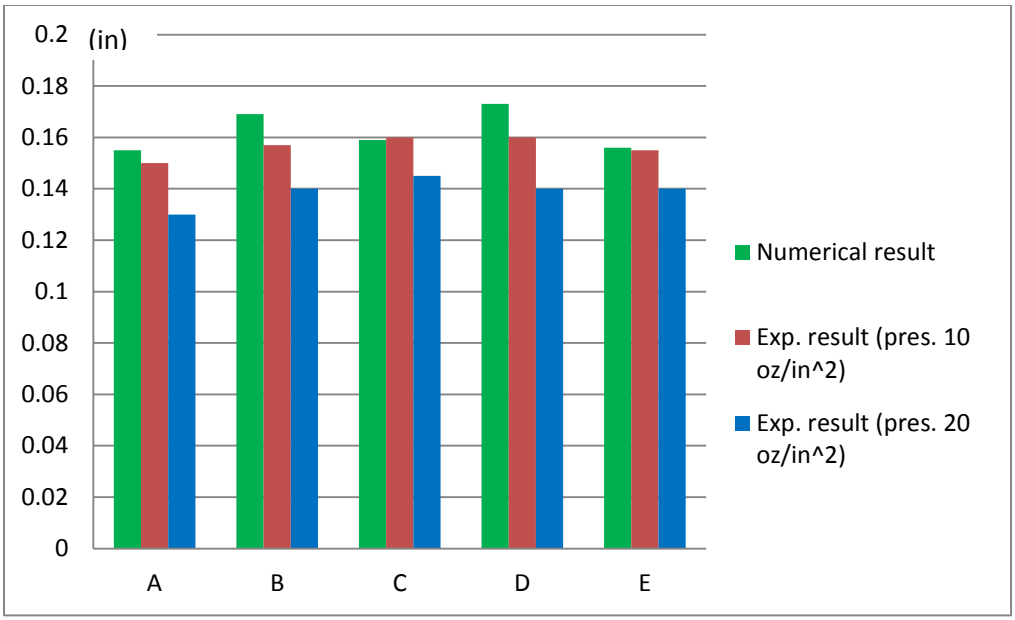

Figure 4-9 Fabric Thickness Comparison

In order to investigate micro-structures, the preform specimen is consolidated by resin and then cut into several pieces, as seen in Figure 4-10a. Micro-structures of cross-sections H-M and H-R of piece H are studied. Satisfactory visual agreements are reached between numerical simulation and experimental observation, as seen in Figure 4-10b and Figure 4-10c, respectively.

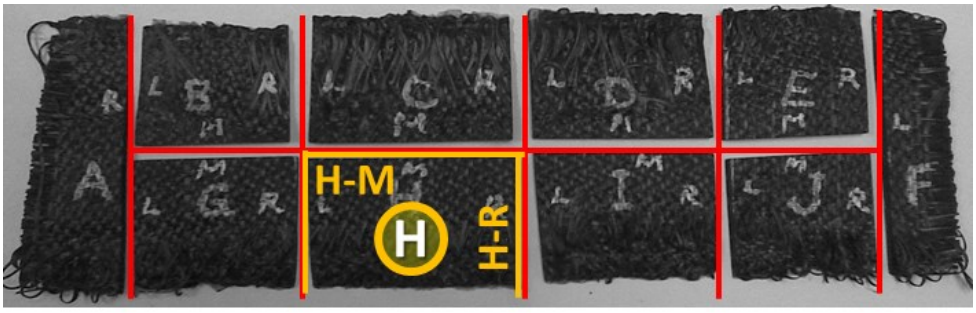

(a) The entire sliced specimen

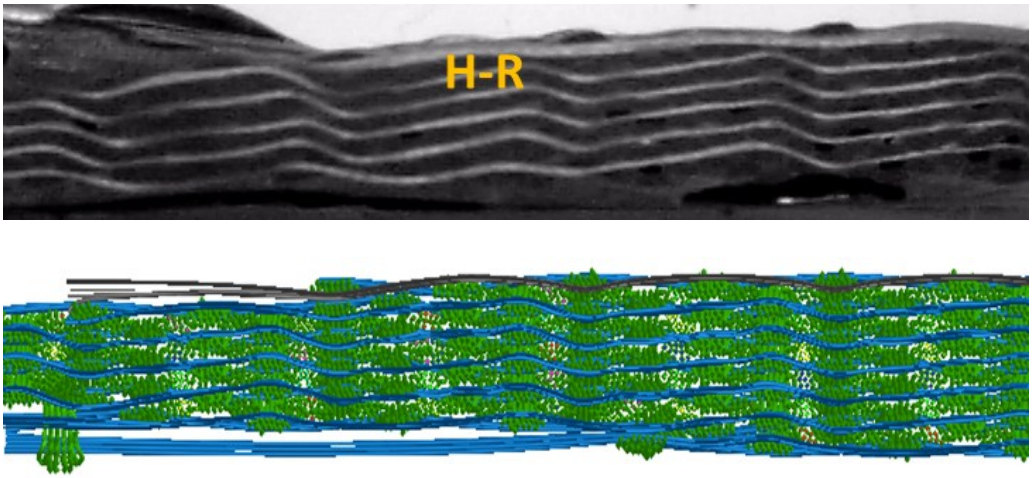

(b) Cross-section H-R

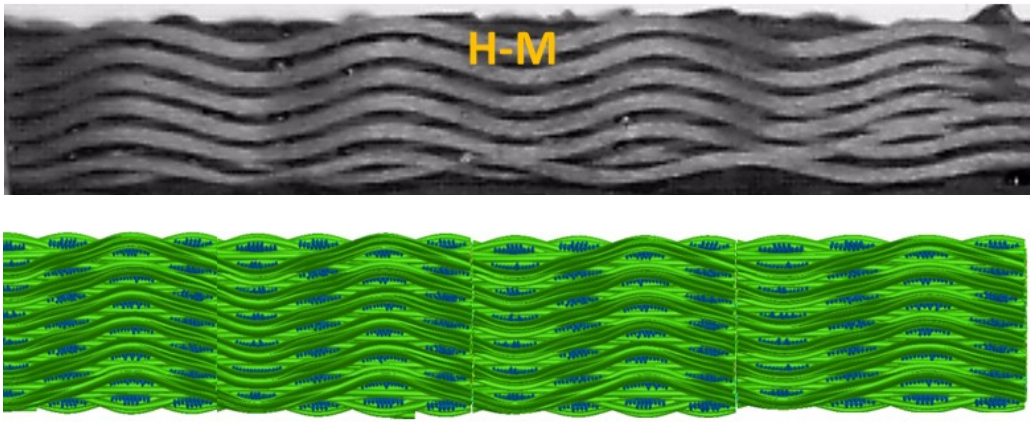

(c) Cross-section H-M

Figure 4-10 Micro-structure Comparison

4.3 Remarks

A 3-D woven near-net shape fabric is modeled using dynamic DEA by a full-field relaxation. All theories used in modeling the fabric unit cell discussed in Chapter 3 are adopted except the periodic boundary condition.

In setting up the boundary condition, weft yarns are connected and boundary walls are added at both ends of warp yarns. These settings can keep fibers running out the fabric domain during the simulation process.

For the full-field relaxation, a parallel processing is performed to handle the large amount of memory. In studying the speed up of parallel computing, different numbers of computing processors are used and three different numbers of fibers per yarn, 1, 7, and 14, are adopted for fabric representation. Optimal number of processors is found for parallel processing.

Numerical results are compared with experimental results on two aspects: fabric thickness and fabric micro-structures. Satisfactory agreements are reached.

Chapter 5 - 3-D Woven Net-shape Composite and Molding Process

A net-shape composite is a final composite product, such as a rib composite structure and a turbine blade. It directly serves as a net part in the whole system. To make a composite part, many composite manufacturing processes have been adopted and the resin transfer molding (RTM) process is a common one. In a typical RTM process, fabric is first placed between two molds; then the top mold moves towards the bottom mold and deforms the fabric accordingly; the fabric fully conforms to the cavity shaped by both molds. Meanwhile, resin is injected to consolidate the fabric into a composite part.

In modeling the fabric reinforced composite and corresponding molding process, common simulation issues are: fabric representation, mold surface representation, and mold-to-fabric contact modeling. In fabric representation, two models are commonly adopted: continuum model and discrete model. The former uses finite shell or membrane element and only focuses on the macro-level deformation. The latter models each yarn and needs empirical or experimental results for yarn shape determination. Researchers at Kansas State University have developed a sub-yarn model DEA, which can correctly reflect the fabric micro- and macro-geometry. In mold surface representation, three-node or four-node elements generated by commercial software are generally used. This may involve inconveniences of searching for contact between mold and fabric. The author has suggested a standard mesh to overcome this issue. Mold-to-fabric contact is modeled by a spring-like element with one-way movement.

Fabric representation has been discussed in Chapter 4. Other issues are covered in this chapter in four sections: 1) Mesh of mold surface; 2) Nodal force calculation; 3) Dynamic

molding procedure; and 4) Numerical results. Corresponding research work has been published in reference [10].

5.1 Mesh of Mold Surface

A mold surface, created by SolidWorks, is shown in Figure 5-1a. The mold needs to be meshed in order to build contacts with fabric. 3-D triangluar elments are first adopted for the mesh, as seen in Figure 5-1b.

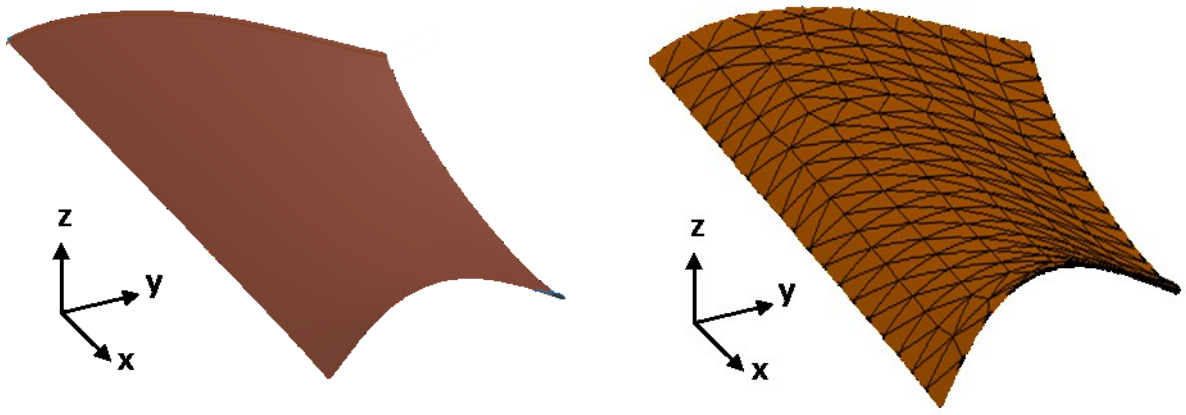

Figure 5-1 Mold Surface and Its Triangular Mesh

Because the mold mesh is irregular, difficulties arise in identifying contact points on the mold mesh. This is because all triangluar elements have to be searched to locate the contact point on mold mesh for a node on fabric, which is time consuming. Hence, a standard mesh is proposed to facilitate contact establishment. Referring to Figure 5-2, procedures of mesh conversion are as follows:

1) On the x-y plane, build a mesh whose elements are all quads with the size of *a*.

2) Locate the projection of an element of mold mesh on the x-y plane. For the element 1-2-3, its projection on the x-y plane is 1'-2'-3'.

3) Determine which nodes of quad element mesh on the x-y plane are inside the projection element. For example, *j*' is inside 1'-2'-3'.

4) Finds the intersection node between a vertical line starting from the node identified in step 3 and the element of the mold mesh. For example, a vertical ine starting from node *j* intersects the element 1-2-3 at node *j*. Node *j'* can be thus treated as a projection of node *j* on the x-y plane.

5) Calculate cooridnates of the intersection node identified in step 4. For node *j*, its x and y coordinates are identical to those of node *j*', and its z-coordinate is calculated by

$$z_j = N_1 z_1 + N_2 z_2 + N_3 z_3 \tag{5.1}$$

where z_1, z_2, and z_3 are the vertical distances between the nodes of element 1-2-3 and nodes of element 1'-2'-3', respectively; N_1, N_2, and N_3 are the shape functions that can be calculated on the x-y plane respectively by

$$N_1 = \frac{A_1}{A},\ N_2 = \frac{A_2}{A},\ N_3 = \frac{A_3}{A} \tag{5.2}$$

where A, A_1, A_2, and A_3 denote the areas of elements 1'-2'-3', 2'-*j'*-3', 1'-*j'*-3', and 1'-*j'*-2', respectively, as seen in the right picture of Figure 5-2.

The same procedure is applied to other triangular elements of the mold surface. Thus, new mesh of the mold surface is formed, as seen in Figure 5-3. The red curve marks the original mold surface and black dots describe the nodal positions of new mesh. In this standard mesh, the mold surface is discretized into four-node elements, with each element having a square projection on the x-y plane and having an exact size, as seen in Figure 5-3b. In addition, fabric domain is also

marked using the green box in the second picture. It is seen that new mesh of the mold surface has been extended. This is to completely cover the fabric so that the boundary irregularities are eliminated during the molding process simuation. The standard mesh also allows an easy mesh partition for parallel processing.

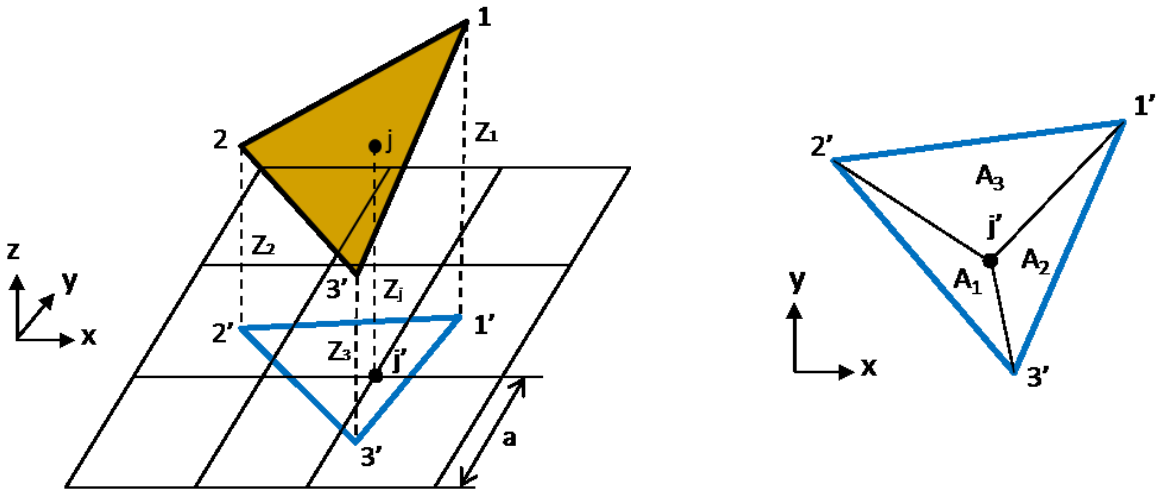

Figure 5-2 Mold Mesh Conversion

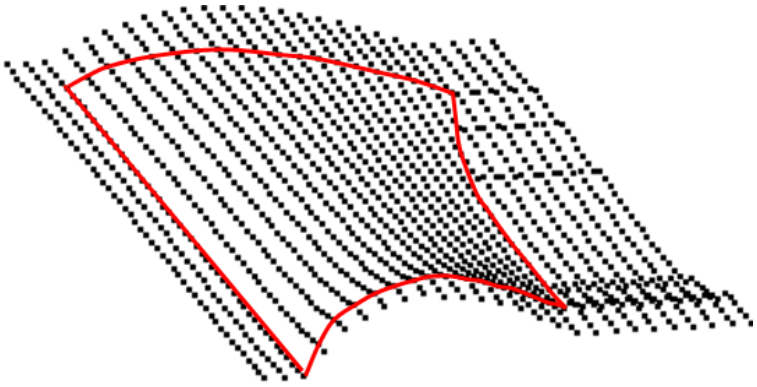

(a) 3-D view

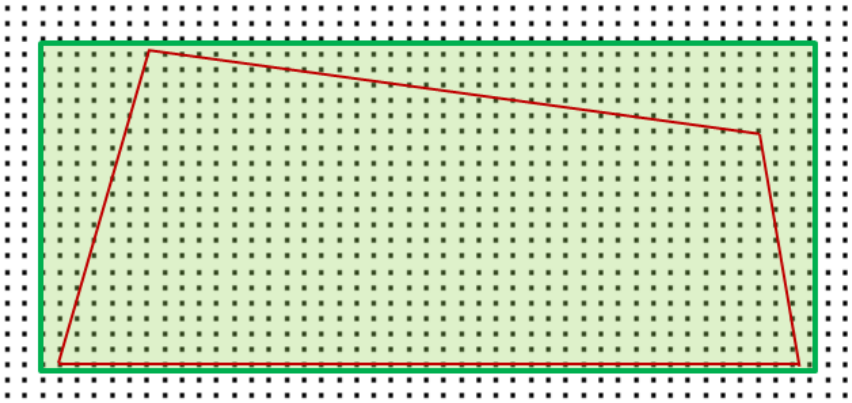

(b) Top view

Figure 5-3 Standard Mold Mesh

5.2 Nodal Force Calculation

In simulation of the molding process, nodal forces that exist in modeling the fabric unit cell or fabric are still maintained: fiber tensile force, fiber-to-fiber contact force, and damping force. Details have been presented in Section 3.2.1. During the molding process, mold movement creates mold-to-fabric contact force that leads to fabric deformation. Fabric will eventually conform to the cavity shape formed by both molds. In addition, mold-to-fabric force may cause irregularities of fiber arrangements especially at fabric boundaries. Consequently, fiber-to-fiber friction is added to generate sufficient fiber-to-fiber sticking force during the molding process. As such, two forces will be discussed in this section: 1) Fiber-to-fiber friction force, and 2) Mold-to-fabric contact force.

5.2.1 Fiber-to-Fiber Friction Force

Fiber-to-fiber friction force is generated by nodal movements and the relevant contact evolution. Refer to Figure 5-4a. There are two fibers, the solid curve on the left denotes fiber 1,

and the dashed curve and the solid curve on the right respectively denote fiber 2 before and after one step movement. Node *i* at position 0, denoted by *i*(0), is on fiber 1, and node *j* at position 1, denoted by *j*(1), is on fiber 2 before movement. Assume *j*(1) is in contact range of *i*(0). Then *j*(1) and *i*(0) can be called a contact pair. After one simulation step, *j*(1) moves to position 2, denoted by *j*(2), while assuming node *i* stays at position 0 and *j*(2) is still in the contact range of node *i*. Then *j*(2) and *i*(0) are the new contact pair. A friction force is thus created by nodal movement. Let vectors $\mathbf{u}_1$, $\mathbf{u}_2$, and $\mathbf{u}_{12}$ describe the direction of contact element at previous step, the direction of contact element at current step, and contact element deformation, respectively. The contact element deformation can then be decomposed along current contact direction and its orthogonal direction. Figure 5-4b shows a decomposition of vector $\mathbf{u}_{12}$ at *j*(2), where orthogonal vectors $\mathbf{u}_n$ and $\mathbf{u}_s$ describe nodal movements in current contact direction and the sliding direction, respectively. Fiber-to-fiber contact force calculation has been introduced in Section 3.2.1.2. For fiber-to-fiber friction force, it is expressed along the sliding direction by

$$F_s = -\mu k_c \Delta l_s \tag{5.3}$$

where μ is the friction coefficient, ranging between 0.1~0.7, k_c is the fiber-to-fiber contact element stiffness and its calculation is presented in Section 3.2.1.2, and Δl_s is the length of vector $\mathbf{u}_s$.

A Coulomb friction model [80] is used to account for the sliding of two fiber surfaces. If $|F_s| > \mu F_n$, sliding will occur and then let $|F_s| = \mu F_n$, where F_n denotes the contact force.

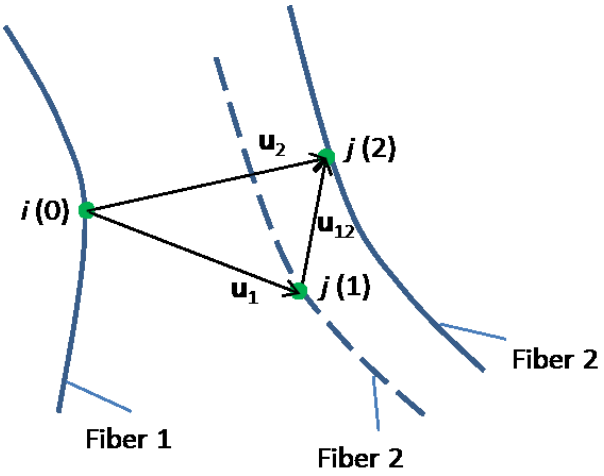

(a) Contact evolution

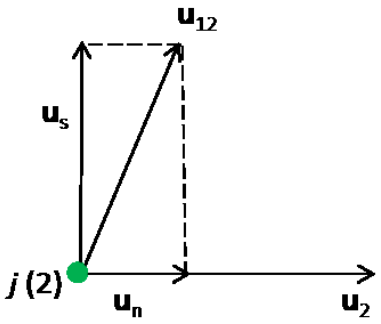

(b) Decomposition of vector $\mathbf{u}_{12}$

Figure 5-4 Friction Force Calculation

5.2.2 Mold-to-Fabric Contact Force

Mold-to-fabric contact force plays a major role in deforming the fabric. Contact elements are inserted between mold and fabric. In general, mold-to-fabric contact element length is set approximately to the digital element length which is half the fiber diameter. A shorter contact element length should be accompanied with larger contact element stiffness to create a reasonable contact force. But this setting has two disadvantages: establishing an exact contact element from each node on fabric to mold surface is inefficient; larger contact element stiffness may incur simulation instability. Thus, fairly long contact element length with relatively small contact element stiffness is adopted. Contact element length can be set at the magnitude of fabric dimension, allowing quicker mold movement with the simulation stability assured. Figure 5-5 shows a 2-D view illustration of mold-to-fabric contact element approximation. For node *i* on the fabric, ideally, the contact element should be element *i-k* with the length of *l*' and the element is perpendicular to the mold surface. Since mold surface has a low curvature and the distance of mold-

to-fabric is fairly long, element *i-k* can be represented by the vertical element *i-j* with the length of *l*.

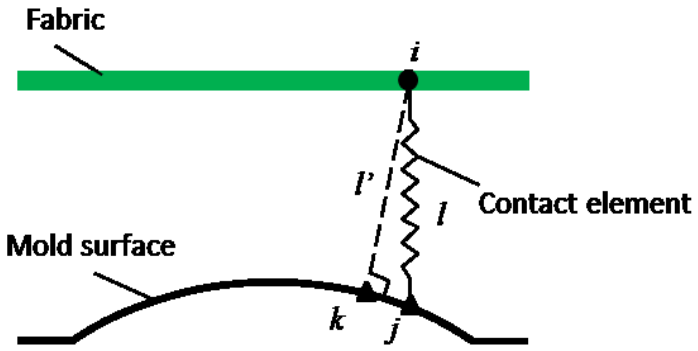

Figure 5-5 Mold-to-fabric Contact Element Approximation (2-D View)

Calculation of mold-to-fabric contact element is described in Figure 5-6. As seen in Figure 5-6a, node *i* is on fabric, element 1-2-3-4 is an element of standard mold mesh, the quad element 1'-2'-3'-4' is the projection of element 1-2-3-4 on the x-y plane, point *j* is the contact point between the vertical element passing node *i* and the element 1-2-3-4. Point *j*' is the projection of point *j* on x-y plane. The contact element length between node *i* and point *j* is determined by

$$l = N_1 z_1 + N_2 z_2 + N_3 z_3 + N_4 z_4 \tag{5.4}$$

where z_1, z_2, z_3, and z_4 are vertical distances between node *i* and four nodes of the mold element 1-2-3-4, respectively. N_1, N_2, N_3, and N_4 are the shape functions that can be calculated on the x-y plane, as seen in Figure 5-6b:

$$
\begin{aligned}
N_1 &= \frac{1}{4}(1-\frac{2\Delta x}{a})(1-\frac{2\Delta y}{a}),\\
N_2 &= \frac{1}{4}(1+\frac{2\Delta x}{a})(1-\frac{2\Delta y}{a}),\\
N_3 &= \frac{1}{4}(1+\frac{2\Delta x}{a})(1+\frac{2\Delta y}{a}),\\
N_4 &= \frac{1}{4}(1-\frac{2\Delta x}{a})(1+\frac{2\Delta y}{a})
\end{aligned}
\tag{5.5}
$$

where a is the element length of 1'-2'-3'-4', and Δx and Δy are the distances between the point j' and the center of this square element, denoted by point o, on the x-y plane.

Mold-to-fabric contact force is then calculated as

$$F_m = k_m \Delta l \tag{5.6}$$

where k_m is the mold-to-fabric contact element stiffness, and Δl is the contact element shortening at each simulation step.

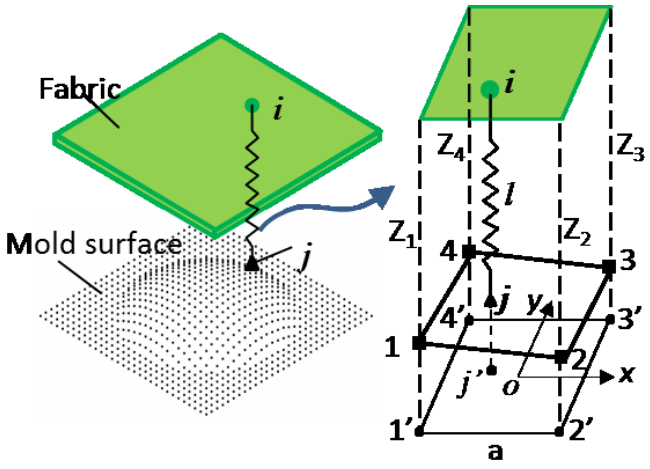

(a) 3-D view

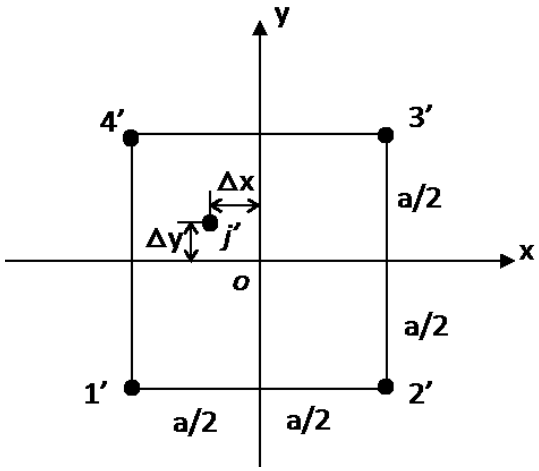

(b) Shape function calculation on x-y plane

Figure 5-6 Mold-to-fabric Contact Element Calculation

5.3 Dynamic Molding Procedure

The dynamic molding process is described in Figure 5-7.

Figure 5-7a describes the initial settings. Fabric is placed between two molds, while the top mold is fixed and the bottom one is free to move. Contact elements are set up according to the shortest distance between fabric and each mold. The shortest distance is also the defined contact distance l_0. If the vertical distance from a node on the fabric to the mold surface is smaller than defined contact distance, a contact element is then inserted.

After initial settings are established, the bottom mold moves upwards to deform the fabric. During each step of the movement, the distance from the node on fabric to each mold surface is checked to determine whether a mold-to-fabric contact element needs to be established. Contact forces are then applied and fabric deforms accordingly. The bottom mold continues to move upwards and more and more contact elements are added. A deceleration is assigned to the mold movement so that adequate relaxation time is provided for fiber movements when the fabric

receives more external contact forces. Bottom mold stops until lengths of all contact elements are equal, as seen in Figure 5-7b. At this balanced position, fabric fully conforms to mold shapes.

Figure 5-7c shows a finished product, which is formed after removing both molds and the corresponding contact elements at the balanced position. Mold-to-fabric friction and resin effect are both neglected in the simulation of this molding process.

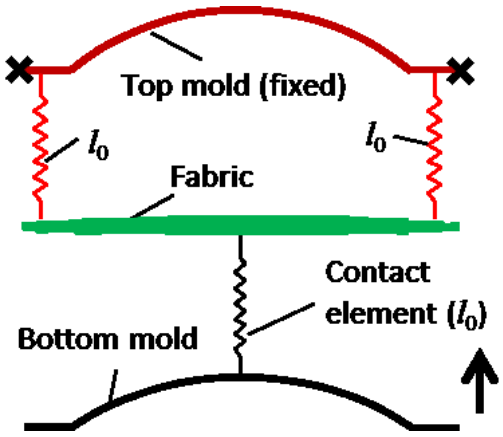

(a) Initial settings

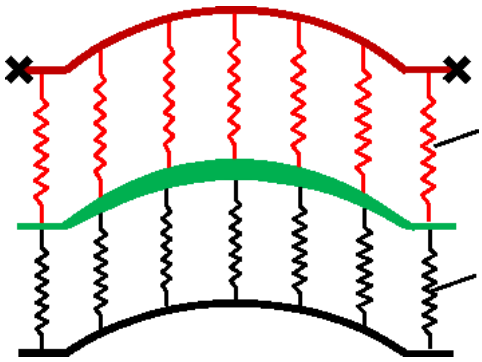

(b) Final balanced positions

(c) Finished product

Figure 5-7 Dynamic Molding Process

5.4 Numerical Results

Numerical simulations of fabric reinforced composite obtained from the molding process are shown in Figure 5-8.

Fabric macro-geometry after the molding process is shown in Figure 5-8a, where the red curve marks the original mold surface profile. Fabric has gracefully conformed to the extended mold shapes. It is then trimmed to be a net-shape fabric reinforced composite component that follows original mold shapes, as seen in Figure 5-8b. The net-shape component is then sliced for micro-geometry observation. Section A-A, displayed in Figure 5-8c, presents various thicknesses at different locations. This shape reaches the targeted shape without surface debulking. A local view of sliced section A-A, section A'-A', is shown in Figure 5-8d. Every digital yarn is represented by 14 digital fibers and various yarn shapes are also presented.

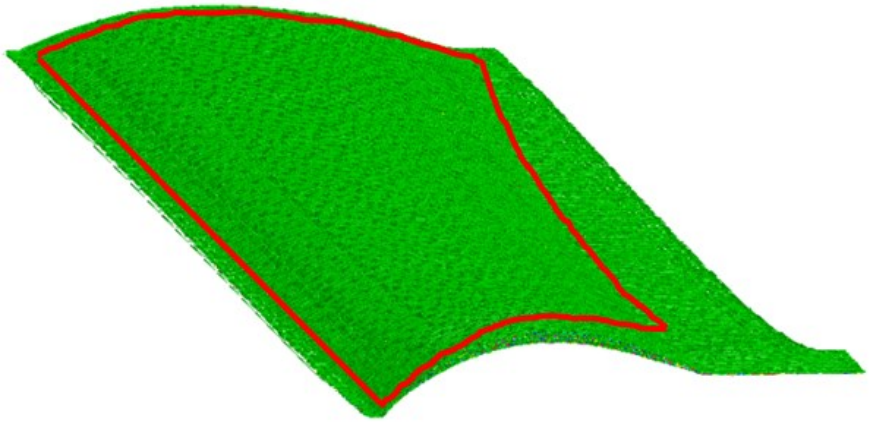

(a) Molded fabric

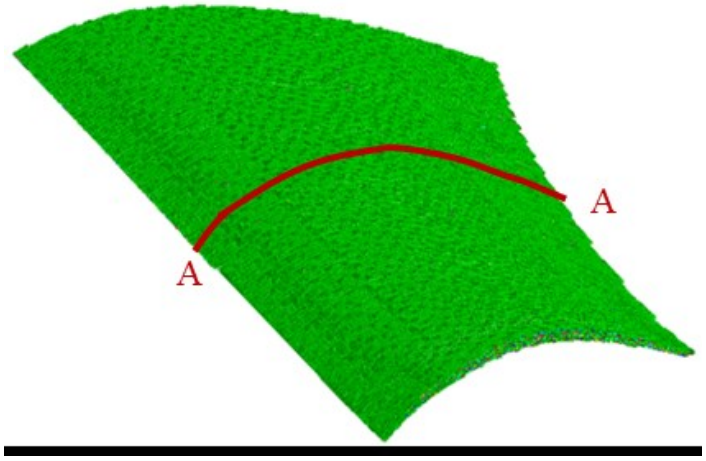

(b) Net shape composite component

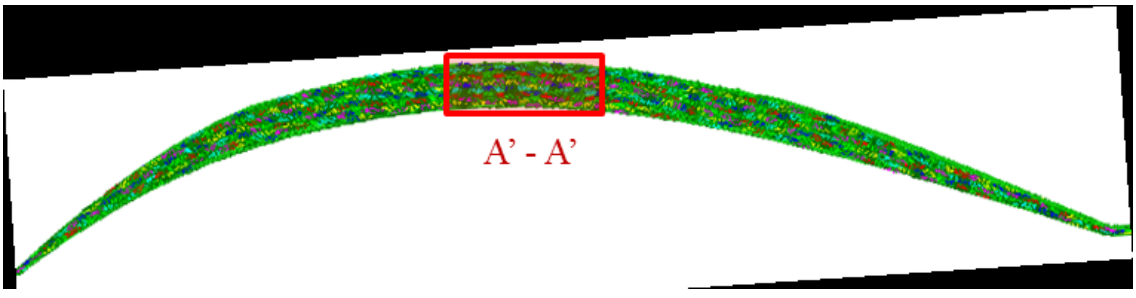

(c) Section view (A - A)

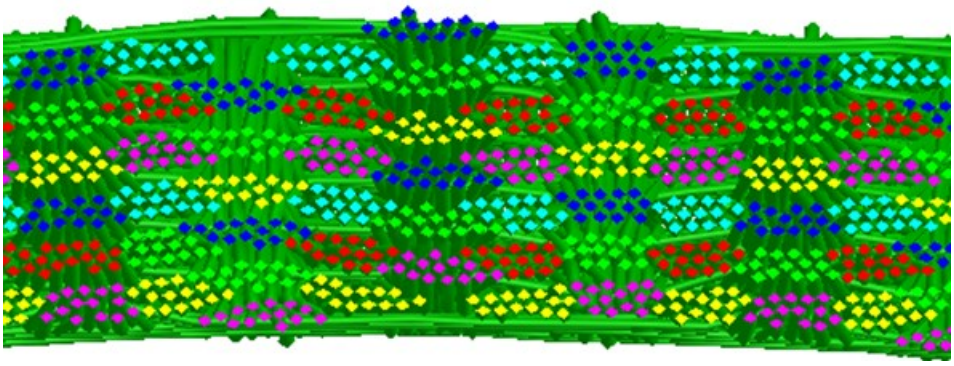

(d) Section view (A' - A')

Figure 5-8 Macro- and Micro-geometries of Net Shape Composite

5.5 Remarks

A fabric reinforced composite and the corresponding molding process are simulated. Fabric is modeled using dynamic DEA. Mold surface is represented by a standard mesh. In this standard mesh, projections of elements of the mold mesh on the x-y plane are all quad elements. Contact between mold and fabric is modeled using long vertical element. Standard mold mesh and the long vertical element are able to facilitate the mold-to-fabric establishment and contact force calculation. The long vertical element with soft contact element stiffness also allows quicker mold movement with the stability of fabric deformation guaranteed.

Besides nodal forces introduced in Chapter 3, two other nodal forces are discussed: mold-to-fabric contact force and fiber-to-fiber friction force. The former is to deform the fabric and the latter is to reduce irregularities of fiber arrangements especially at fabric boundaries. The dynamic molding procedure is explained: fabric is placed between two molds while the top one is fixed and the bottom one is free to move; more elements are added while the bottom mold moves upward and fabric deforms accordingly until a balanced position is reached; a finished product is obtained by removing both molds and corresponding mold-to-fabric contact elements.

Macro- and micro-geometry of the fabric reinforced composite are obtained. Resin effects are neglected during the simulation.

Chapter 6 - Conclusions and Future Works

Composite design and analysis require a good understanding of macro- and micro-geometry of fabric and fabric reinforced composite. Micro-geometry of fabric is determined by the weaving process. Macro- and micro-geometry of fabric reinforced composite is determined by fabric geometry and the molding process.

6.1 Conclusions

A fabric consists of a number of yarns or tows, and a yarn is a bundle of fibers. Fabric micro-geometry can be analyzed either at the yarn level or at the fiber level. For the yarn-level analysis, yarn shape is described by yarn path and yarn cross-section shape. For the fiber-level analysis, yarn shape is described by fiber paths and fiber arrangements on yarn cross-section, and each fiber is assumed to have a circular cross-section shape.

The objective of this research is to model macro- and micro- geometry of fabric and fabric reinforced composite using a fiber-level approach DEA. A dynamic explicit algorithm is employed in this approach. The following conclusions can be reached from this dissertation:

1. Fabric micro-geometry determination should follow the textile weaving mechanics. First, fabric topology is established based on the textile weaving pattern, followed by yarn discretization, then a dynamic explicit solver is employed to obtain the detailed fabric geometry.
2. An explicit algorithm with a periodic boundary condition is employed to model micro-geometry of the fabric with unit cell property. Nodal forces, nodal

accelerations, nodal velocities, and nodal displacements within the unit cell are calculated. The renewed nodal displacements are then mapped to the external boundary zone of unit cell in order to calculate nodal forces in the ensuing simulation step. An efficient contact search algorithm and a multi-level mesh and relaxation procedure are proposed. Those improvements save a great amount of computer resources compared to the previous algorithm developed in this group. A yarn-level fabric micro-geometry is also created and data can be read by commercial software packages for further composite/fabric analysis.

3. An explicit algorithm with a boundary that follows the weaving physics is employed to simulate the near-net shape fabric component. A parallel processing is conducted to handle the large amount of memory required by full-field simulation.
4. A dynamic molding process is simulated. Fabric is modeled by using dynamic DEA. Mold surface is represented by a standard mesh to quickly establish contact between mold and fabric. Mold-to-fabric contacts are modeled by long vertical elements that only take compressive force, which allows quicker mold movements with simulation stability ensured during the molding process. A net-shape composite component is obtained.

6.2 Future Works

From the major conclusions presented in the preceding section, additional works could be made in the future, as follows:

1. Typical composite/fabric structures include woven, braided, stitched, and knitted structures. Only 3-D woven structures have been studied in this research. Other types of structures also need to be studied to enrich applications of DEA.
2. In parallel processing, one dimensional data partition and memory allocation has been used. This is applicable for uniform or near-uniform fabric other than hybrid fabric. For a hybrid fabric used in ballistic-proof, it has a higher density in the impact zone than other zones. In this case, a two dimensional data partition needs to be applied in parallel processing to ensure data in all sections are approximate.
3. The structure of composite has been studied without considering resin effect. In many cases, resin is not a slighting role in determining composite structure and should be considered in the future.
4. Composite structures determine composite mechanical properties. Only composite structures have been studied in this research. Their roles in determining composite mechanical properties should be investigated.

References

[1] Huang, L.J., Wang, Y.Q., Miao, Y.Y., Swenson, D., Ma, Y., & Yen, C.F. (2013). Dynamic relaxation approach with periodic boundary conditions in determining the 3-D woven textile micro-geometry. Composite Structures, 106, 417-425.

[2] Wang, Y.Q., & Sun, X.K. (2000, September 23-27). Determining the geometry of textile preforms using finite element analysis. The 15th Annual Technical Conference for Composites, College Station, Texas, USA.

[3] Wang, Y.Q., & Sun, X.K. (2001). Digital element simulation of textile processes. Composites Science and Technology, 63, 311-319.

[4] Zhou, G.M., Sun, X.K., & Wang, Y.Q. (2004). Multi-chain digital analysis in textile mechanics. Composites Science and Technology, 64, 239-244.

[5] Miao, Y.Y., Zhou, E., Wang, Y.Q., & Cheeseman, B.A. (2008). Mechanics of textile composites: micro-geometry. Composites Science and Technology, 68, 1671-1678.

[6] Miao, Y.Y., Huang, L.J., Wang, Y.Q., Swenson, D., Sullivan, B., & Yen, C.F. (2009, September 15-17). Explicit digital element approach with periodic boundary in determining textile micro-geometry. The 24th Conference of American Society for Composites, Newark, DE, USA.

[7] Wang, Y.Q., Miao, Y.Y., Swenson, D., Cheeseman, B.A., & Yen, C.F. (2010). Digital element approach for simulating impact and penetration of textiles. International Journal of Impact Engineering, 37, 552-560.

[8] Yang, X.Y., Wang, Y.Q., & Yen, C.F. (2012, October 1-3). Dynamic Simulation of 3-D Weaving Process. The 27th Conference of American Society for Composites, Arlington, Texas, USA.

[9] Ma, Y., Huang, L.J., Wang, Y.Q., Swenson, D., Sullivan B, & Yen, C.F. (2012, October 1-3). Validation of explicit digital element dynamic relaxation approach in determining

micro-geometry of 3-d woven fabrics. The 27th Conference of American Society for Composites, Arlington, TX, USA.

[10] Huang, L.J., Wang, Y.Q., Miao, Y.Y., Yen, C.F., Bayraktar, H., & Goering, J. (2013, July 28 - August 02). Simulation of fabric deformation under molding process. The 19th International Conference on Composite Materials, Montreal, Canada.

[11] Peirce, F.T. (1937). The geometry of cloth structure. Journal of the textile institute, 28(3), T45-T96.

[12] Hu, J. (2004). Structure and mechanics of woven fabrics. CRC Press.

[13] Kemp, A. (1958). An extension of Peirce's cloth geometry to the treatment of nonlinear threads. Journal of Textile Institute, 49, T44-T48.

[14] Hearle, J.W.S., & Shanahan, W.J. (1978). An energy method for calculations in fabric mechanics. Part I: Principles of the method. Journal of Textile Institute, 69, 81-110.

[15] Ito, M., & Chou, T.W. (1997). Elastic moduli and stress field of plain-weave composites under tensile loading. Composites Science and Technology, 57, 787-800.

[16] Naik, N.K., & Shembekar, P.S. (1992). Elastic behavior of woven fabric composites: I-Lamina analysis. Journal of Composite Material, 26(15), 2196-2225.

[17] McBride, T.M., & Chen, J. (1997). Unit-cell geometry in plain-weave fabrics during shear deformations. Composites Science and Technology, 57(3), 345-351.

[18] Hivet, G., & Boisse, P. (2005). Consistent 3D geometrical model of fabric elementary cell. Application to a meshing preprocessor for 3D finite element analysis. Finite Elements in Analysis and Design, 42(1), 25-49.

[19] Kuhn, J., & Charalambides, P. (1999). Modeling of plain weave fabric composite geometry, Journal of Composite Material, 33(3), 188-220.

[20] Hivet, G., & Boisse, P. (2008). Consistent mesoscopic mechanical behaviour model for woven composite reinforcements in biaxial tension. Composites Part B: Engineering, 39, 345-361.

[21] Hivet, G., Wendling, A., Vidal-Salle, E., Laine, B., & Boisse, P. (2010). Modeling strategies for fabrics unit cell geometry-application to permeability simulations. International Journal of Material Forming, 3(1), 727-730.

[22] Sullivan, B. (2010). Microscopic images of 3-D woven fabric, Materials Research & Design, Inc., private communication.

[23] Tsukrov, .I, Bayraktar, H., Giovinazzo, M., Goering, J., Gross, T., Fruscello, M., & Martinsson, L. (2012). Finite element modeling to predict cure-induced microcracking in three-dimensional woven composites. International Journal of Fracture, 172(2), 209-216.

[24] Mahadick, Y., & Hallett, S.R. (2008, October 13-15). Finite element modelling of yarn geometry in 3D woven fabrics. Proceedings of the 9th International Conference on Textile Composites, Newark, Delaware, USA.

[25] Mahadick ,Y., & Hallett, S.R. (2010). Finite element modelling of tow geometry in 3D woven fabrics. Composites Part A: Applied Science and Manufacturing, 41, 1192-1200.

[26] Durville, D. (2005). Approach of the constitutive material behaviour of textile composites through simulation. II International conference on Textile Composites and Inflatable Structures, France.

[27] Durville, D. (2010). Simulation of the mechanical behaviour of woven fabrics at the scale of fibers, International Journal of Material Forming, 3(2), 1241-1251.

[28] Durville, D. (2011). Microscopic approaches for understanding the mechanical behaviour of reinforcement in composites. Composite Reinforcements for Optimum Performance, 461-485.

[29] Lomov, S.V., Huysmans, G., Luo, Y., Parnas, R., Prodromou, A., Verpoest, I., & Phelan, F.R. (2001). Textile composites: modelling strategies. Composites Part A: Applied Science and Manufacturing, 32(10), 1379-1394.

[30] Verpoest, I., & Lomov, S.V. (2005). Virtual textile composites software Wisetex: integration with micro-mechanical, permeability and structural analysis. Composites Science and Technology, 65(15-16), 2563-2574.

[31] Lomov, S.V., Ivanov, D.S., Verpoest, I., Zako, M., Kurashiki, T., Nakai, H., & Hirosawa, S. (2007). Meso-FE modelling of textile composites: Road map, data flow and algorithms. Composites Science and Technology, 67, 1870-1891.

[32] Lomov, S.V., Perie, G., Ivanov, D.S., Verpoest, I., & Marsal, D. (2011). Modelling 3D fabrics and 3D reinforced composites: challenges and solutions. Textile Research Journal, 81(1), 28-41.

[33] Retrieved from http://www.mtm.kuleuven.be/Onderzoek/Composites/software/wisetex, May 20, 2013.

[34] Robitaille, F., Clayton, B.R., Long, A.C., Souter, B.J., & Rudd, C.D. (1999). Geometric modelling of industrial preforms: woven and braided textiles. Proceedings of the Institution of Mechanical Engineers, Part L: Journal of Materials Design and Applications, 213, 69-83.

[35] Robitaille, F., Long, A.C., Jones, I.A. & Rudd, C.D. (2003). Automatically generated geometric descriptions of textile and composite unit cells. Composites PartA: Applied Science and Manufacturing, 34, 303-312.

[36] Schubel, P.J., Warrior, N.A., & Rudd, C.D. (2006 October 16-18). Surface roughness modelling of textile composites using TexGen. 8th International Conference on Textile Composites, Nottingham, UK.

[37] Sherburn, M. (2007). Geometric and mechanical modelling of textiles. PhD thesis, University of Nottingham.

[38] Lin, H., Brown, L.P., & Long, A.C. (2011). Modelling and simulating textile structures using TexGen. Advanced Materials Research, 331, 44-47.

[39] Sherburn, M., Long, A., Jones, A., Crookston, J., & Brown, L. (2012). Prediction of textile geometry using an energy minimization approach. Journal of Industrial Textiles, 41(4), 345-369.

[40] Retrieved from http://texgen.sourceforge.net/index.php/Main_Page, May 30, 2013.

[41] Goering, J., & McClain, M. (2007, September 17-19). Recent developments in 3D woven Pi preforms. 22nd Technical Conference of the American Society for Composites, Seattle, Washington.

[42] McClain, M., & Goering, J. (2012, March). Overview of recent developments in 3D structures. Society of Manufacturing Engineers, Composites Manufacturing.

[43] McClain, M., & Goering J. (2012, May 21-24). Rapid assembly of fiber preforms using 3D woven components. Society for the Advancement of Material and Process Engineering, Baltimore, Maryland.

[44] Retrieved from www.albint.com, June 01, 2013.

[45] Wang, Y.Q., & Wang, A.S.D. (1997). Spatial distribution of yarns and mechanical properties in 3d braided tubular composites. Applied Composite Materials, 4, 121-132.

[46] Schreiber, F., Ko, F.K., Yang, H.J., Amalric, E., & Gries, T. (2009, July 27-31). Novel three-dimensional braiding approach and its products. 17th International Conference on Composite Materials, Edinburgh, UK.

[47] Hampton, F.P., Ko, F.K., Doyle, C., & Runyen, R.W. (2009, July 27-31). Development of ductile-hybrid composites (DHC) by the braidtrusion process. 17th International Conference on Composite Materials, Edinburgh, UK.

[48] Schreiber, F., Theelen, K., Schulte Südhoff, E., Lee, H.Y., Ko, F.K., & Gries, T. (2011, August 21-26). 3D-hexagonal braiding: possibilities in near-net shape preform production

for lightweight and medical applications. 18th International Conference on Composite Materials, Jeju Island, Korea.

[49] Horrocks, A.R., & Subhash, S.C. (2000). Handbook of Technical Textiles, Woodhead Publishing.

[50] Cebulla, H., Diestel, O., & Offermann, P. (2002). Fully fashioned biaxial weft knitted fabrics. AUTEX Research Journal, 2(1), 220-227.

[51] Boisse, P., Aime`ne, Y., Dogui, A., Dridi, S., Gatouillat., S., Hamila, N., …, Vidal-Sallé, E. (2010). Hypoelastic, hyperelastic, discrete and semi-discrete approaches for textile composite reinforcement forming. International Journal of Material Forming, 3(2), 1229-1240.

[52] Van West, B.P., Pipes, R.B., & Keefe, M. (1990). A simulation of the draping of bidirectional fabrics over arbitrary surfaces. Journal of Textile Institute, 81(4), 448-460.

[53] Van Der Ween, F. (1991). Algorithms for draping fabrics on doubly-curved surfaces. International Journal for Numerical Methods in Engineering, 31, 1414-1426.

[54] Mark, C., & Taylor, H.M. (1965). The fitting of woven cloth to surfaces. Journal of Textile Institute, 47, T477-T88.

[55] Potter, K.D. (1979). The influence of accurate stretch data for reinforcements on the production of complex structural mouldings: Part 1 and 2. Composites, 10(3), 161-173.

[56] Robertson, R.E., Hsiue, E.S., & Sickafus, E.N. (1981). Fiber rearrangements during the molding of continuous fiber composites. I. Flat cloth to a hemisphere. Polymer Composites, 2(3), 126-131.

[57] Vanclooster, K., Lomov, S.V., & Verpoest, I. (2009). Experimental validation of forming simulations of fabric reinforced polymers using an unsymmetrical mould configuration. Composites Part A: Applied Science and Technology, 40, 530-539.

[58] Walther, J., Simacek, P., & Advani, S.G. (2012). The effect of fabric and fiber tow shear on dual scale flow and fiber bundle saturation during liquid molding of textile composites. International Journal of Material Forming, 5, 83-97.

[59] Collier, J. R., Collier, B.J., O'Toole, G., & Sargan, S.M. (1991). Drape prediction by means of finite-element analysis. Journal of the Textile Institute, 82(1), 96-107.

[60] Eischen, J.W., Deng, S.G., & Clapp, T.G. (1996). Finite-element modeling and control of flexible fabric parts. IEEE Computer Graphics and Applications, 16(5), 71-80.

[61] Dong, L., Lekakou, C., & Bader, M.G. (2000). Solid-mechanics finite element simulations of the draping of fabrics: a sensitivity analysis. Composites Part A: Applied Science and Manufacturing, 31, 639-652.

[62] Dong, L., Lekakou, C., & Bader, M.G. (2001). Processing of composites: simulations of the draping of fabrics with updated material behavior law. Journal of Composite Materials, 35(2), 138-163.

[63] Cherouat, A., & Billoët, J.L. (2001). Mechanical and numerical modelling of composite manufacturing processes deep-drawing and laying-up of thin pre-impregnated woven fabrics. Journal of Materials Processing Technology, 118, 460-471.

[64] Cherouat, A., Borouchaki, H., & Giraud-Moreau, L. (2010). Present state of the art of composite fabric forming: geometrical and mechanical approaches. Materials, 2(4), 1835-1857.

[65] Sidhu, R., Averill, R.C., Riaz, M., & Pourboghrat, F. (2001). Finite element analysis of textile composite preform stamping. Composite Structures, 52, 483-497.

[66] Lin, H., Wang, J., Long, A.C., Clifford, M.J., & Harrison, P. (2007). Predictive modelling for optimization of textile composite forming. Composites Science and Technology, 67, 3242-3252.

[67] Jauffres, D., Sherwood, J., Morris, C., & Chen, J. (2010). Discrete mesoscopic modeling for the simulation of woven-fabric reinforcement forming. International Journal of Material Forming, 3(2), S1205-S1216.

[68] Duhovic, M., Mitschang, P., & Bhattacharyya, D. (2011). Modelling approach for the prediction of stitch influence during woven fabric draping. Composites Part A: Applied Science and Manufacturing, 42, 968-978.

[69] Sharma, S.B., & Sutcliffe, M.P.F. (2004). A simplified finite element model for draping of woven material. Composites: Part A, 35, 637-643.

[70] Skordos, A.A., Monroy Aceves, C., & Sutcliffe, M.P.F. (2007). A simplified rate dependent model of forming and wrinkling of pre-impregnated woven composites. Composites Part A: Applied Science and Manufacturing, 38, 1318-1330.

[71] Boubaker, B.B., Haussy, B., & Ganghoffer, J.F. (2007). Discrete models of woven structures. Macroscopic approach. Composites Part B: Engineering, 38, 498-505.

[72] Boisse, P., Gasser, A., & Hivet, G. (2001). Analyses of fabric tensile behavior: determination of the biaxial tension-strain surfaces and their use in forming simulations. Composites Part A: Applied Science and Manufacturing, 32, 1395-1414.

[73] Boisse, P., Zouari, B., & Gasser, A. (2005). A mesoscopic approach for the simulation of woven fibre composite forming. Composites Science and Technology, 65, 429-436.

[74] Hamila, N., & Boisse, P. (2008). Simulations of textile composite reinforcement draping using a new semi-discrete three node finite element. Composites Part B: Engineering, 39, 999-1010.

[75] Gatouillat, S., Vidal-Sallé, E., & Boisse, P. (2010). Advantages of the meso/macro approach for the Simulation of fibre composite reinforcements. International Journal of Material Forming, 3(1), 643-646.

[76] Tavana, R., Najar, S.S., Abadi, M.T., & Sedighi, M. (2013). Meso/macro-scale finite element model for forming process of woven fabric reinforcements. Journal of Composite Materials, 47(17), 2075-2085.

[77] Johnson, K.L. (1985). Contact Mechanics. Cambridge University Press, Cambridge, UK.

[78] Inman, D.J. (1996). Engineering Vibration, Prentice-Hall, Inc..

[79] Cook, R.D., Malkus, D.S., & Plesha, M.E. (1974). Concepts and applications of finite element analysis. New York. John Wiley & Sons.

[80] Anh, L.X. (2003). Dynamics of mechanical systems with coulomb friction. Springer, New York.